EXPERIMENTAL INVESTIGATION OF UNINTERRUPTED AND
INTERRUPTED MICROCHANNEL HEAT SINKS

A THESIS SUBMITTED TO
THE GRADUATE SCHOOL OF NATURAL AND APPLIED SCIENCES
OF
MIDDLE EAST TECHNICAL UNIVERSITY

BY

AYŞE GÖZDE ULU

IN PARTIAL FULFILLMENT OF THE REQUIREMENTS

FOR

THE DEGREE OF MASTER OF SCIENCE

IN

MECHANICAL ENGINEERING

FEBRUARY 2012

Approval of the thesis:

EXPERIMENTAL INVESTIGATION OF UNINTERRUPTED AND INTERRUPTED MICROCHANNEL HEAT SINKS

submitted by **AYŞE GÖZDE ULU** in partial fulfillment of the requirements for the degree of **Master of Science in Mechanical Engineering Department, Middle East Technical University by,**

Prof. Dr. Canan ÖZGEN
Dean, Graduate School of **Natural and Applied Sciences**   _____

Prof. Dr. S. Süha Oral
Head of Department, **Mechanical Engineering**   _____

Assist. Prof. Dr. Cüneyt SERT
Supervisor, **Mechanical Engineering Dept, METU**   _____

Assoc. Prof. Dr. Almıla GÜVENÇ YAZICIOĞLU
Co-Supervisor, **Mechanical Engineering Dept., METU**   _____

Examining Committee members:

Prof. Dr. Haluk AKSEL
Mechanical Engineering Dept., METU   _____

Assist. Prof. Dr. Cüneyt SERT
Mechanical Engineering Dept., METU   _____

Assoc. Prof. Dr. Almıla GÜVENÇ YAZICIOĞLU
Mechanical Engineering Dept., METU   _____

Assist. Prof. Tuba OKUTUCU ÖZYURT
Mechanical Engineering Dept., METU   _____

M. Sc. Uğur Etiz
Design Leader, ASELSAN   _____

Date: 09.02.2012

I hereby declare that all information in this document has been obtained and presented in accordance with academic rules and ethical conduct. I also declare that, as required by these rules and conduct, I have fully cited and referenced all material and results that are not original to this work.

Name, Last name : Ayşe Gözde ULU

Signature :

ABSTRACT

EXPERIMENTAL INVESTIGATION OF UNINTERRUPTED AND INTERRUPTED MICROCHANNEL HEAT SINKS

Ulu, Ayşe Gözde
M. Sc., Department of Mechanical Engineering
Supervisor: Assist. Prof. Dr. Cüneyt Sert
Co-Supervisor: Assoc. Prof. Dr. Almıla Güvenç Yazıcıoğlu

February 2012, 115 pages

Experimental measurements are conducted on uninterrupted and interrupted aluminum microchannel heat sinks of 300, 500, 600 and 900 μm channel widths. Two different versions of interrupted channels are tested; with single interruption and with 7 interruptions. Distilled water is used as the working fluid and tests are conducted at volumetric flow rates in a range of 0.5-1.1 lpm. Thermoelectric foils are used to supply uniformly distributed heat load to the heat sinks such that for all the tests the heat removed by water is kept constant at 40 W. Pressure drop and temperature increase are measured along the channels of different configurations for a number of different flow rates.

For the interrupted channels thermal boundary layers re-initialize at the leading edge of each interrupted fin, which decreases the overall boundary layer thickness. Also the flow has been kept as developing, which results in better heat transfer performance. Due to the separation of the flow into branches, secondary flows appear which improves the mixing of the stream. Advanced mixing of the flow also enhances the thermal performance.

In the experiments, it is observed that interruption of channels improved the thermal performance over the uninterrupted counterparts up to 20% in average Nusselt number, for 600 micron-wide channels. The improvement of average Nusselt number

between the single interrupted and multi interrupted channels reached a maximum value of 56% for 500 micron-wide channels. This improvement did not cause a high pressure drop deviation between the uninterrupted and interrupted microchannels even for the maximum volumetric flow rate of 1.1 lpm. Highest pressure drop through the channels was measured as 0.07 bar, which did not require to change the pump. In the tests, maximum temperature difference between the inlet of the fluid and the base of the channel is observed as 32.8°C, which is an acceptable value for electronic cooling applications.

Keywords: Interrupted Microchannels, Heat Sink, Electronics Cooling, Phased Array Radar Cooling

ÖZ

BÖLÜNMÜŞ VE BÖLÜNMEMİŞ MİKROKANAL TİPİ ISI ALICILARININ DENEYSEL KARŞILAŞTIRILMASI

Ulu, Ayşe Gözde

Yüksek Lisans, Makine Mühendisliği Bölümü

Tez Yöneticisi: Yrd. Doç. Dr. Cüneyt Sert

Ortak Tez Yöneticisi: Doç. Dr. Almıla Güvenç Yazıcıoğlu

Şubat 2012, 115 sayfa

Deneysel ölçümler 300, 500, 600 ve 900 mikron kanal genişliklerinde bölünmemiş ve bölünmüş alüminyum mikro kanal ısı alıcıları yürütülmüştür. Bölünmüş kanalların tek noktadan bölünmüş ve 7 noktadan bölünmüş olmak üzere 2 tipi test edilmiştir. Çalışma sıvısı olarak saf su kullanılmıştır ve testler 0,5-1,1 lpm hacimsel akış hızlarında gerçekleştirilmiştir. Termoelektrik malzeme, suyun sabit 40 W ısı aldığı tüm testlerde, düzgün dağıtılmış ısı yükünü ısı alıcılara sağlamak amacıyla kullanılmıştır. Farklı kanal konfigürasyonda kanal boyunca basınç düşüşü ve sıcaklık artışı farklı debi dizilerinde ölçülmüştür.

Bölünmüş kanallarda ısıl sınır tabakalar bölünmüş her fin başlangıç ucunda yeniden başladığı için genel sınır tabaka kalınlığı azalır. Aynı zamanda akışın gelişmemiş durumunun muhafaza edilmesinin bir sonucu olarak daha iyi bir ısı transferi performansı elde edilir. Akışın dallara ayrılması nedeniyle, akışın karışmasını arttıran ikincil akışlar görülür. Akışın karışması termal performansı ayrıca geliştiren bir etkidir.

Kanalların bölünmesi, 600 mikron genişlikli kanallarda, bölünmemiş türevlerine göre termal performansın ortalama Nusselt sayısında % 20'ye kadar artmasını sağlamıştır.

Bir kere bölünmüş ve çok kez bölünmüş kanallar arasında ortalama Nusselt sayısının iyileştirilmesi 500 mikron çapında kanallar için % 56 maksimum değerine ulaşmıştır. Bu gelişmeler maksimum debi olan 1.1 lpm de dahi bölünmüş ve bölünmemiş kanallar arasında kanal boyunca gözlenen basınç düşüşünde büyük bir sapmaya neden olmamıştır. Kanallardaki en yüksek basınç farkı 0.07 bar olarak ölçülmüştür ve bu fark pompanın değiştirmesine gerek duyulmadan sağlanabilmiştir. Testlerde akışkanın girişi ve kanalın tabanı arasındaki maksimum sıcaklık farkı 32.8°C olarak ölçülmüştür ki bu değer elektronik soğutma uygulamaları için kabul edilebilirdir.

Anahtar kelimeler: Bölünmüş Mikro Kanal, Isı Alıcı, Elektronik Soğutma, Faz Dizili Radar Soğutma Metodları

ACKNOWLEDGEMENTS

TABLE OF CONTENTS

LIST OF TABLES

TABLES

LIST OF FIGURES

FIGURES

LIST OF SYMBOLS

c_p : Specific heat at constant pressure

f : Friction factor

f_{app} : Apparent friction factor

h : Convection heat transfer coefficient

k : Conduction heat transfer coefficient

$\dot{m}$: Coolant mass flow rate

p : Pressure

q : Rate of heat transfer

q_f : Rate of heat transfer between fin and coolant

q_{max} : Maximum possible rate of heat transfer between fin and coolant

q_t : Rate of total heat transfer between heat sink and coolant

q'' : Channel wall surface heat flux

t : Time

u_m : Mean velocity

w : Fin width

x : Distance along channel from inlet

A_b : Fin prime surface area

A_c : Fin cross sectional area

A_{ch} : Channel flow area

A_f : Fin surface area

A_{ht} : Heat transfer area

A_t : Fin total area

C_D : Smallest channel dimension

D_h : Hydraulic diameter

$K(x)$: Incremental pressure defect

K_{90} : Pressure loss coefficient of 90° bends

K_c	: Pressure loss coefficient of sudden contraction
K_e	: Pressure loss coefficient of sudden expansion
K_L	: Pressure loss coefficient
l	: Stream wise length of flow circulation
L	: Fin length
L_c	: Corrected fin length
L_{ch}	: Channel length
L_h	: Hydrodynamic development length
L_t	: Thermal development length
N	: Number of fins
Nu	: Nusselt number
P	: Heat power input
Po	: Poiseuille number
Pr	: Prandtl number
P_w	: Wetted perimeter
Q	: Coolant inlet volumetric flow rate
R_{HS}	: Heat sink thermal resistance
Re	: Reynolds number
Re_t	: Reynolds number based on interrupted fin thickness
T_b	: Heat sink base temperature
T_i	: Fluid inlet temperature
T_m	: Fluid mean temperature
T_o	: Fluid outlet temperature
W_c	: Channel width
w_w	: Interrupted fin thickness
α_c	: Channel aspect ratio
ΔT	: Temperature difference
ΔT_{LMTD}	: Log Mean Temperature Difference
Δp	: Pressure difference
μ	: Dynamic viscosity
η_f	: Fin efficiency
η_o	: Overall fin efficiency

ρ	: Density
σ	: Characteristic length
τ	: Molecular length scale
ν_f	: Coolant kinematic viscosity

CHAPTER 1

INTRODUCTION

This preparatory chapter demonstrates the main thoughts which instigate to consider the microchannel concept at length. These interrelated notions are miniaturization of devices, the requirement to comprehend developing electronic cooling trends especially the subjects which comes to a conclusion with a product suitable for national military standards and could be manufactured in domestic infrastructure

1.1 Thermal Management of Electronics and Cooling Technologies

The increasing capability of electronic devices resulted in higher heat flux dissipation at the chip level. This heat generation causes thermal failures in devices such as thermal de-bonding, mechanical stresses, and thermal fracture; due to the reaching the operation temperature limits of components, unless it is removed in reliable advanced methods. Anandan et al. point out that sustaining the junction temperature in allowable limits is a momentous challenge for thermal engineers which necessitate handling thermal management in three different cooling levels at the same time. According to scientists these levels are maintaining the chip temperature at a reasonably low values in spite of high heat flux, handling the heat flux at a system or module level and thermal management of the environment of system or module for instance computer machine room, office space or telecommunication enclosure [1]. In 1974, Scott [2] was classified the cooling methods of all these levels into four main groups in the order of increasing heat transfer effectiveness, for the temperature difference of 80°C between the surface and the ambient. The comparison of the methods is shown in Figure 1.1.
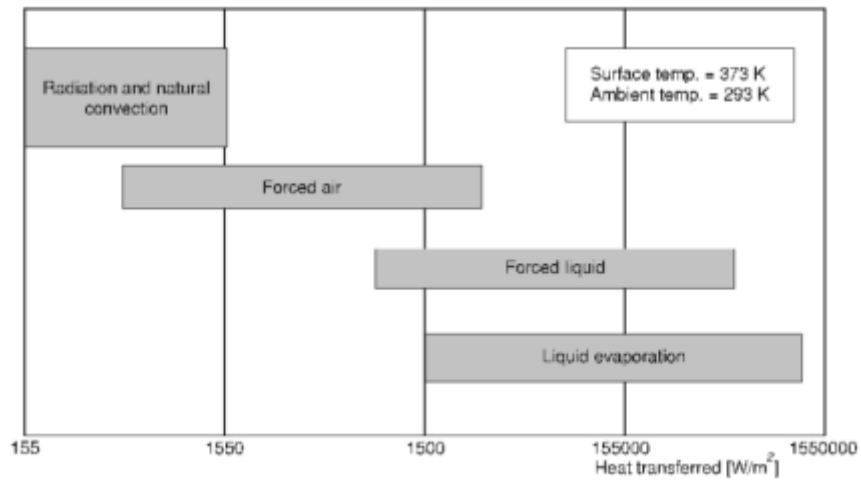
Figure 1.1: Range of conventional heat transfer modes for 80°C temperature difference

Although Scott's prediction of order of cooling methods was validated with time, it was not explicit for each method. According to the detailed survey conducted in 1997 by Lasance [3], the heat transfer coefficients for different cooling techniques had been updated and as shown in Figure 1.2.

.
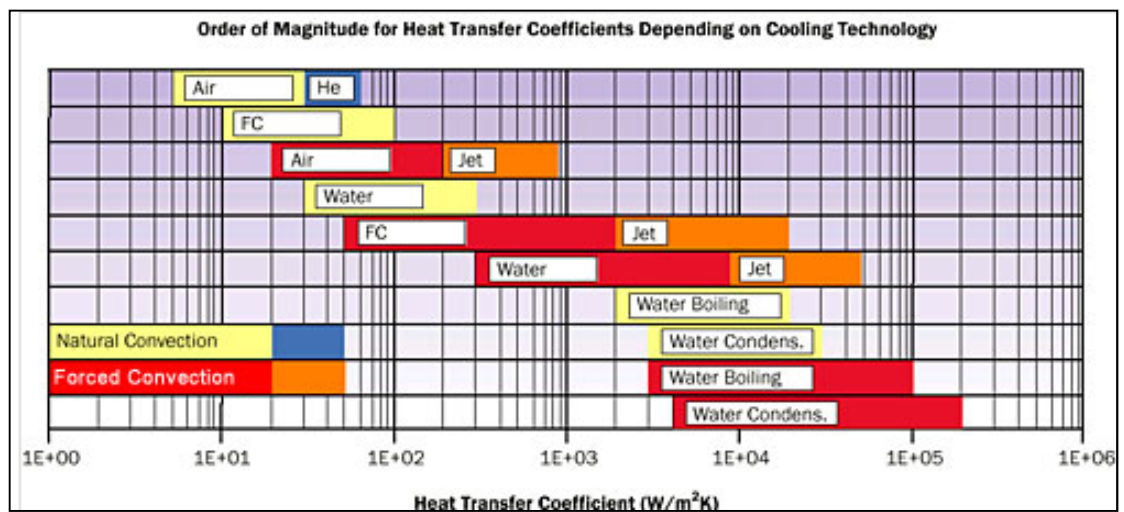
Figure 1.2: Achievable heat transfer coefficients with natural convection, single-phase liquid force convection and boiling for different coolants.

The principal method for electronics cooling is air cooling which is the most frequently utilized one, due to the ease of application and ready availability. On the other hand, it is conceded that traditional air cooling techniques are about to reach the cooling performance limits. For this reason, numerous enhancement methods have been attempted to increase the cooling performance of the natural and force convection of air cooling systems. In 2007 Florio and Harnoy [4] put forward an alternative cooling technique that enhances the free convection heat transfer from discrete sources. The study demonstrated that combined effects of vibrating plate and the opening flow have the potential to improve in the thermal performance of natural cooling over pure free convection. They assessed that up to 70% enhancement in the local heat transfer coefficient over free convection was achieved with only a board opening.
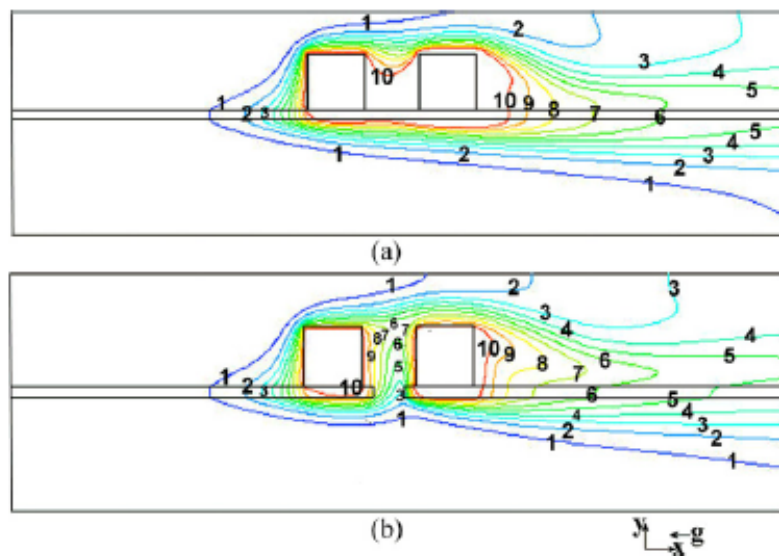
Figure 1.3: Steady state dimensionless temperature contours (a) without an opening (b) with an opening on the plate.

3

When the cooling performance of natural convection is not enough forced convection is used with the equipments such as conventional fans, micro air jets and piezoelectric fans. Although conventional fans have the disadvantages of noise pollution and power consumption they are preferred in various areas such as commercial personal computers or military task equipments. Fans are generally used with extended surfaces such as fins in heat sinks or heat pipe- heat sink assemblies where high fluxes required to remove. An example for heat pipe-heat sink fan assembly is shown in Figure 1.4.
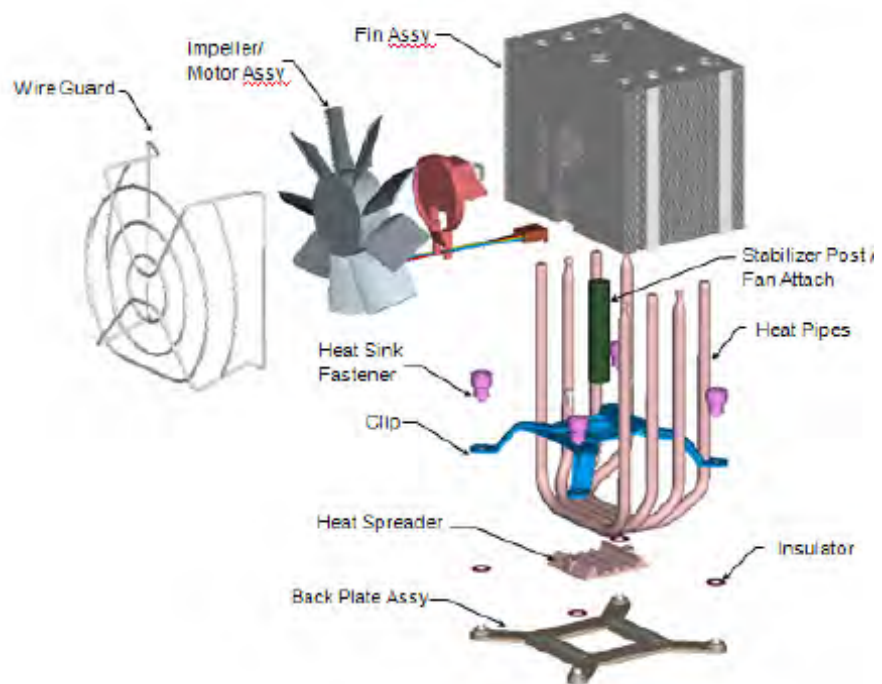
Figure 1.4: Reference heat pipe thermal solution assembly for i7 processor

Comparatively fresh electronic cooling method piezoelectric fan assembly experimental studies are generally research by scientists from in Purdue University. The assembly generally includes a power supply, thin shim stock and piezoelectric

module as seen in Figure 1.5. During the alternating voltage loading into the system the piezoceramic module contradicts and expands which causes bending moment at the shim stock. These bending moments result in oscillations at the shim stock end with the same frequency as applied alternating voltage. Oscillations engender beneficial air mixing and air flow for cooling applications. [6] Sydney et al, emphasized that piezoelectric fans are gaining popularity owing to their low power consumption and low noise level for limited volume devices. Scientists also highlight that at the high frequency domain power consumption increases and fluid motion reduces which brought to a conclusion that the technology is limited to first resonance mode for portable cooling applications.

Figure 1.5: Oscillating piezoelectric fan under applied voltages owing to contradiction and expansion of piezoceramic patch.

Increasing power removal demand of electronics forces scientists to investigate liquid cooling applications. Jet impingement and spray cooling are the generally investigated water cooling applications which are explained in detail in this section as well. Jet impingement is one of the significant methods in removing high heat fluxes dissipated by electronic constituents. High heat transfer liquid jet is pointed to the hot spot in order to remove heat and cool the surface. In this manner high heat transfer rates are obtained in the vicinity of the stagnant point. Due to the surface temperature of the hot spot and jet working fluid, the jet impingement resulted in

single phase or two phase transfer. Different jet impingement configurations are presented in Figure 1.6 [7].
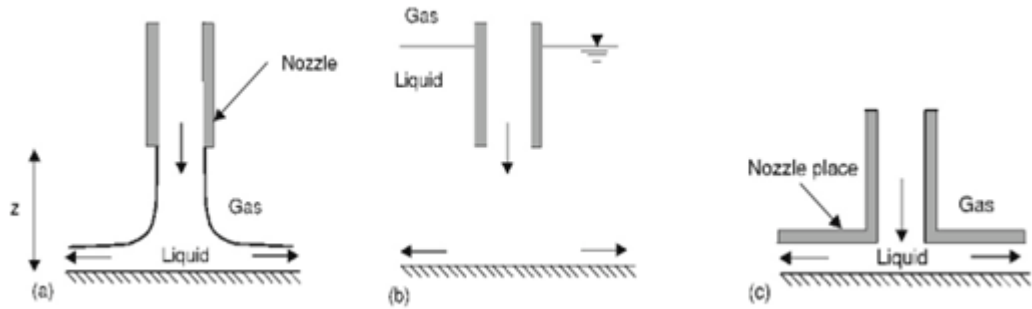
Figure 1.6: Different configurations of jet impingement: (a) free-surface jet, (b) submerged jet, (c) confined submerged jet

Spray cooling is another method used for removing high heat fluxes from electronic components generating heat from integrated circuits. In the electrospray evaporative cooling (ESEC) system atomized working fluid is obtained by electrospray technique as shown in Figure 1.7. During the voltage application between the nozzles and the collecting electrode, charges surrounded by the fluid are driven to the surface of the fluid meniscus of each nozzle. Due to the Coulombic force the charged fluid particles sprayed from the tip of the fluid cone repel each other and generate fine aerosol droplets. Electrostatic force accelerates these droplets towards the collecting electrode surface. Consequently; phase change of droplets from liquid to vapor enable to dissipate large amounts of heat at the thermal exchange surface [8].
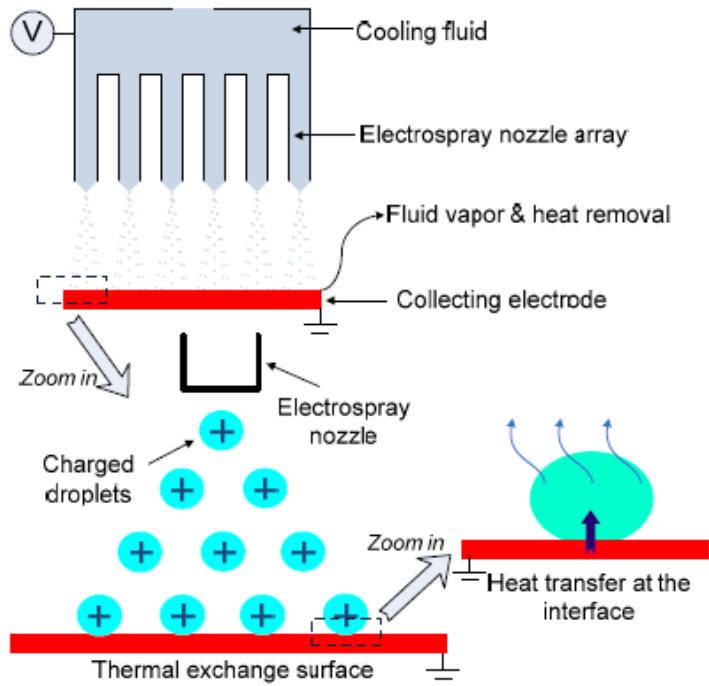
Figure 1.7: Fluid atomization and heat transfer mechanism of ESEC device using an ESEC microfluidic chamber

Besides the affords performed in order to increase the heat transfer coefficients various advanced techniques, such as thermoelectric foils and heat pipes are also used to cool down the hot spots. Among these techniques, heat pipes are the passive heat transfer tools where the two phase heat transfer mechanism takes places inside of the sealed vacuum vessels partially filled with water which is used as a heat transfer medium. Details of working mechanism of a heat pipe are given in Figure 1.8 [9].
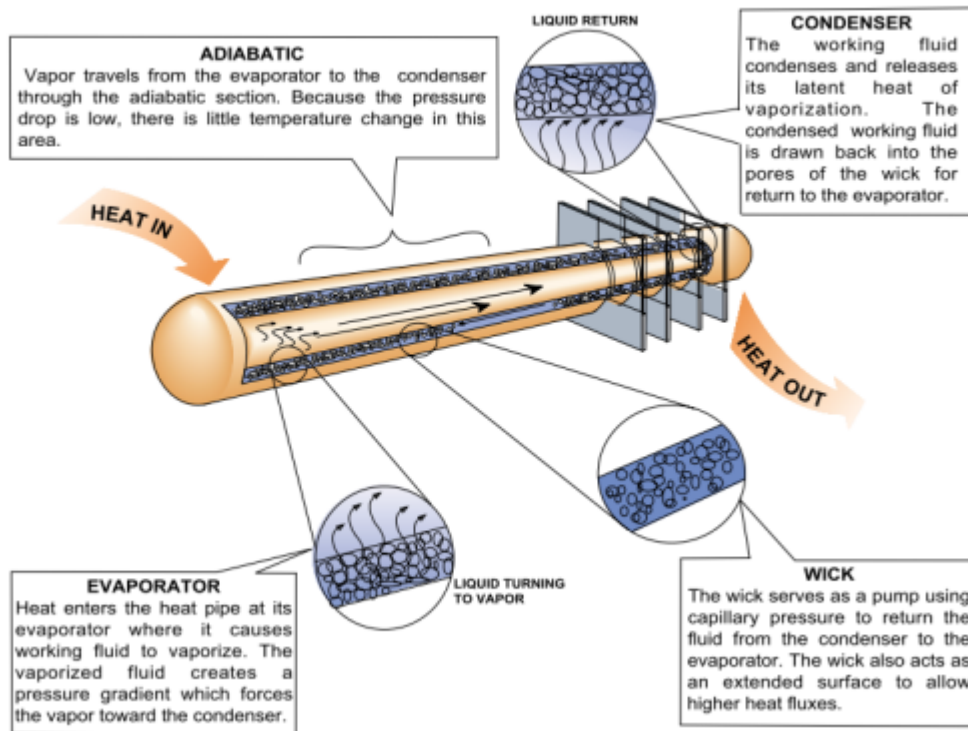
Figure 1.8: Heat pipe operation

A recent study performed by Hiroyuki Ryoson et al., from Sony Chemical & Information Device Corporation demonstrate the thermal performance of thin heat pipe with a new type of wick structure as shown in

Figure 1.9 [10]. Such thin heat pipes with high thermal conductivity; in this example up to 16000 W/m˚K is observed, are getting attraction in the area of consumer electronics as exemplified by LCD TVs and notebook PCs which are becoming thinner and smaller day by day.
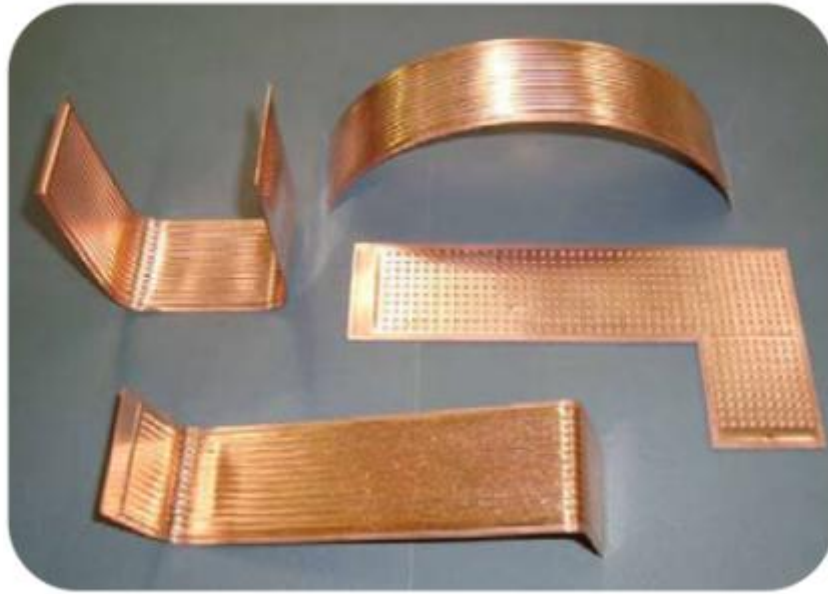
Figure 1.9: Photo of thin heat pipes

Another electronics cooling technique mentioned in the review of Anandan et al. [1] is thermoelectric cooling which converts electrical energy into thermal energy via depending on the several phenomenon namely; the Peltier, Seeback and Thomson effects. The device is mainly used in temperature stabilization, temperature cycling and cooling below ambient temperature. One of thermoelectric equipment exemplar is shown in Figure 1.10. In some treatments, it is essential to have entirely isolated working environment for electronics in order to prevent large built up of particles which could harm to electronics. Conventional cooling methods cannot be efficient under these conditions. For these cases, hermetic thermo coolers are suggested by Palacios et al. [11]. According to study, which was carried for personal computers and present different cooling alternatives namely natural convection using standard radiators and forced convection using radiators and fans, by using thermoelectricity the heat transfer is significantly increased.
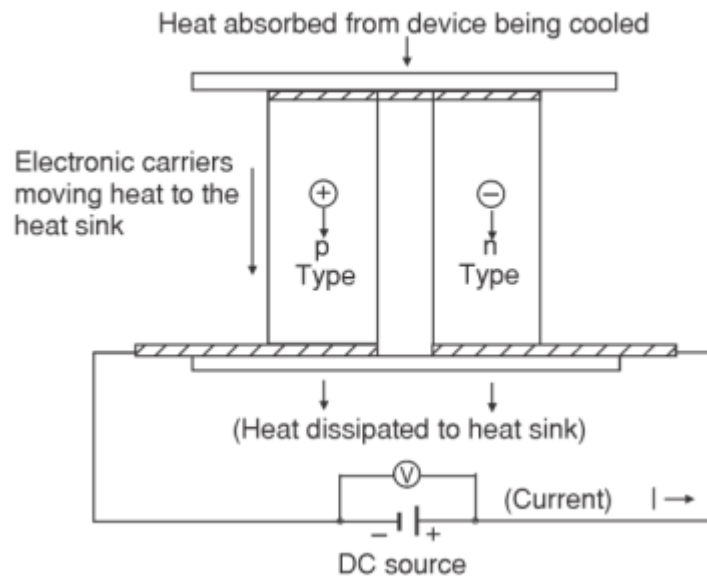
Figure 1.10: Working diagram of thermoelectric cooler

The techniques explained in this section are getting more and more importance with the demand to remove increasing heat fluxes and trend of miniaturization. Cooling performance limits of these techniques have been researched to enhance further and disadvantages for example lack of ruggedness, dependency to additional devices such as pumps, secondary cooling systems etc., high manufacturing costs and complexity have been investigated to diminish. In order to reach mentioned goals, scope of electronics cooling becomes more challenging and intricate.

1.2 Miniaturization and Microchannels

The perception of miniaturization was uttered at first by Richard Feynmann [12] in the talk at the annual meeting of American Physical Society in 1959. In his speech the possibility of transferring information into small scale, enhancing electron microscopes, miniaturizing computers, solving lubrication problems are brought to light. His striking remark "In the year 2000, when they look back at this age, they will wonder why it was not until the year 1960 that anybody began to seriously move in this direction." is confirmed before the pointed time.

10

Owing to the fact that observed by Moore in 1965; diminishing trend in relative manufacturing cost per component with increasing number of components per integrated circuit; as shown in Figure 1.11 the 20th century become the era of increasing number of transistors on an integrated circuit which introduce word minimization in technology outcome products and brought the requirement of cooling down the minimized-shaped electronic components of the devices in packets in a challenging way.
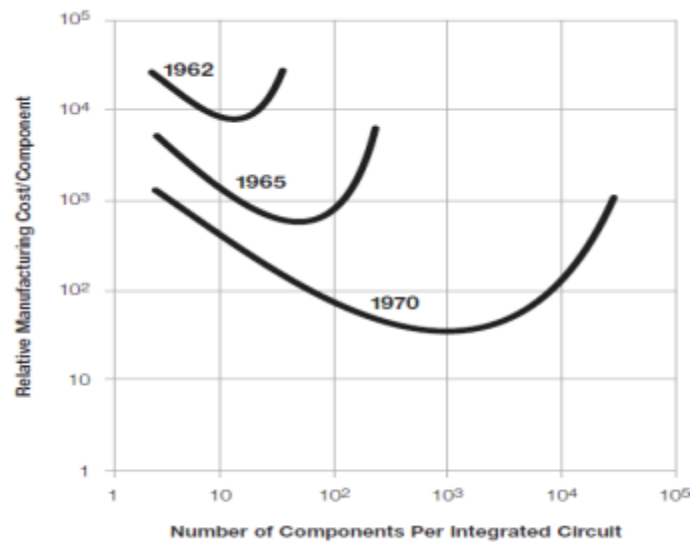
Figure 1.11: The relative manufacturing cost per component reduced with the time

As the developments force engineers to design smaller devices generating high heat generations, different electronic cooling methods have been proposed. Among these methods liquid cooling is a reasonable alternative solution to conventional techniques due to having high heat transfer coefficients. In 1981, Tuckerman and Pease furthered liquid cooling technique to one step forward by constructing a more compact structure owning high heat transfer area to volume ratio and heat transfer

11

coefficients [14]. In the test it was seen that it had been possible to remove 790 W from 1 cm^2; via microchannels having wall depth of 300 μm and width of 50 μm hydraulic diameter with relatively high temperature differences between the inlet and exit of the channel. Although the channel was not optimized in terms of thermal resistance and temperature difference; it has been the pioneer survey of microchannel for scientist dealing with electronics cooling and since this study followers have been tried to improve performance and diminish the mentioned disadvantages.

1.3 Motivation

The factors encouraged to research microchannel cooling can be listed as the tendency of temperature failure of electronic components, the requirement to remove high heat fluxes in military design applications under harsh environmental conditions, and overall performance and applicability of microchannel heat sink among other techniques. The tendency of electronic devices to various types of failure was analyzed by Kristiansen [15]. According to his study more than half of the breakdowns are sourced from temperature related issues. In military designs it is expected to have a greater failure percentage for this aspect due to higher heat fluxes generated from complicated devices working under harsh environmental conditions. In defense systems, typical operating condition is specified between -30°C/+55°C range. Generally, lower limit does not cause any failure for functionality or reliability; in occasional cases additional heater design would be a simple solution. However; the upper bound is a tough criterion for designers owing to the fact that temperature endurance of most of the electronic components is under +85 °C level. For this reason, thermal engineers working in military design sector is bounded in a narrow thermal band and necessitates having advance cooling techniques with high heat transfer coefficients.
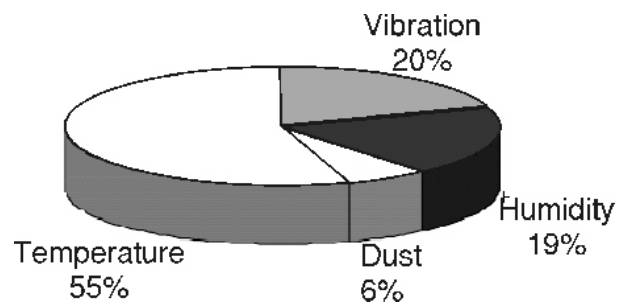
Figure 1.12: Failure in electronic components

Although it is emphasized that high transfer capacity of cooling methods is vital for harsh environmental electronics, the cooling performance is not the only criteria for rugged designs. The complexity, weight, cost and reliability form the overall picture. In the survey conducted by engineers from Smart and Small Thermal Systems Laboratory and CALCE Electronics Systems and Products Center collaborated with University of Maryland [16], these features of cooling methods are compared. According to the survey, among these methods liquid cooling; even if it does not serve the best cooling capacity; has been selected as the best in overall rank.

Consequently, the requirement for advanced cooling techniques to minimize temperature based problems in electronics, attainable cooling performance for military designs, and the reasonable features for harsh environmental conditions motivated writer to investigate liquid cooling.

13
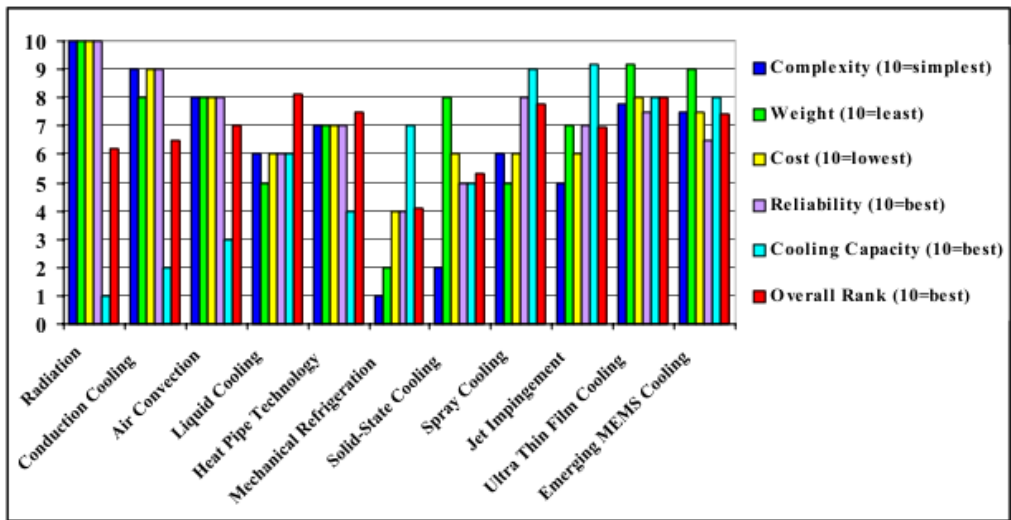
Figure 1.13: Summary of thermal management techniques for harsh environmental electronics.

CHAPTER 2

CURRENT LITERATURE ON MICROCHANNEL HEAT SINKS

This chapter is composed of selected surveys about microchannels and enhancement techniques.

2.1 Related Early Work on Microchannel Heat Sinks

The pioneer work on microchannels was conducted by Tuckerman and Pease [14]. Up until this study liquid cooling techniques had not been observed at this scale. In the study, effective and compact heat removal for high speed, high density very-large-scale integrated (VLSI) circuits were aimed. As mentioned in the first chapter, they managed to remove 790W from 1cm^2 through channels having wall depth of 300μm and width of 50 μm with a relatively high temperature difference penalty of 71˚C. The scientists asserted that high heat fluxes could be removed via a merit of small characteristic length in the micro-scale channels. Later than this pioneer study numerous scientists analyzed the flow and heat transfer in microchannels. Although high heat flux removal capabilities of microchannels were assessed ratified through these studies; different phenomena of flow and heat transfer in microchannels and micro tubes were detected [17].

2.1.1 Flow Considerations

The first investigations for measuring the friction factors of microchannels were done by Wu and Little in 1983 [18]. They conducted tests for measuring friction factors of nitrogen in silicon an glass trapezoidal channels and compared the results with Moody's chart values for commercial channels. They asserted friction factors for

glass channels 3-5 times larger than smooth-pipe predictions. A few years after this study, R. J. Phillips from MIT claimed in the master of science thesis that turbulent flow designs performs equal or better thermal performance over laminar flow designs, and due to tolerable pumping power requirement it is feasible to manufacture comparatively large turbulent flow channels with conventional machine shop technology [19]. In 1990, Pfahler et al. [20, 21] observed that in relatively large cross-section channels, the Navier-Stokes predictions could be applied; however in decreased channel depth experimental observations deviated from the predictions. For different cooling fluids in decreased channel depth, friction factor relations differed in terms of dependency to Reynolds number and channel size. For instance; in tests, it was found that isopropyl friction constant was independent of Reynolds number and dependent on the channel size. Contrary to isopropyl, for silicone oil friction constant was slightly dependent on Reynolds number and independent of channel size. The scientist attributed this behavior of channels for liquid flow to reduction of viscosity due to very small dimensions and for the rarefaction effect in the small channel for gas flow.

Another experimental study on friction factor for rectangular stainless steel channels with water flow was conducted by Peng et al. [22]. According to this study friction factor findings were significantly different from the characteristics of the macro-sized channel flow. They investigated the flow for Reynolds number from 50 to 4000, and argued that the flow transition had been occurred at a Re of 200 to 700 contrary to the generally accepted value 2300. They ascribed the deviation of the findings from theoretical predictions to the hydraulic diameter; and claimed that decreasing in the value of hydraulic diameter causes the lower transition Re numbers. Although this article was referred by many scientists; this study was refuted in a review accomplished by scientists from Israel Institute of Technology, due to the disunity with other researchers' observations [23].

Since the work of Wu and Little; numerous researchers studied on fluid flow characteristics of circular, rectangular and trapezoidal microchannel heat sinks for smooth and rough tubes. A recent comprehensive comparison of these experimental

16

studies, for Reynolds number range of 0.002<Re<5000 and a hydraulic diameter range of 8< D_h < 990 μm, stated that the experiments which did not account for the entrance, exit losses or developing flow in the microchannel experienced a deviation from the conventional study [24]. Steinke and Kandlikar uttered that the experiments considering the mentioned effects showed an agreement with the conventional friction factor theory for the range of Reynolds number and hydraulic diameter. They also noted that uncertainties for microchannel heat exchangers could be very high and added that "Even a very accurate pressure drop measurement will often be overshadowed by geometry measurement uncertainties."

2.1.2 Heat Transfer Considerations

Since the survey of Tuckerman and Pease, working on heat transfer of microchannel exchangers attracted many scientists attention as well as the friction factor analyses. Wu and Little were the first example of these scientists who also published the study about the heat transfer in microchannels 1 year after their study about friction factors. In this study [25] they worked with trapezoidal glass and silicon type channels with working fluid of nitrogen. The channels hydraulic diameter range were at 55< D_h < 76 μm and they offered a Nusselt number correlation which were afterwards contended as higher than conventional correlations for both laminar and turbulent region by Lee at al. in 2005 [26].

After few years later than the study of Wu and Little, Choi et al. also measured the Nusselt numbers higher than correlations for turbulent flow for microtubes having diameters of 3,7, 10, 53, 81 μm [27]. In the tests they observe a Re- dependence for laminar flow as well.

An interesting test results came after 2 years from the mentioned study by Rahman and Gui [28]. According to this investigation; which had been carried out for rectangular etched silicon channels with cooling fluid of water; Nusselt numbers

were determined higher than analytical prediction for developing laminar flow, whereas it was measured lower for turbulent regime.

Yu et al. [29] also investigated the heat transfer in microtubes for turbulent flow with a considerably wide Reynolds number range at 2500< Re < 60000 for micro tubes having inner diameter of 19 to 102μm. They measured Nusselt numbers higher than correlation for turbulent flow.

Another interesting test results are obtained by Peng et al. [30]. Unlike to Rahman and Gui; they measured Nusselt numbers lower than correlation for laminar flow and higher for turbulent flow for rectangular channels having width of 100 to 300 μm and height 200 to 400 μm. They observed the transition to fully developed turbulent flow at smaller Reynolds number than the ordinary channel flow.

Likewise many scientists Ravigururajan and Drost [31] measured the heat transfer coefficients different than the laminar prediction. Their test results for rectangular microchannels were higher than the previous correlations for channels having channel width of 270 μm, height of 1000 μm and lengthf 20.5 mm.

Similar to study of Yu et al; Adams et al. who worked with micro tubes having diameter of 760 μm for turbulent flow with a Reynolds number range at 2600< Re < 23000; also measured the Nusselt numbers higher than correlation for turbulent flow [32].

In contrast to many scientist Harms et al. [33] measured local Nusselt numbers in good agreement with laminar prediction for rectangular microchannels having channel width of 251 μm, height of 1000 μm and lengthf 25 mm with a Reynolds number range at 173< Re < 12900.

In 2002, Qu and Mudawar carried out both experimental and numerical investigations for pressure drop and heat transfer in rectangular microchannel having width of 231 μm and height of 713μm [34]. They showed that the conventional

Navier-Stokes equations are acceptable for microchannels and observed an agreement between the numerical and experimental predictions.

In a recent review study published in 2005 by scientists from Cooling Technologies Research Center, School of Mechanical Engineering, Purdue University stated that the divergence from the conventional correlations is sourced from the mismatch in the boundary and the inlet conditions between the experiments and the conventional correlations [26]. They also noted that numerical results; which are based on Navier-Stokes analysis using both a full 3D conjugate approach model and a simplified thin wall model were found to be in a satisfactory agreement with the experimental data, validating that if entrance and boundary conditions were carefully matched withed the correlations; the numerical analysis could be applied with confidence in order to predict heat transfer behavior in microchannels in the reviewed dimensional range.

2.2 Enhancement Techniques on Microchannels

Numerous scientists attempted to increase the heat transfer performance of microchannel heat sinks via adopting the idea of using microchannel geometries which are similar to conventional microchannel heat sinks with optimized geometry and which are not similar to conventional counterparts. In addition to geometrical considerations, in recent years, improving heat transfer performance by nanofluid and two phase fluid employment were also evaluated. In the study of Lee and Chou [35], oblique and sectional fins are used in microchannels in contrast to continuous fins, in order to reinitiate boundary layer growth at the leading edge and shrink boundary layer thickness. Not only the doubling of entrance effect but also improved mixing of the fluid by the regenerated secondary flows at the ends of the oblique fins increased the heat transfer performance of the microchannel when compared with the parallel conventional counterparts. According to the experiments average Nusselt number increased from 8.6 to 15.8 which correspond to a 83.7% increase against to regular microchannels. On the contrary to general expectation, high pressure drop penalty has not been observed when compared with the conventional improvement techniques.
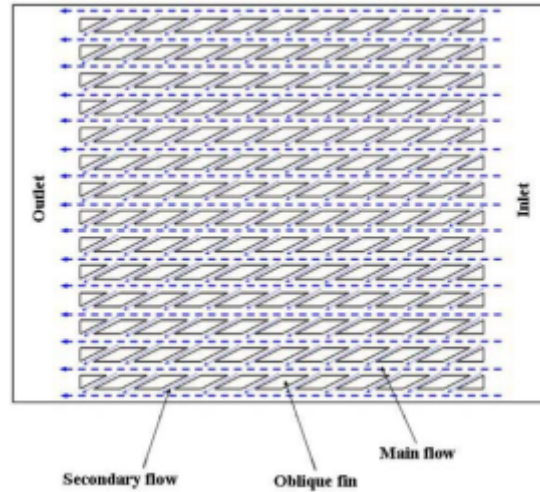
Figure 2.1: Top view of microchannel heat sink with oblique fins

Li and Peterson [36] managed to decrease total thermal resistance of a geometrically optimized microchannel heat sink compared to the microchannel of the pioneer study of Tuckerman and Pease [14]. They initially used a semi-normalized 3-dimesional heat transfer model to optimize parameters of a parallel water-cooled, silicon microchannel heat sink. The optimized geometry has channel depth of 700μm, channel width of 60 μm and pitch of 100 μm with a constant pumping power of 0.05W. Performance of this heat sink is calculated with different pumping powers based on the full 3-D conjugate model. Heat sink with the best performance required pumping power of 2W under a total resistance of 0.068 ^{o} C/W which is 20 % lower than the pioneers.
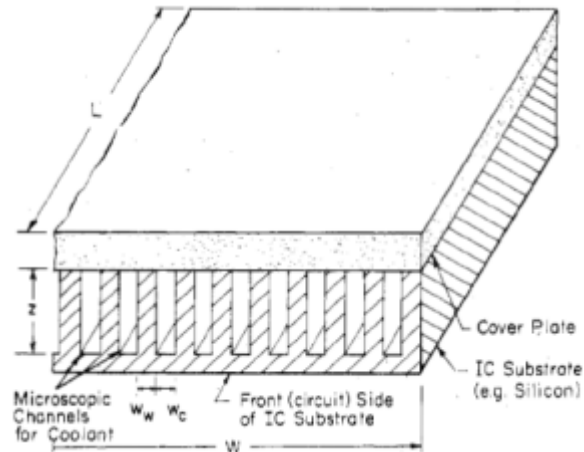
Figure 2.2: Schematic view of Tuckerman and Pease's compact heat sink integrated into an integrated circuit chip

In 2000, Bejan and Errera investigated optimization of interior configuration of a volume that generates heat at each point, which is removed by a single flow via adopting the constructal theory. According to the theory, the constructal tree networks are flow paths which are subjected to local and global constraints and inferred from the idea of minimizing the global resistance to flow between a single point (source, or sink) and a finite size-volume. The scientists broaden the constructal method to systems which are cooled volumetrically by tree networks of channels with fluid flow.

The coolant enters the volume through a single port and leaves from another single port. All points of the heat generating volume are placed in contact with coolant fluid. The generated heat flows primarily by thermal diffusion through solid material, before it is gathered by the first stream of the fluid. The scientists managed to minimize the flow resistance for a parallel plate and round tube between a volume and point by considering the theory [37].
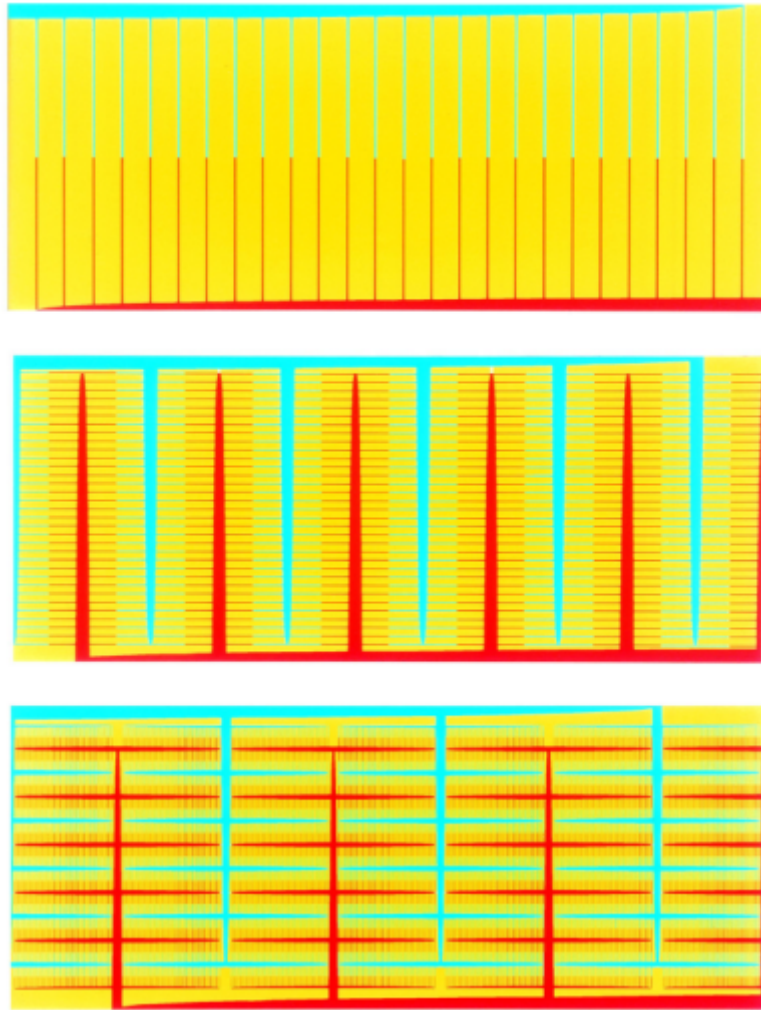
Figure 2.3: Three types of fluid flow network

D.V. Pence is another example to the researchers implemented the idea of studying alternative geometries to improve the performance of the conventional microchannels. Pence analyzed fractal-like branching microchannels in order to minimize pumping power and wall temperature [38]. In 2002 he compared heat sinks with a straight channel array against those utilizing a fractal-like branching channel network. Both geometries have identical channel lengths, heat fluxes and hydraulic diameters. He assumed that both hydrodynamic and thermal boundary layers are reinitiated after each branching. Pence concluded that fractal-like channels provided

a 30 °C lower wall temperature and 60 % lower pressure drop for the same volumetric flow rate of a conventional straight channel array.
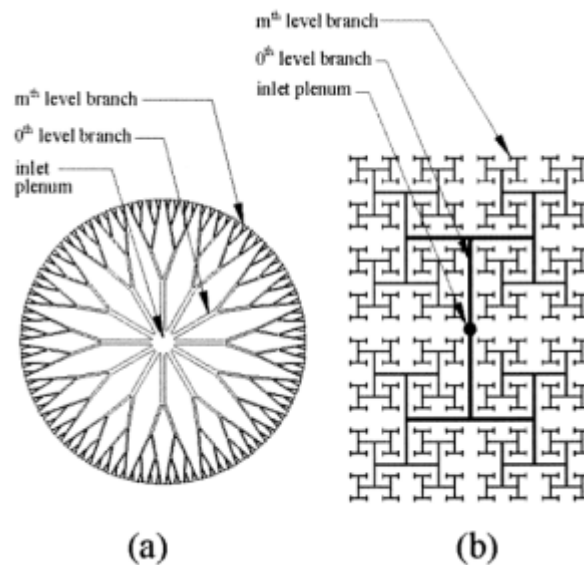
Figure 2.4: Examples of fractal-like branching channel flow networks: (a) having bifurcation angle less than 90° ; (b) bifurcation angle is 90°

In 2010 D.V. Pence and D. Heymann performed numerical optimization studies on fractal-like branching flow networks in disk-shaped heat sinks in order to reduce pressure drop and pumping power [39]. The study is based on a genetic algorithm with gradient-based optimization and direct numerical search. One dimensional formerly approved heat transfer and pressure drop model with working fluid of water is used in the numerical analysis. The methodology is compared with results from direct numerical search and generic algorithm.

In the study geometric features of the optimized flow networks are investigated as a function of disk radius, applied heat flux, and maximum allowable wall temperature. Maximum inlet plenum radius, minimum interior channel spacing, and ranges of

terminal channel widths and periphery channel spacing remained constant. The study revealed that all geometric limits and the heat flux have a considerable effect on the design of an optimal flow network, and results from geometrically derived network design are shown within 15 % of the direct search and gradient-base optimized configurations.

Although most of the research on fractal-like branching and tree shaped configurations is based on numerical analysis and simulations, due to the requirement on complex manifold design and for distribution and collection of coolant liquid, Chen and Cheng conducted experiments on fractal-like shape microchannels. The scientists experimentally confirmed that heat transfer rate per unit power, i.e., thermal efficiency; of fractal tree-like microchannel heat sink is considerably higher than the conventional parallel counterparts under the same circumstances namely temperature difference and inlet velocity.[40]
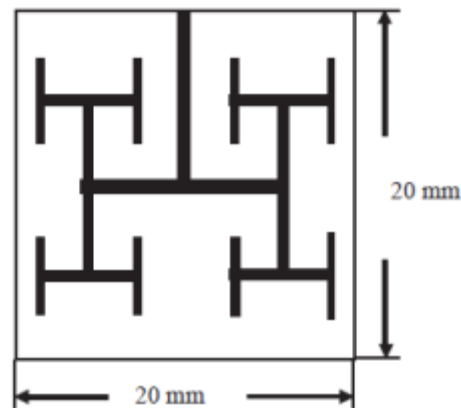
Figure 2.5: Fractal-like microchannel schematics

In order to reduce the overall pressure drop with its short flow length, optimization of split-flow manifold is performed by Ryu et al. using 3D simulations [41]. They succeed to lower the thermal resistance more than a half and enhanced the temperature uniformity on the heated wall by tenfold when compared with the traditional microchannel heat sink. It is concluded that the more imperative design parameters are the channel width and depth on the heat sink performance.
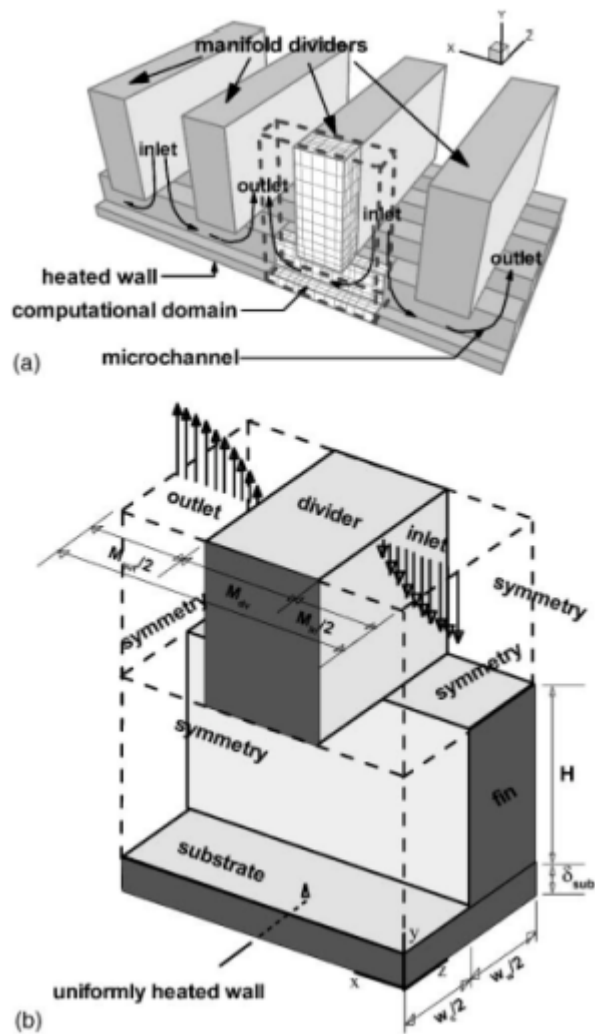
Figure 2.6: Manifold microchannel; (a) general configuration (b) computational domain with boundary conditions; w_c, w_w, M, H, and δ_{sub} stand for channel width, fin thickness, manifold dimensions, channel depth and substrate thickness

Kandlikar and Upadhye attempted to optimize the microchannel size in order to overcome high pressure drop penalty while improving the heat removal performance of the heat sink. For this purpose, the enhanced microchannels having offset strip in single pass and split-flow arrangements are examined. The consequences demonstrated that the split flow microchannels can remove heat fluxes up to $3MW/m^2$ with pressure drop of 35kPa [42].
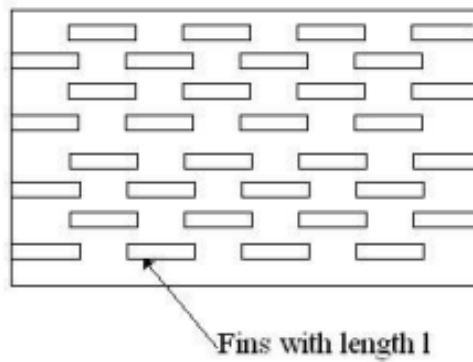
Figure 2.7: Top view of offset strip fins

(a) Single-pass arrangement   (b) Split-flow arrangement
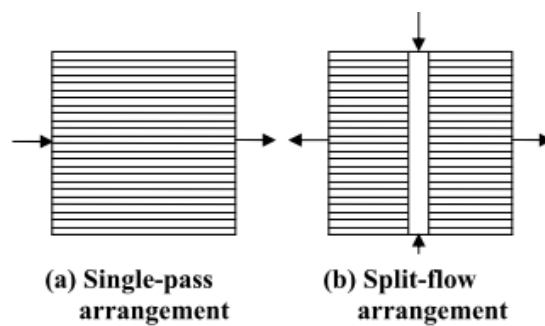
Figure 2.8: Schematics of single-pass and split-flow arrangements with fluid flow directions

Colgan et al. worked on offset strip-fin coupled with a split flow configuration. They revealed a practical implementation of microchannel cooler for high heat fluxes which are above 300W/cm^2 with tolerable pressure drops that is below 35kPa [43].
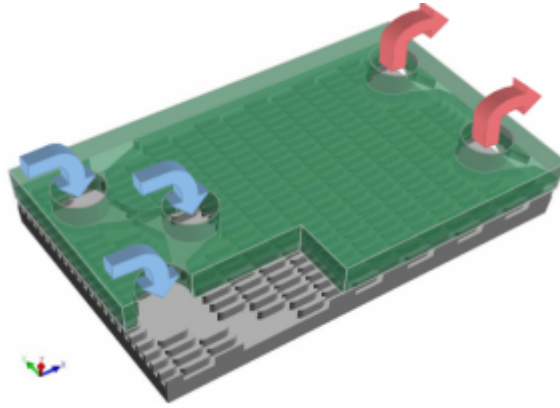
Figure 2.9: Schematics of offset strip fin microchannel

In 2005, Lee and Garimella [44] managed to augment the heat transfer performance of a parallel flow heat sink both globally and locally. They modify the conventional cover lid geometry of microchannel heat sink via adding the recesses. They utilized the boundary layer re-initialization effect to enhance heat transfer. The local Nusselt number is improved up to 150% in the regions at the downstream of the recesses owing to the re-initialization of boundary layers while the flow re-enters the microchannel.
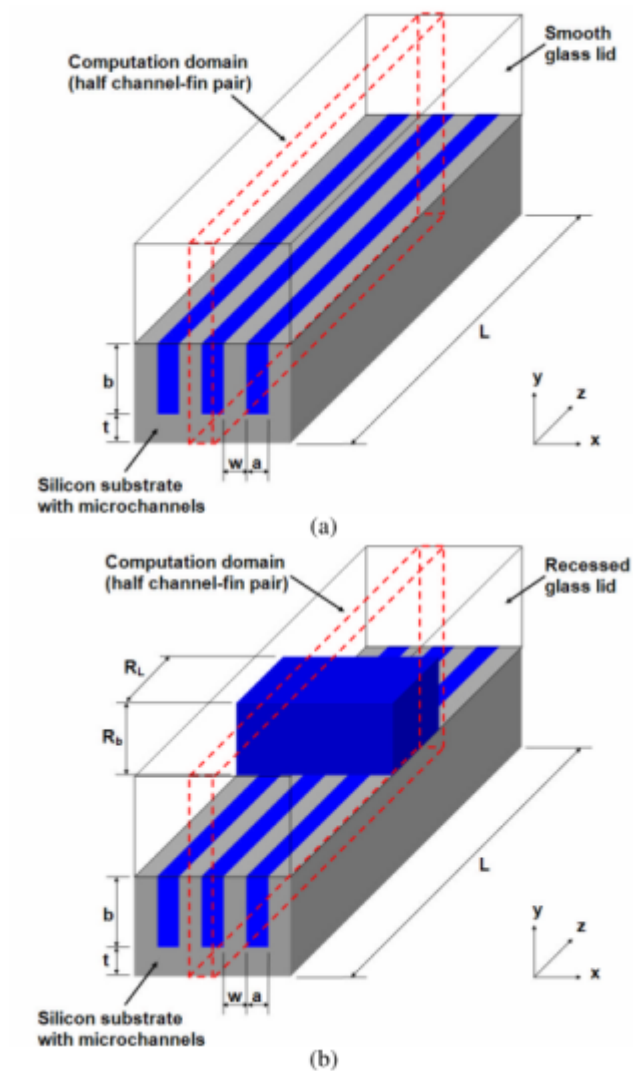
Figure 2.10: (a) Conventional microchannel heat sink with smooth lid; (b) microchannel heat sink with a single recess in the lid. Computational domain is shown in red dashed lines

Xu et al. analyzed boundary layer re-initialization effect in their experiments and numerical simulations [45]. In the study, transverse cuts were added across the main microchannel heat sink fin direction. These transverse cuts assist thermal boundary layer re-initialization and result in local heat transfer performance improvement. The scientist followed a distinct method in measuring the wall temperature of the

microchannel. They managed to have local temperatures of the wall which is used to calculate local Nusselt number.
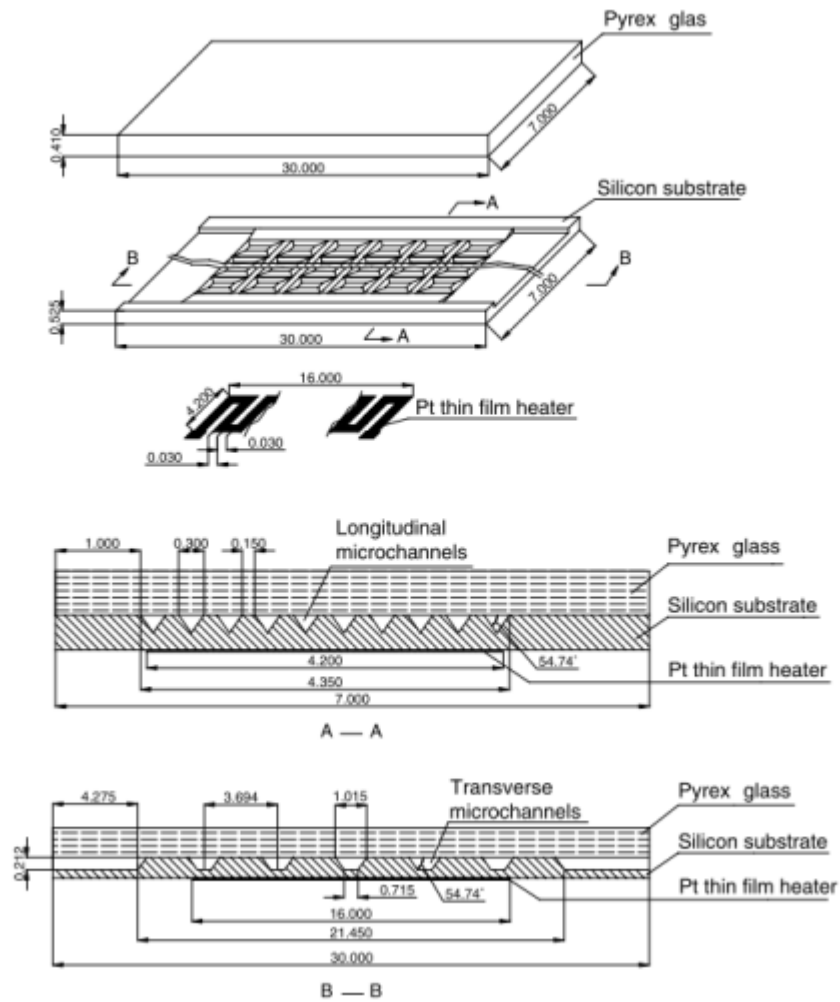
Figure 2.11: Heat sink with crosswise microchannels
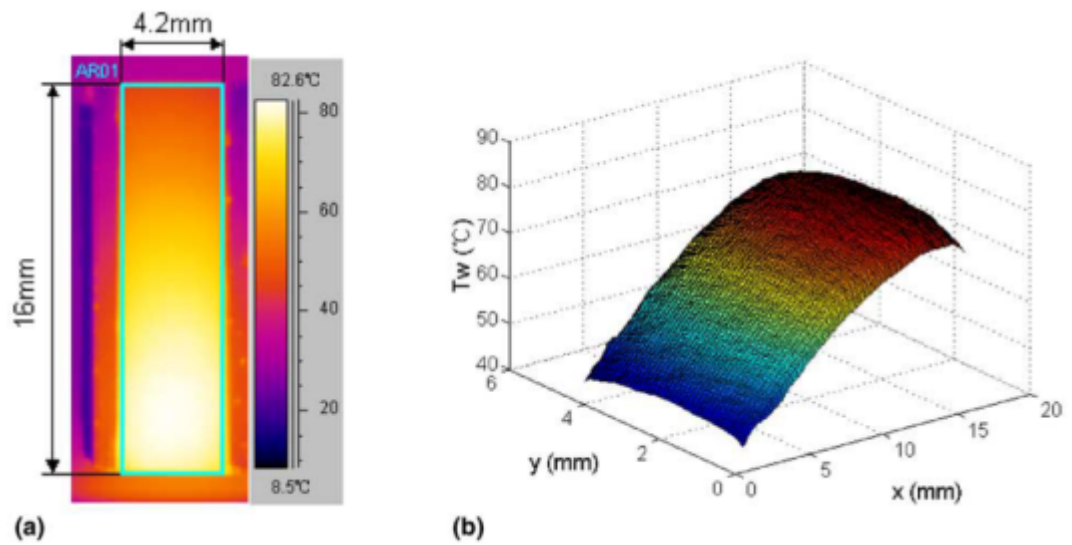
Figure 2.12: (a) High resolution thermal image of the thin film heater; (b) temperature distribution of the thin film heater

One another improvement technique based on geometry variation was applied by scientists from Georgia Institute of Technology [46]. The scientist confirmed that sinusoidal wavy channels were able to provide 26% improvement in heat transfer performance for low Reynolds number (<20) laminar flows while sustaining pressure drop in tolerable limits over straight channels. The schematic of wavy channels are given in Figure 2.13.
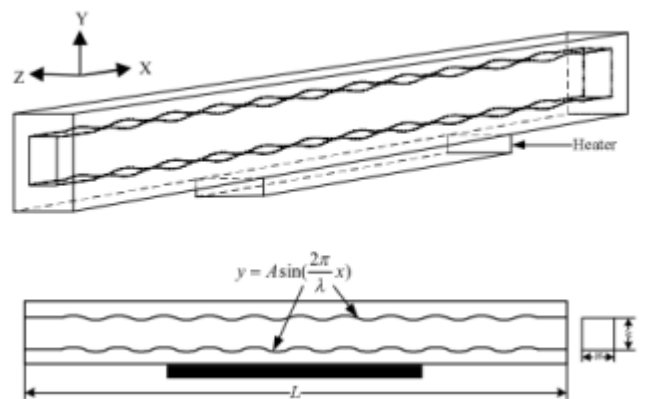
Figure 2.13: Wavy channel with square cross section

30

Some scientists also tried to improve the heat transfer performances of microchannel heat sinks via applying nanofluid into channels. An experimental example for this approach was conducted by Ho et al. in 2010 [47]. The scientist used copper rectangular microchannels having dimensions of 283μm width and 800μm with Al_2O_3 as a nanofluid. According to test results, for the largest flow rate they observed 70% improvement in the average heat transfer coefficients of nanofluid cooled microchannels when compared with the water cooled counterpart. In spite of this remarkable enhancement in heat transfer performance, scientists observed slightly increased in friction factor.

Number of researchers investigated the saturated flow boiling in microchannels due to capability of high-flux heat removal in microelectronic device applications. A recent comprehensive review which compares the predictions from 25 heat transfer correlations with 1847 measurements from 10 independent sources put forward that nucleate boiling seems to dominate the heat transfer process in microchannels and state that predictions had only achieved a partial success. According to study predictions from 12 out of the 25 correlations presented errors higher than 100% when compared with the experimental data base [48].

CHAPTER 3

FLOW AND HEAT TRANSFER ANALYSIS IN MICROCHANNELS

In this chapter analytical calculations and correlations suggested in the literature for fluid flow and heat transfer analyses of microchannels are presented.

3.1 Classification of Channels

The definition of "microchannel" is still a debatable issue for the researchers in the field. Mehendale et al. classified channels as follows, based on manufacturing techniques and smallest channel dimension C_D [49]

1 μm < C_D < 100 μm	: Microchannels
100 μm < C_D < 1 mm	: Minichannels
1 mm < C_D < 6 mm	: Compact passages
5 mm < C_D	: Conventional passages

Kandlikar and Grande classified channels based on the rarefaction effect of gasses as seen below [50]

1 μm < C_D < 10 μm	: Transitional Microchannels
10 μm < C_D < 200 μm	: Microchannels
200 μm < C_D < 3 mm	: Minichannels
3 mm < C_D	: Conventional passages

Another simpler classification was suggested by Obot, based on hydraulic diameter, according to which channels having hydraulic diameter under 1 mm are said to be

microchannels [51]. According to this classification the channels used in the current study can be treated as microchannels.

3.2 Flow in Closed Conduits

It is considered appropriate to remind the basic geometrical parameters for rectangular conduits which are aspect ratio, α, and hydraulic diameter, D_h. Aspect ratio is defined as the ratio of short side of a rectangular channel to long one (1).

$$\alpha = \frac{a}{b} \tag{1}$$

Hydraulic diameter is defined for rectangular channels as follows

$$D_h = \frac{4A_{ch}}{P_w} \tag{2}$$

where $A_{ch} = ab$ is the channel cross-sectional area and $P_w = 2(a+b)$ is the wetted perimeter. As mentioned in the previous chapter, recent review studies showed that conventional correlations are applicable to analyze the flow and heat transfer in microchannels. Kandlikar et al. stated that incompressible flow in a smooth circular pipe forms the basis for pressure drop analysis in internal flows and derived the following equations for Newtonian liquid flows in minichannels and microchannels based on continuum assumption [52]. For the equilibrium of a fluid element of length dx in a conduit of hydraulic diameter D_h, frictional force due to shear stress at the wall balances the force due to infinitesimal pressure difference, dp, as given below

$$\left(\frac{\pi D_h^2}{4} \right) d_p = \left(\pi D_h d_x \right) \tau_w \tag{3}$$

which yields the following correlation between the pressure gradient and the wall shear stress

$$\frac{d_p}{d_x} = \frac{4\tau_w}{D_h} \qquad (4)$$

It is known that for Newtonian fluids, the wall shear stress is related to velocity gradient at the wall as follows

$$\tau_w = \mu \frac{d_u}{d_y}\bigg|_w \qquad (5)$$

where μ stands for the dynamic viscosity. Defining the Fanning friction factor as follows

$$f = \frac{\tau_w}{(1/2)\rho u_m^2} \qquad (6)$$

where u_m stands for the mean flow velocity in the channel, equations (5-7) can be combined to get the following pressure drop for a channel of length L_{ch}

$$\Delta p = \frac{2f\rho u_m^2 L_{ch}}{D_h} \qquad (7)$$

According to Kandlikar et al. the Fanning friction factor is related to the flow conditions such as being laminar or turbulent or being developing or fully-developed, the channel wall geometry and surface conditions [52]. For fully developed laminar flow in a circular pipe the velocity profile gradient at the channel wall can be

calculated from Hagen-Poiseuille parabolic velocity profile and using this profile f can be represented as

$$f = \frac{Po}{\mathrm{Re}} \qquad (8)$$
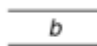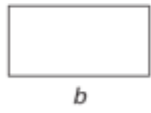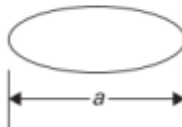
where Po and Re are Poiseuille and Reynolds numbers, respectively, defined as follows

$$\mathrm{Re} = \frac{\rho u_m D}{\mu} \qquad (9)$$

$$Po = f\,\mathrm{Re} \qquad (10)$$

For different channel cross-sections Poiseuille number varies as seen in the Table 3.1

Table 3.1: Fanning friction factor and Nusselt number for fully developed laminar flow in ducts with different cross-sections

Duct shape			Nu_H	Nu_T	$Po = f\,Re$
Circular			4.36	3.66	16
Flat channel			8.24	7.54	24
Rectangular, aspect ratio, $b/a =$		1	3.61	2.98	14.23
		2	4.13	3.39	15.55
		3	4.79	3.96	17.09
		4	5.33	4.44	18.23
		6	6.05	5.14	19.70
		8	6.49	5.60	20.58
		∞	8.24	7.54	24.00
Hexagon			4.00	3.34	15.05
Isosceles Triangle, Apex angle $\theta =$		10°	2.45	1.61	12.47
		30°	2.91	2.26	13.07
		60°	3.11	2.47	13.33
		90°	2.98	2.34	13.15
		120°	2.68	2.00	12.74
Ellipse, Major/Minor axis $a/b =$		1	4.36	3.66	16.00
		2	4.56	3.74	16.82
		4	4.88	3.79	18.24
		8	5.09	3.72	19.15
		16	5.18	3.65	19.54

$Nu = hD_h/k$; $Re = \rho u_m D_h/\mu$; Nu_H – Nu under a constant heat flux boundary condition, constant axial heat flux, and uniform circumferential temperature; Nu_T – Nu under a constant wall temperature boundary condition; f – friction factor.

Another Poiseuille number derivation is provided by Shah and London as follows where α is the aspect ratio [54]

$$Po = f\,Re = 24(1 - 1.3553\alpha + 1.9467\alpha^2 - 1.7012\alpha^3 + 0.9564\alpha^4 - 0.2537\alpha^5) \quad (11)$$

These correlations are valid for fully developed laminar flow. In most of the microchannel applications developing flow region, where the velocity profile has not yet reached the Hagen-Poiseuille velocity profile, forms the major portion of the flow [52]. Length of this hydrodynamic developing region L_h, is defined as:

$$\frac{L_h}{D_h} = 0.05\,\mathrm{Re}$$
(12)

The effect of developing flow region can be considered by defining an apparent friction factor, f_{app}. Pressure drop for developing flow in a channel over a length x from the entrance can now be expressed as

$$\Delta p = \frac{2 f_{app} \rho u_m^2 x}{D_h}$$
(13)

An incremental pressure defect $K(x)$ is defined as follows to express the difference between f_{app} and f

$$K(x) = (f_{app} - f)\frac{4x}{D_h}$$
(14)

For $x > L_h$ the incremental pressure defect reaches a constant value of $K(\infty)$ known as Hagenbach's factor. Steinke and Kandlikar obtained the following Hagenbach's factor expression for rectangular channels through a curve fit [24]

$$K(\infty) = 0.6796 + 1.2197\alpha_c + 3.3089\alpha_c^2 - 9.5921\alpha_c^3 + 8.9089\alpha_c^4 - 2.9959\alpha_c^5 \quad (15)$$

For fully developed and developing turbulent flow in smooth channels several friction factor correlations were suggested by numerous scientists. Phillips put

37

forward the following equation, which covers both the developing and fully developed regions [19]

$$f_{app} = A\,\mathrm{Re}^B \tag{16}$$

where;

$$
\begin{aligned}
A &= 0.09290 + \frac{1.01612}{x/D_h} \\
B &= -0.26800 - \frac{0.32930}{x/D_h}
\end{aligned}
\tag{17}
$$

Jones suggested the following equation for rectangular channels by replacing *Re* with a laminar-equivalent diameter D_{le} [55]

$$\mathrm{Re}^* = \frac{\rho u_m D_{le}}{\mu} = \frac{\rho u_m [(2/3)+(11/24)(1/\alpha_c)(2-1/\alpha_c)]D_h}{\mu} \tag{18}$$

3.3 Total Pressure Drop in a Microchannel Heat Exchanger

Equations given in the previous section consider the pressure drop due to wall friction. However as seen in Figure 3.1, practically the pressure drop across the inlet and outlet plenum of a microchannel, which includes the combined effect of losses in bends, entrance and exit losses, developing region effects and the core frictional losses is of interest
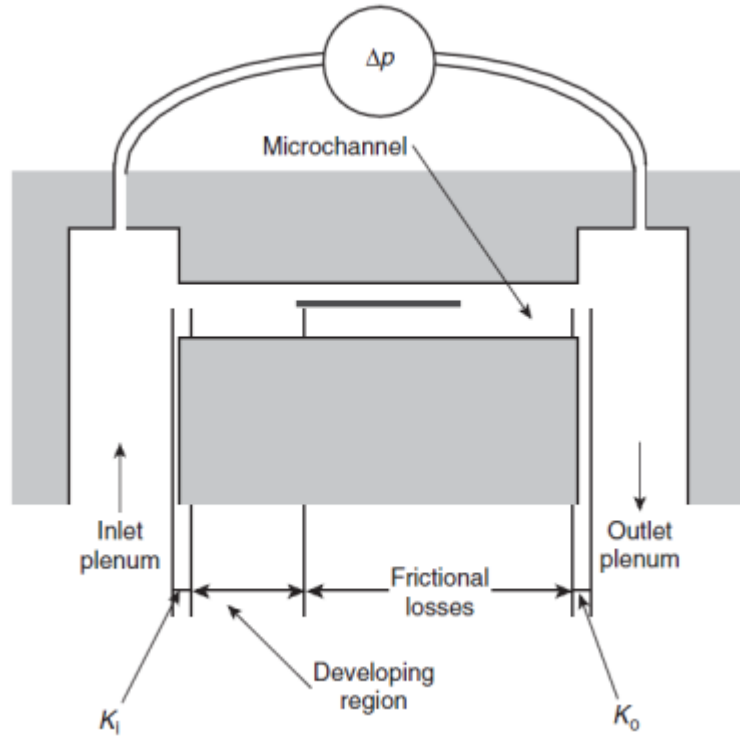
Figure 3.1: Schematic representation of the effects on pressure drop along the microchannel inlet and outlet plenum.

The total pressure drop including all these effects is formulated by Philips as follows [19]

$$\Delta p = \frac{\rho u_m^2}{2}[(A_c / A_p)^2 (2K_{90}) + (K_c + K_e) + \frac{4 f_{app} L}{D_h}] \qquad (19)$$

where A_c and A_p are the total channel area and the total plenum area, respectively. K_{90} stands for the loss coefficient at the 90° bends, K_c and K_e are the contraction and expansion loss coefficients due to the area changes and f_{app} stands for the apparent friction factor. Philips suggested using a bend loss coefficient value of 1.2. Kays and London worked on contraction and exit losses and presented tables for circular and parallel channels as seen in Figure 3.2 [56]:
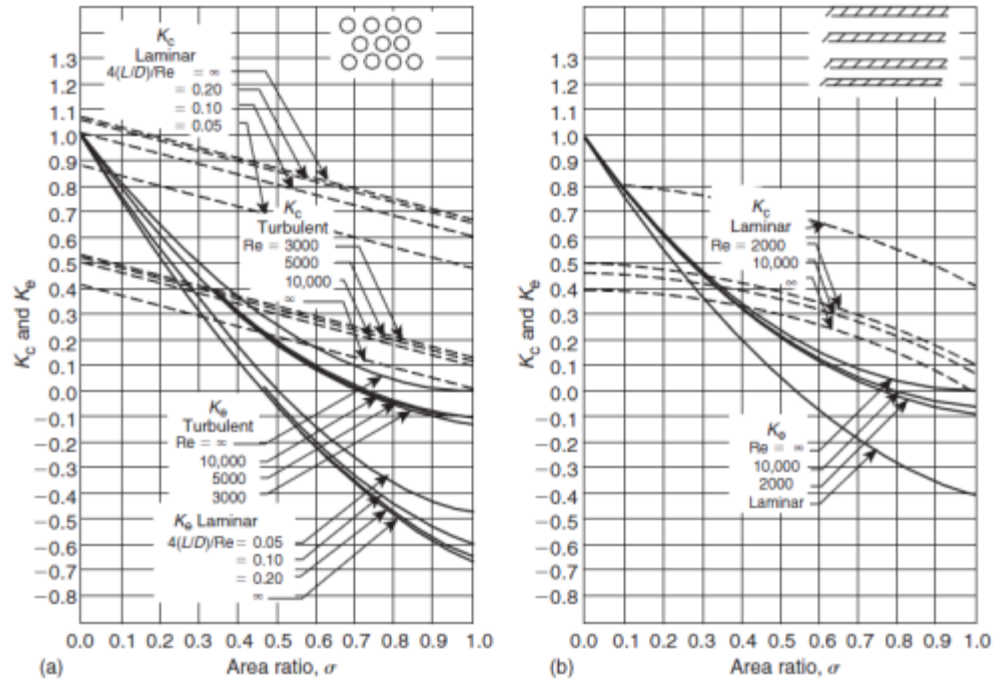
Figure 3.2: Expansion and contraction loss coefficients between inlet and outlet plenum for microchannel flows

Equation (19) can be rewritten in terms of fully developed friction factor, f including the pressure drop defect $K(x)$ seen as follows

$$\Delta p = \frac{\rho u_m^2}{2}[(A_c / A_p)^2 (2K_{90}) + (K_c + K_e) + \frac{4fL}{D_h} + K(x)]$$ (20)

3.4 Heat Transfer in Microchannels

According to Newton's law of cooling, the convective heat transfer to/from the channels to the fluid is given by:

$$q = h_{ave}(A_{ht})(T_s - T_m) \tag{21}$$

where q stands for the heat transfer rate, A_{ht} is the total heat transfer area, h_{ave} is the average convective heat transfer coefficient and T_s and T_m are the inner channel wall surface temperature and fluid mean temperature, respectively. Using a log mean temperature difference as seen below is more suitable for the cases where the surface temperature is not constant

$$\Delta T_{LMTD} = \frac{(T_s - T_i) - (T_s - T_o)}{\ln\dfrac{T_s - T_i}{T_s - T_o}} \tag{22}$$

where T_i and T_o are the fluid inlet and outlet temperatures, respectively. The heat transfer from the channel surface to the inner fluid can be expressed in terms of heat flux as follows

$$q'' = \frac{q}{A_{ht}} = h_{ave}(T_s - T_m) = h_{ave}\Delta T_{LMTD} \tag{23}$$

where h_{ave} is the average heat transfer coefficient. The total heat transfer rate can also be stated as the energy gain between the inlet and outlet of the channel as follows

$$q = \dot{m}c_p(T_o - T_i) \tag{24}$$

Where $\dot{m}$ stands for the mass flow rate and c_p stands for the specific heat under constant pressure. The measure of convection heat transfer occurring at the surface for a prescribed geometry is characterized by the following Nusselt number

$$Nu = \frac{hD_h}{k} \qquad (25)$$

where h stands for the local convective heat transfer coefficient and k stands for the thermal conductivity of the fluid.

3.5 Thermal Performance Measures of Liquid Cooled Heat Sinks

In the previous sections it was underlined that Nusselt number and friction factor are two of the main performance criteria for thermal and hydraulic characteristics, respectively. Besides these parameters, the thermal resistance of a heat sink given below is also accepted as a representative of thermal performance, especially for electronics cooling applications

$$R_{HS} = \frac{T_b - T_i}{q} = \frac{\theta_b}{q} \qquad (26)$$

where T_b is the heat sink base temperature, T_i is the coolant fluid inlet temperature and q is the heat power dissipated at the heat sink base. In electronics cooling applications it is important to hold the heat sink base temperature below certain limits; due to the temperature endurance of the heat dissipating element. Thermal resistance not only symbolizes the importance of low heat sink base temperature, but also relates the thermal performance to geometric features of the channel and the coolant flow rate. The temperature difference between the coolant inlet and base depends on the convective heat transfer coefficient, which is determined by the Nusselt number; function of aspect ratio and/or Reynolds number, hence the channel geometry and coolant flow rate. It is well known that pressure drop and the friction factor is also a function of Reynolds number, and it can be concluded that coolant flow rate has a noticeable impact on both pumping power required to drive the flow and cooling performance of the heat sink. Alpsan drew attention to the challenge for finding a compromise between the cooling performance and pumping power in electronics cooling applications [58]. He stated that the maximum allowable thermal

resistance for a heat sink to satisfy adequate cooling is determined as a first step and suitable design could then be selected from a set of flow rate / channel geometry pairs that provide the necessary thermal resistance.

3.6 Heat Transfer from Extended Surfaces

Incrope and DeWitt related the dissipated heat load from a heat sink to its coolant via the temperature rise between the heat sink base and coolant; θ_b; with the concept of fin efficiency [57]. The fin efficiency given below is the ratio of the actual heat transferred from the fin to coolant, q_f, to the amount of heat that would be transferred from all the surfaces of the fin if they were at the base temperature

$$\eta_f = \frac{q_f}{q_{max}} = \frac{q_f}{hA_f\theta_b} \tag{27}$$

where h is the convection heat transfer coefficient and A_f is the surface area of the fin. The fin efficiency for rectangular fins with adiabatic fin tip condition is found as [57]

$$\eta_f = \frac{\tanh(mL_c)}{mL_c} \tag{28}$$

where L_c stands for corrected fin length used to take the fin tip into account. For a fin with a thickness of t_f and length L L_c is defined as

$$L_c = L + \frac{t_f}{2} \tag{29}$$

In equation (28) m is defined as

$$m = \sqrt{\frac{hP_w}{kA_c}} \qquad (30)$$

where h is the convective heat transfer coefficient, k is the thermal conductivity of the fin material, P_w is the fin perimeter and A_c is the cross-sectional area o the fin.

In cases, like microchannels where there is an array of fins, overall surface efficiency, η_o given below can be defined

$$\eta_o = \frac{q_t}{q_{max}} = \frac{q_t}{hA_t\theta_b} \qquad (31)$$

where q_t is the actual heat transferred from the heat sink to the coolant at a total surface area of A_t that is exposed to the coolant. In this relation A_t includes the total finned surface area and it is related to the prime (unfinned) surface area, A_b as follows

$$A_t = NA_f + A_b \qquad (32)$$

where N stands for the number of fins in the array and A_f stands for the surface area of each fin. The total heat transfer rate from total exposed area can be expressed as

$$q_t = h[N\eta_f A_f + (A_t - NA_f)]\theta_b = hA_t[1 - \frac{NA_f(1-\eta_f)}{A_t}]\theta_b \qquad (33)$$

In the above equation convective heat transfer coefficient, h, is considered to be the same for prime and fin area [57]. The overall surface efficiency can now be written as

$$\eta_o = 1 - \frac{NA_f(1-\eta_f)}{A_t} = \frac{q_t}{hA_t\theta_b} \tag{34}$$

The temperature difference between the heat sink base and coolant inlet can be rewritten from Equation 34 as

$$\theta_b = \frac{q_t}{hA_t\eta_o} \tag{35}$$

As mentioned in the previous section, the thermal resistance is the ratio of the temperature rise to the applied heat power. Thermal resistance for a fin array can be written as

$$R_{t,o} = \frac{\theta_b}{q_t} = \frac{1}{hA_t\eta_o} \tag{36}$$

Another thermal resistance relation is proposed by Garimella in the microchannel heat exchangers tutorial of Itherm 2010 [65]. According to his suggestion thermal resistance includes three components which are namely conduction, convective and calorical thermal resistances

$$R_{overall} = R_{cond} + R_{conv} + R_{cal} \tag{37}$$

Conduction thermal resistance is calculated by Fourier's law as

$$q_{cond} = \frac{k_s \times A_s}{t_b}(T_w - T_b) \tag{38}$$

$$R_{cond} = \frac{(T_w - T_b)}{q_{cond}} = \frac{t_b}{k_s \times A_s} \tag{39}$$

45

where t_b stands for the base thickness of the channel, k_s is the thermal conductance of the microchannel material and A_s is the base surface area of the channel.

$$q_{conv} = \bar{h} \times A_f \times (\bar{T_b} - \bar{T_f}) \qquad (40)$$

$$R_{conv} = \frac{(\bar{T_b} - \bar{T_f})}{q_{conv}} = \frac{1}{\bar{h} \times A_f} \qquad (41)$$

where $\bar{T_f}$ stands for the average fluid temperature and A_f is the fin area of the microchannel.

$$q_{cal} = \rho \times Q \times c_p \times (T_{fo} - T_{fi}) \qquad (42)$$

$$R_{cal} = \frac{(T_{fo} - T_{fi})}{q_{cal}} = \frac{1}{\rho \times Q \times c_p} = \frac{1}{\rho \times u_m \times n \times H \times w_c \times c_p} \qquad (43)$$

where T_{fo} and T_{fi} stand for the fluid outlet temperature and inlet temperature, respectively. Q is the volumetric flow rate, c_p is the specific heat of the fluid under constant pressure, u_m is the fluid velocity, n is the number of channels, H is the channel depth, w_c is the width of the channel and ρ is the density of the fluid. According to Garimella's point of view conceptual optimization for channel width is possible with respect to convective and calorical thermal resistances as seen in the following figure
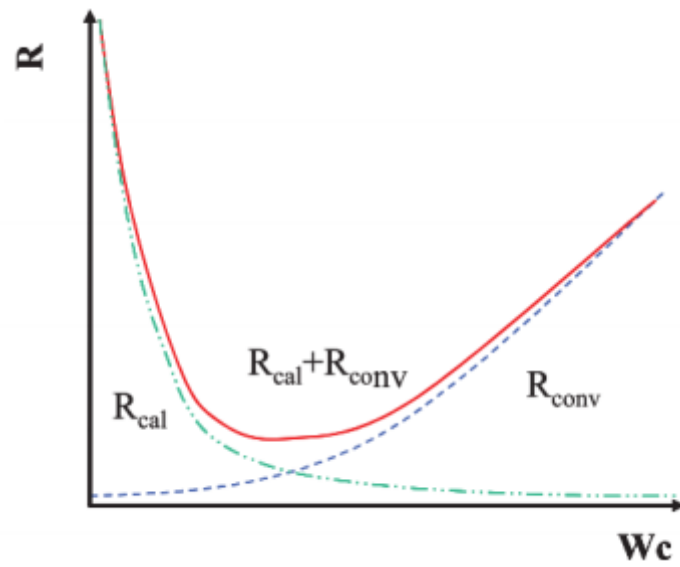
Figure 3.3: Conceptual optimization for uninterrupted microchannels.

3.7 Interrupted Fins

Phillips argued that thermal performance is higher for channels where the flow has not been fully developed at the exit [19]. To amplify the performance, two ways had been attempted; increasing the hydraulic diameter by increasing the channel width and reducing the fin length. The second way was called as interrupted fin and includes two main geometries namely in-line and staggered as shown in Figure 3.4.
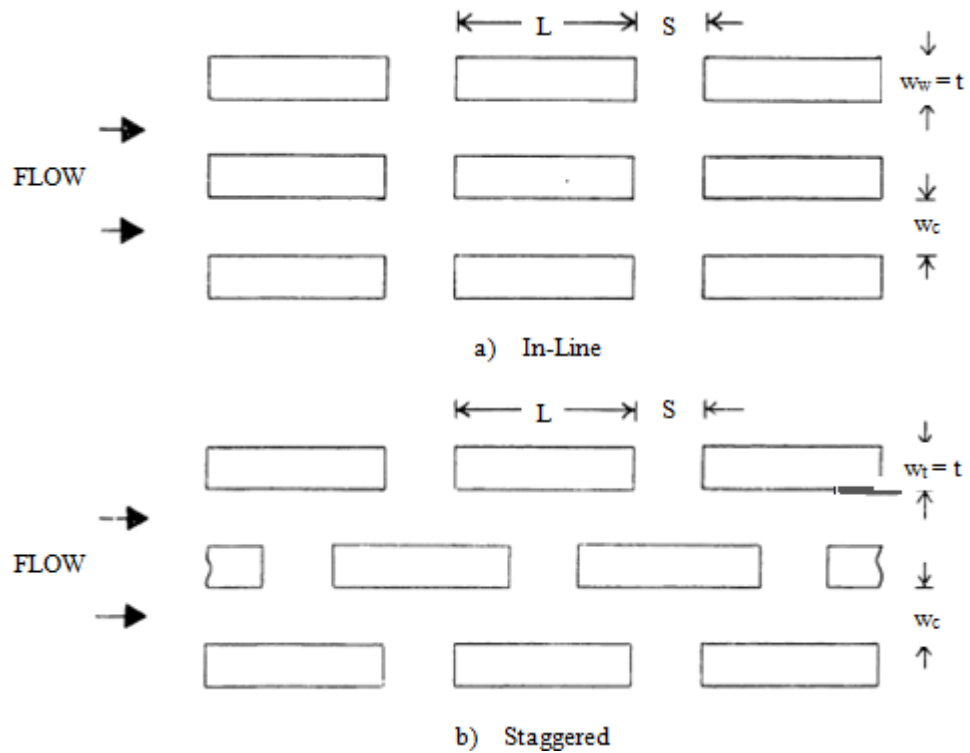
Figure 3.4: In-line and staggered fin microchannels

The superior properties of the interrupted-fin microchannels over uninterrupted ones can be listed as follows

- The interrupted fins could enhance the overall heat transfer coefficient up to 50-100 % owing to flow separation, secondary flow and periodic starting of the boundary layer on fins [19].
- Moreover; interrupted flows achieve transverse coolant mixing that spread the high coolant temperatures from the hot points [19].
- Interrupted fin channels are less vulnerable to catastrophic thermal failures occurred by channel blockage as a result of this they are less susceptible to inconveniences trigged by manufacturing tolerance errors [19].

Philips emphasized that the performance of interrupted fins are better than the uninterrupted ones only if they are designed correctly. He also stated that due to the lack of general correlations for interrupted fins, requires the investigation of each individual microchannel experimentally [19]. He also provided the main design criteria to minimize recirculation as follows

- If the S and w_c are designed larger, the fin behaves as a bluff body in a uniform velocity, uniform temperature flow field
- If the Reynolds number is high, this bluff body creates recirculation zones owing to the flow separation in the leading edge as seen in the following figure:
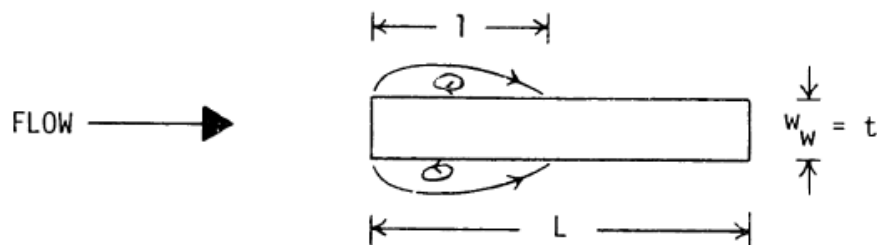
Figure 3.5: Recirculation zones in interrupted fin channels

- These recirculation zones yield to insulation effect in laminar flows. For turbulent flows this insulation effect is less due to periodic shedding and mass transform across the recirculation boundary.
- Increasing Re_t, which is the Reynolds number based on interrupted fin thickness, enlarges the recirculation to a maximum value of $l=1.65t$ at

49

$Re_t=325$ where l is the stream wise length of the recirculation and t is the interrupted fin thickness

- At higher Re_t, the recirculation is found to be unsteady, resulted in a decrease in l due to enlarged momentum transfer.
- For $Re_t>500$, l is almost constant and equals to 4 times of the interrupted thickness for both laminar and turbulent flows.

Lane and Loehrke discovered the following features of the interrupted channels [62]

- For laminar flow over long plates ($8<L/w_w<16$) recirculation zone first appears when $Re_t =100$ [62].
- For short plates of water pass ($8<L/w_w<16$), length of stream wise recirculation converges to plate length, L for $Re_t>200$.
- There was not any flow separation for small plate interruption ($S<4w_w$) and concluded recirculation zones occurred due to flow separation will not be occurred for such designs.

Cur and Sparrow [63] worked on co planar plates including pair of interrupted fins in order to analyze the phenomena inside the interrupted fins
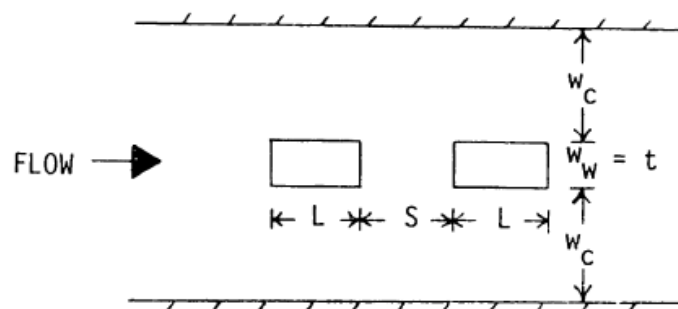
Figure 3.6: Schematics of collinear planes

Their experimental results are shown in the following figure
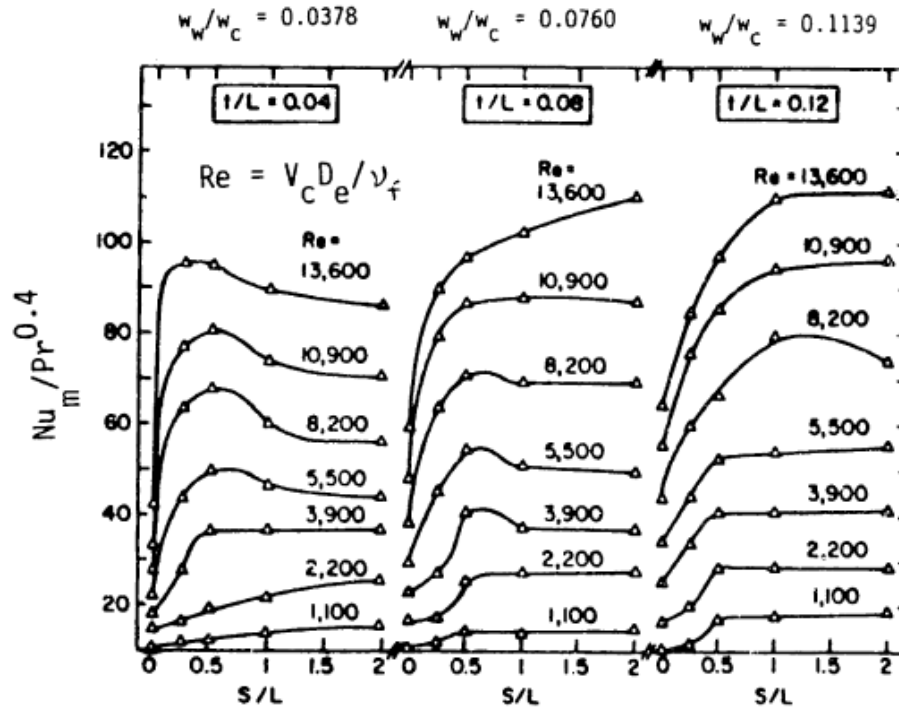
Figure 3.7: Nusselt number variation with inter-plate spacing

Potential acoustic noise problem was investigated by Johnson and Loehrke [64] and settle that in order to avoid from noise problem S should not be equal to $4nw_w$ where n is a term of a series of integer starting from 2 and increasing by 1. In other words should not be equal to $8w_w$, $12w_w$…

Phillips summed up the discussions clarified in this section for interrupted microchannels [19]

- S/L=0.5 seems have best thermal performance according to Figure 3.7

- To have enhanced mixing it is suggested to have $2<S/w_w<4$; noticing that $S/w_w = 2$ applies for large Re_t ($\sim 10^4$), $S/w_w = 4$ applies for small Re_t (~ 200). And considering that $S/w_w = 8$ is the first significant acoustic peak and $S/w_w = 4$ also includes a small acoustic peak.

- From the first two constraints it follows that $4<L/w_w<8$.

- In order to minimize the pressure drop the ratio of fin thickness to channel width should be minimized; for the best optimization w_w/ w_c should be kept below 0.1.

- In order to ensure turbulent flow or at least in order to satisfy highly mixed laminar flow Re should be above 1000-2000.

- In line or staggered arrays could be applied but in-line microchannels are quite simpler to manufacture.

- Re_t must be small (<100) or $L>>4t$ for large Re_t (>500); or else the recirculation zones will expand over a significant segment of the fin length and blockages the heat transfer in that region.

CHAPTER 4

EXPERIMENTAL SET-UP AND PROCEDURE

4.1 Overview of Microchannels

For this study 12 microchannels having 3 different configurations with a single channel depth of 4 mm and four different widths of 0.3, 0.5, 0.6 and 0.9 µm were produced. The three configurations seen in Figure 4.1 are called uninterrupted, single interrupted and the multi-interrupted. Technical drawings of these channels are given in Appendix A.
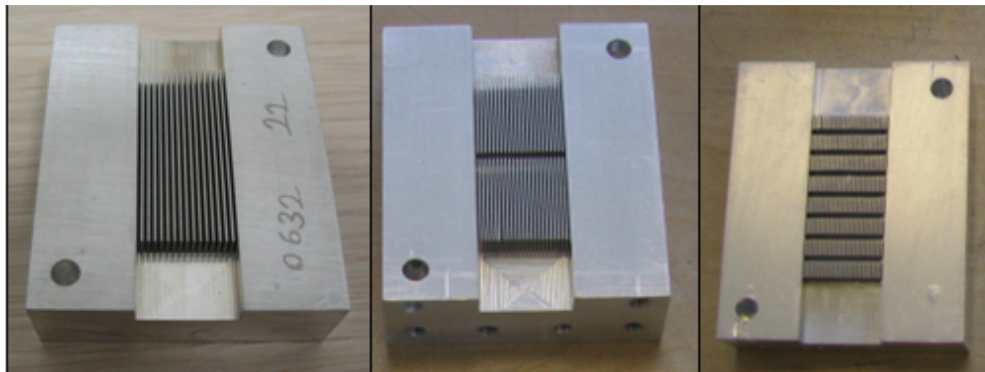
Figure 4.1: Sample photographs of uninterrupted, single interrupted and multi interrupted microchannels

The parameters defining configurations are presented in the following figure:
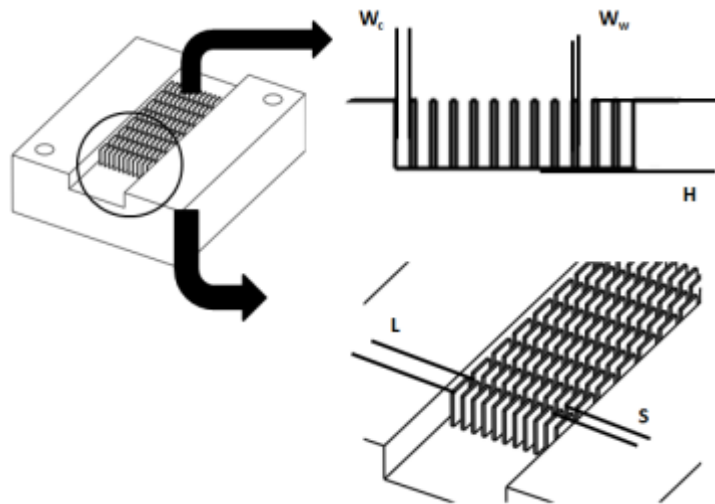
Figure 4.2: Definition of geometric parameters for interrupted channels

Dimensions of channels and the parameters affecting the flow characteristics are summarized in the following table:

Table 4.1: Design parameters of microchannels

Channel	Material	Channel Width (μm)	Secondary Channel Displacement (mm)	Channel Height (mm)	Aspect Ratio	Hydraulic Diameter (μm)	# of Channels
1	Aluminum	300	0	4	0.075	558	24
2	Aluminum	300	15.5	4	0.075	558	24
3	Aluminum	300	3	4	0.075	558	24
4	Aluminum	500	0	4	0.125	889	18
5	Aluminum	500	15.5	4	0.125	889	18
6	Aluminum	500	3	4	0.125	889	18
7	Aluminum	600	0	4	0.15	1043	16
8	Aluminum	600	15.5	4	0.15	1043	16
9	Aluminum	600	3	4	0.15	1043	16
10	Aluminum	900	0	4	0.225	1469	12
11	Aluminum	900	15.5	4	0.225	1469	12
12	Aluminum	900	3	4	0.225	1469	12

4.2 Geometrical Details of Uninterrupted and Interrupted Microchannels

Geometrical details of uninterrupted, single- and multi-interrupted channels can be seen in Figure 4.3, Figure 4.4, and Figure 4.5.
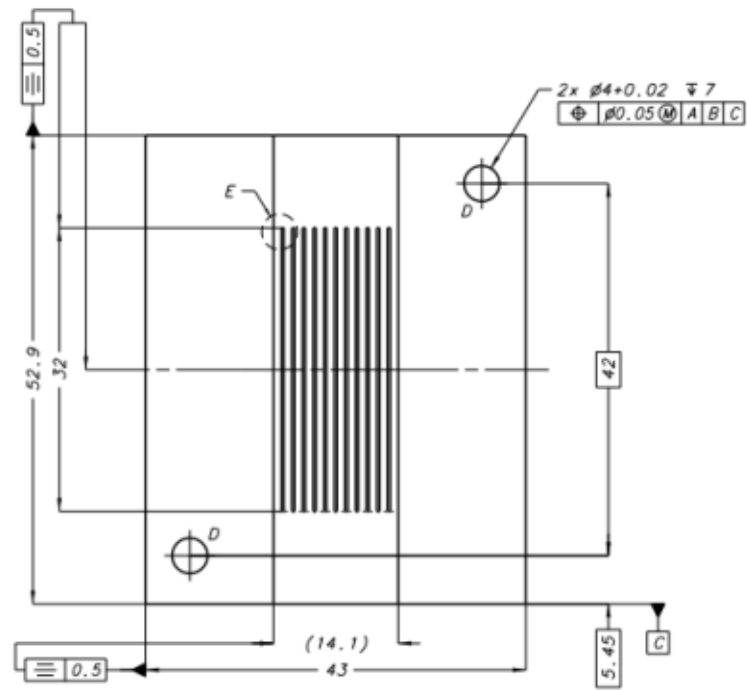
Figure 4.3: Technical drawings of 900 micron wide uninterrupted channel
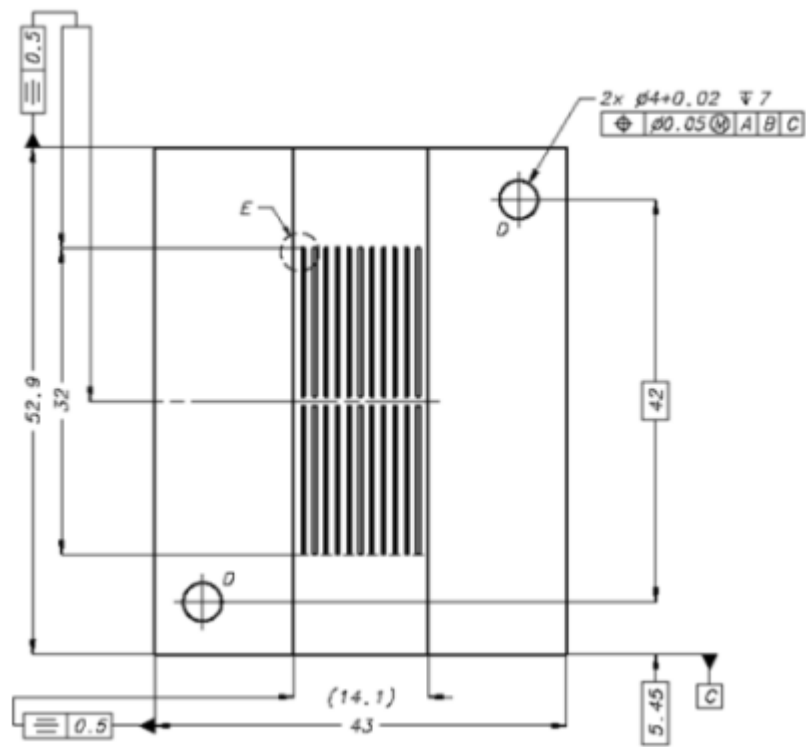
Figure 4.4: Technical drawings of 900 micron single interrupted channel

56
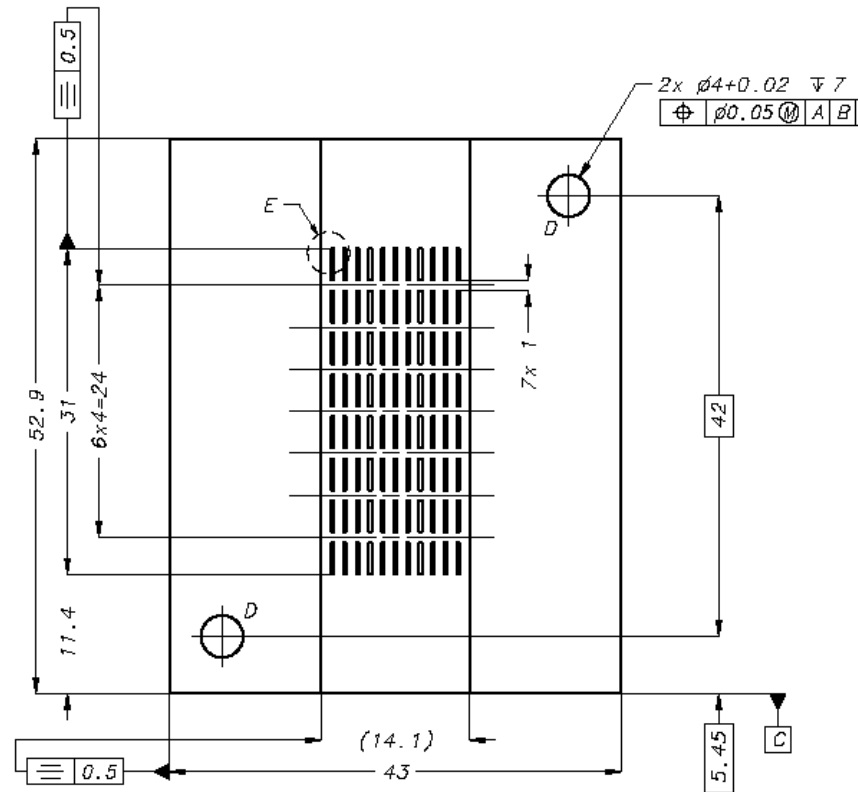
Figure 4.5: Technical drawings of 900 micron wide multi interrupted channel

According to criteria summed up by Phillips [19] mentioned in the previous chapter;

- For both single- and multi-interrupted channels separation distance is 1 mm. Therefore for single- and multi-interrupted channels, S/L ratio is 1/15.5 = 0.06 and 1/3=0.33, respectively. The value for multi-interrupted ones is closer to 0.5.

- Separation distance to channel thickness is the same for the both single- and multi-interrupted channels as $S/w_w=1/0.3=3.33$, satisfies the limit for enhance mixing. ($2<S/w_w<4$)

- In order to avoid from acoustic noise it is suggested to have S/w_w value lower than 8, where the first acoustic peak of the channels occurs. This condition is satisfied by having $S/w_w=3.33$

- Fin length to channel thickness (L/w_w) is 15.5/0.3=51.6 and 3/0.3=10 for single- and multi-interrupted channels, respectively. For both of the interrupted channels ratio of fin thickness to channel width (w_w/w_c) is the same and equal to 0.3/0.3=1, 0.3/0.5=0.6, 0.3/0.6=0.5, and 0.3/0.9=0.33 for 4 different channel widths.

4.3 Manufacturing of the Microchannel Heat Sinks

All channels are made up of caps and base subparts which are electro discharge machined (EDM) in Ankara and brazed in Aselsan facilities. Since brazing operation causes bending in small-volume parts and parts get beyond the manufacturing tolerances pre-brazed parts were produced in large volumes which were further machined to form the microchannels. An example for pre-brazed parts is given in Figure 4.6; and an example for brazed channel is given in Figure 4.7. The ultrasonic view of channels after brazing is presented in Figure 4.8.
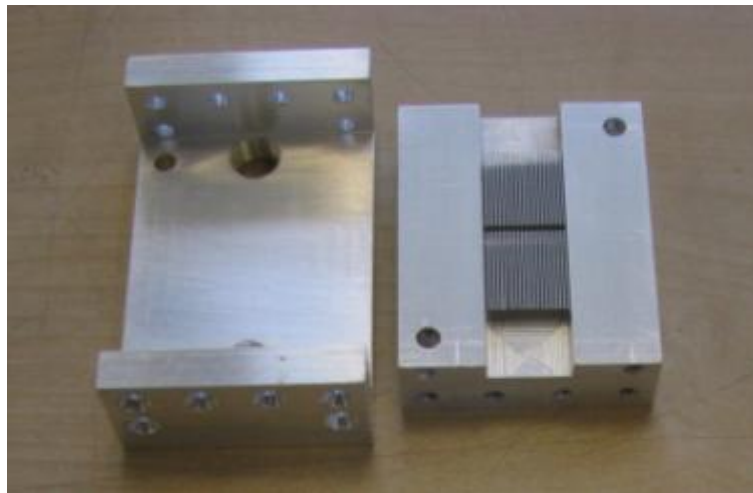
Figure 4.6: Photograph of pre-brazed parts

Figure 4.7: Photograph of a brazed channel before finishing
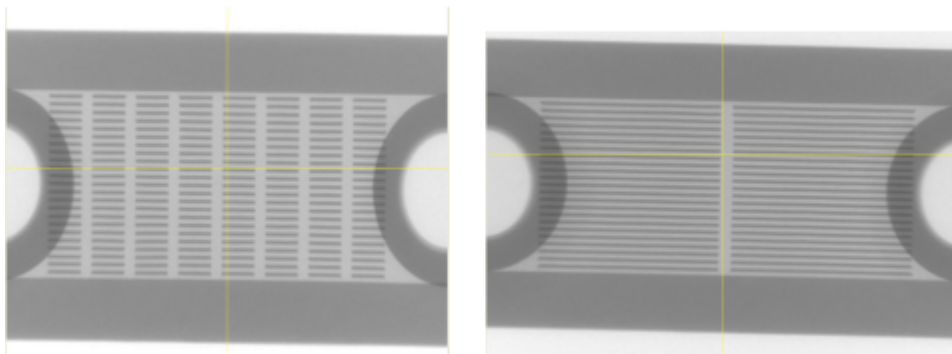
Figure 4.8: Ultrasonic view of interrupted channels after brazing

4.4 The Experimental Setup

The setup is composed of pressure, temperature and volumetric flow rate sensors; heat source, pump, micro filter, expansion tank, hose, couplings and data logging system. The schematic representation of the setup is given in Figure 4.9, and a photograph of the system is given in Figure 4.10. The properties of the setup components are given in Table 4.2, Table 4.3, and Table 4.4.
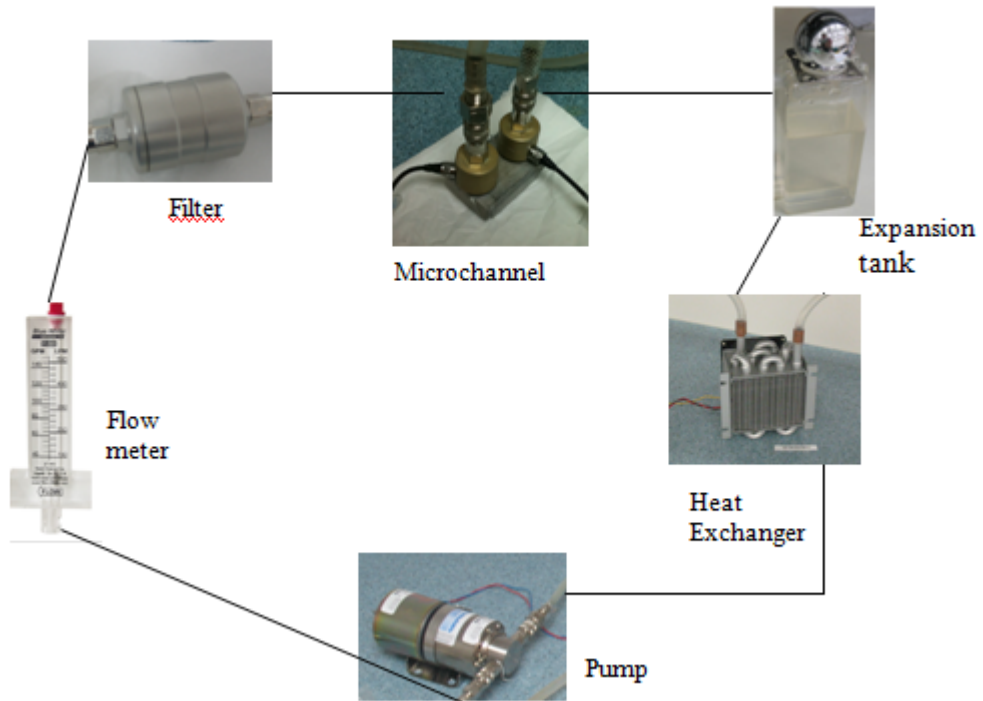
Figure 4.9: Schematic representation of the experimental setup

Figure 4.10: Photograph of the experimental setup

Table 4.2: Components of the experimental setup

Component	Brand	Function & Properties
Power supply 1	Agilent/ E3634A	Supply power for heating up to 25V/7A or to 50V/4A accuracy: 0.05%+10mV 0.2%+10mA
Power supply 2	Agilent/ E3634A	Supply power for the pump
Power supply 3	Agilent/ E3620A	Supply power for the pressure sensors up to 25V/1A accuracy: 0.5%V 0.5%A
Power supply 4	Agilent/ E3620A	Supply power for heat exchanger
Heater	Laird/6529	thermoelectric foiler; simulates heat load max. operating temperature: 175°C max power can be elevates if the hot surface cools below this limit.
Pressure Sensor	Kulite/HKL/T-1-235	combined pressure and RTD temperature sensor measures pressure up to 1,7Bar; rated electrical excitation: 10VDC combined non-linearity, hysteresis and repeatibility ±0,1% FSO (typ.), ±0,5% FSO (max.) full scale output (FSO): 100mV(Nom.) operating temperature range:-55°C to 175°C

Table 4.3: Components of the experimental setup (continue)

Component	Brand	Function & Properties
Data Logger	Agilent /34970A	60 channel data logger with multiplexers that measure temperature, voltage, current, frequency with minimum sampling interval of 40×10^{-3} seconds. Maximum number of reading that can be stored is 65000.
Flow Meter	Cole Parmer	Measures the volumetric flow rate of the fluid at interval between 0.2 lpm to 3lpm with an accuracy of 0.05lpm.
Heat sink-Fan Assembly	Fan:Vantec/TD8038H Heat Exchanger: 72MSLS0A01	80 x 80 x 38 (mm) sized fan which can blow of air flow about 84.1 cfm with 5700 rpm is used to cooled down the cooling fluid. Used to cooled down cooling liquid with forced air with thermal capacity up to 40W/°C.
Pump	Micropump/200.350-000	Pump drives the fluid along the system having maximum differential pressure up to 7.5 bar and at 1400 rpm can provide 840ml/min.
Thermocouple	Omega/MO503	J type, self adhesive thermocouple measures the temperature of the surfaces from -60 °C up to 177°C.

Table 4.4: Components of the experimental setup (continue)

Component	Brand	Function & Properties
Expansion Tank	Aquarius / III	Reservoir with dimensions 40mm x55 mmx 100mm
Micro Filter	ECE /FLP 2421	10 micron filter used to eliminate the particles that can bung up the channels.
Thermal Interface Material	Thermagon T-flex 640	Fills the gaps occurred due to manufacturing tolerances between the heater and the channel.

Schematic representation and photographs of the heater and microchannel assembly are given in Figure 4.11 and Figure 4.12. The heat load is supplied by a thermoelectric foiler (Laird 6529). The foil is attached to the microchannel by pressing with a cap. Thermagon thermal interface material (TIM) is applied between the microchannel and the heater. An insulation material is applied between the heater and the pressing cap. Technical drawings of the assembly are given in Appendix A.
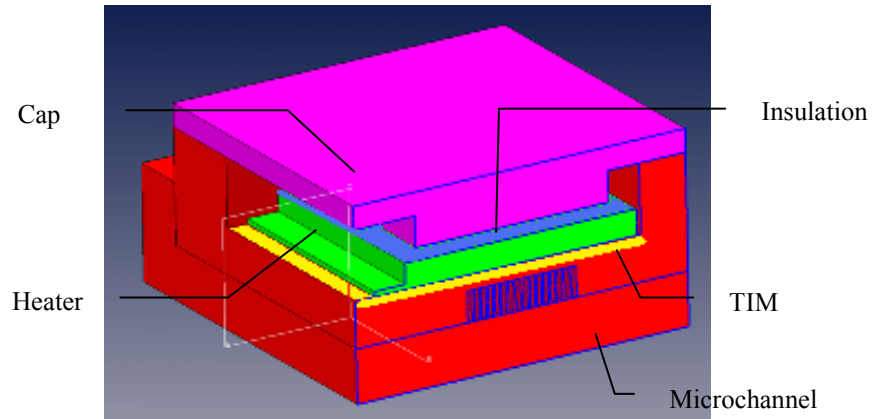
Figure 4.11: Schematic representation of the microchannel heater assembly
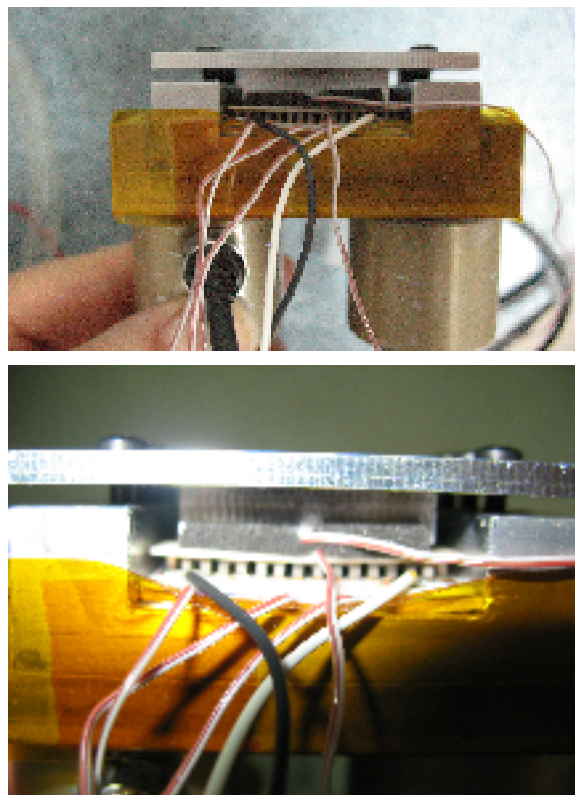
Figure 4.12: Photographs of the microchannel heater assembly

4.5 The Sensor Locations

Temperature data is taken from 8 points. Temperature is measured at the inlet and outlet of the microchannel, at three points on the base of the channel, at the cold and the hot surface of the heater and at the base of the pressing part (cap). Temperature difference between the inlet and the outlet of the channel is measured by 1000 ohm RTD placed in the pressure sensors as seen in Figure 4.13. Temperatures of these points are measured by J type thermocouples as seen in Figure 4.14.

Figure 4.13: Temperature and pressure sensors used to collect data at channel inlet and exit
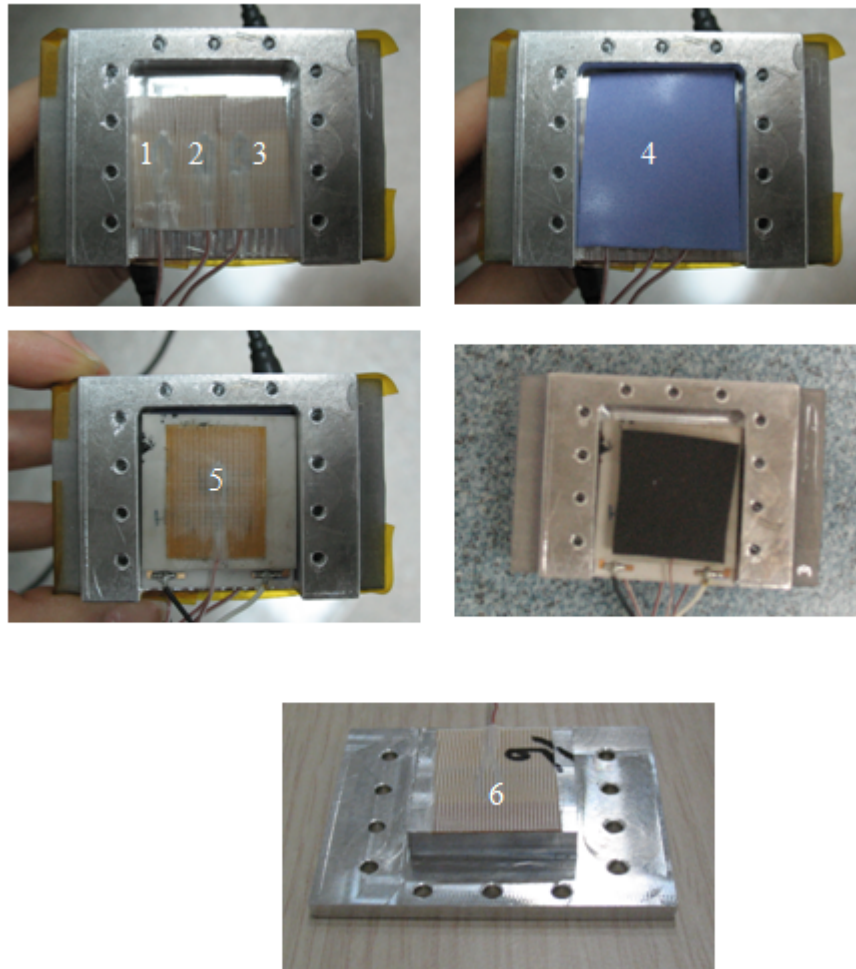
Figure 4.14: Locations of temperature sensors on microchannel and heater

4.6 Uncertainties in the Experimental Setup

Uncertainty can be calculated by evaluating the bias and the precision errors using following equation suggested by Kline and McClintock [66]

$$U = \sqrt{(\frac{\partial R}{\partial v_1}U_1)^2 + (\frac{\partial R}{\partial v_2}U_2)^2 + ...(\frac{\partial R}{\partial v_n}U_n)^2}$$

(44)

where U is the uncertainty in the result, U_n is the uncertainty in the independent variable n and R is a given function of the independent variables $v_1, v_2, v_3, \ldots, v_n$.

During the experiments temperature of the channel inlet and the outlet is measured within an accuracy of ±0.2°C. Pressure difference across the microchannel is measured within an accuracy of 0.1 % FSO (Full scale output) (±0.0025 bar). J type thermocouples used at 6 points provide an accuracy of ±1°C. Power supply provided the 40 W heat load with an accuracy of 0.05 % and 10 mV and 0.2 % and 10mA. Uncertainty of the voltage is calculated by the 0.05 percentage of the measured value and the additional offset of 10mV. Volumetric flow rates are measured with an accuracy of ±0.05 lpm.

CHAPTER 5

RESULTS

In this chapter measurements obtained by different devices and sensors and calculation and comparison of fluid flow and heat transfer related performance parameters are presented. Possible reasons for the particular trends are discussed.

5.1 Measurements

Experimental measurements for examining the pressure drop along the channel length were conducted on uninterrupted; single interrupted, and multi interrupted aluminum microchannel heat sinks of 300, 500, 600 and 900 micron channel widths with working fluids of distilled water with volumetric flow rates of 0.5, 0.7, 0.9, 1.0, and 1.1 lpm. The summarized results of pressure drop measurements are given in Table 5.1. In order to supply uniformly distributed heat load of 40 W without installing additional resistance between the heat load and the heat sink, the heat sink geometries were changed from previous studies carried by Alpsan [58] and Ateş [60]. For this reason microchannels used in these studies could not be used for thermal performance tests. This improvement could be applied to 500, 600 and 900 micron-wide single- and multi interrupted channels; and 600 micron-wide uninterrupted channel. The heat load of uniformly distributed 40 W was applied through these channels with volumetric flow rate of 0.2, 0.5, 0.7, and 1.0 lpm.

Table 5.1: Measured pressure drops for different heat sinks

Channel width (μm)	Channel configuration	Coolant Flow Rate (lpm) 0.5	0.7	0.9	1	1.1	1.2
300	Uninterrupted	949	1694	2416	2862	3057	3693
	Single-interrupted	1359	1992	2684	3254	3571	4100
	Multi-interrupted	1944	2655	3198	3681	4199	7121
500	Uninterrupted	0	323	568	633	926	1066
	Single-interrupted	789	1321	1765	2097	2838	3395
	Multi-interrupted	1648	1848	2248	2646	3326	5321
600	Uninterrupted	0	0	513	583	888	1089
	Single-interrupted	587	1068	1415	1637	1832	2014
	Multi-interrupted	1513	1694	1840	2097	2156	2356
900	Uninterrupted	0	263	487	569	714	853
	Single-interrupted	449	704	1022	1115	1315	1515
	Multi-interrupted	969	1064	1179	1354	1464	1798

Temperature values at eight locations are measured for different flow rates under same heat load of 40 W and the obtained values are presented in the following tables:

Table 5.2: Temperature readings for channels at 0.2 lpm

	Location of sensors	Types of channels						
		500 micron single	600 micron single	900 micron single	600 micron multi	900 micron multi	500 micron multi	600 micron uninter.
1	inlet of microchannel	30.4	30.5	32.5	32.1	31.9	30.7	31.4
2	outlet of microchannel	33.3	33.5	35.5	35.0	34.7	33.6	34.2
3	base of the channel 1	64.5	66.7	69.1	67.8	64.1	61.9	67.7
4	base of the channel 2	59.6	56.5	58.8	56.3	54.4	52.6	54.9
5	base of the channel 3	63.5	58.7	65.3	67.2	62.2	60.1	66.2
6	cold surface of heater	57.2	49.7	48.5	45.6	46.7	55.9	59.6
7	bottom surface of the cap	49.8	41.3	44.7	42.1	42.3	47.3	49.1
8	heater hot surface	115.1	98.9	106.7	95.8	89.7	89.6	95.4

Table 5.3: Temperature readings for channels at 0.5 lpm

Location of sensors	Types of channels						
	500 micron single	600 micron single	900 micron single	600 micron multi	900 micron multi	500 micron multi	600 micron uninter.
1 inlet of microchannel	30.8	30.8	32.9	32.9	30.1	30.6	32.0
2 outlet of microchannel	31.9	32.0	34.0	34.1	31.2	31.8	33.1
3 base of the channel 1	65.0	66.1	67.3	69.2	55.8	59.8	68.9
4 base of the channel 2	60.0	54.9	57.0	56.1	48.1	50.5	56.1
5 base of the channel 3	64.6	57.0	63.1	68.2	54.8	57.6	66.8
6 cold surface of heater	62.4	50.6	45.9	45.9	36.5	52.2	66.8
7 bottom surface of the cap	51.0	40.9	42.6	42.4	34.5	44.4	52.4
8 heater hot surface	121.5	99.4	103.4	94.0	79.4	86.2	101.5

Table 5.4: Temperature readings for channels at 0.7 lpm

	Location of sensors	Types of channels						
		500 micron single	600 micron single	900 micron single	600 micron multi	900 micron multi	500 micron multi	600 micron uninter.
1	inlet of microchannel	31.2	32.7	33.0	33.7	32.8	33.4	31.9
2	outlet of microchannel	32.0	33.6	33.9	34.5	33.7	34.2	32.7
3	base of the channel 1	66.1	69.1	67.4	68.2	64.5	64.8	66.8
4	base of the channel 2	60.8	58.5	56.7	56.9	53.1	54.9	54.9
5	base of the channel 3	64.9	59.6	63.2	69.5	61.6	61.7	65.4
6	cold surface of heater	64.1	53.7	47.0	47.5	49.5	60.1	63.7
7	bottom surface of the cap	53.0	43.6	43.1	43.6	43.1	50.4	50.1
8	heater hot surface	121.8	98.0	105.3	95.8	88.2	99.5	99.4

Table 5.5: Temperature readings for channels at 1 lpm

	Location of sensors	Types of channels						
		500 micron single	600 micron single	900 micron single	600 micron multi	900 micron multi	500 micron multi	600 micron uninter.
1	inlet of microchannel	31.4	33.0	33.8	34.3	33.0	33.7	31.9
2	outlet of microchannel	32.0	33.6	34.4	34.8	33.5	34.3	32.4
3	base of the channel 1	66.4	70.0	68.7	68.5	64.6	65.4	66.0
4	base of the channel 2	61.1	59.1	58.0	57.1	53.4	55.5	54.5
5	base of the channel 3	65.4	60.3	64.2	69.7	62.0	62.1	65.1
6	cold surface of heater	66.4	56.2	48.7	47.5	51.3	62.0	63.0
7	bottom surface of the cap	53.9	44.7	44.0	43.8	43.8	51.4	49.7
8	heater hot surface	124.1	100.2	105.8	96.0	89.7	102.5	99.6

5.2 Evaluation of Pressure Drop Results

Sample analytical pressure drop calculation for 500 micron channel is given in Appendix B. Measured and analytically calculated pressure drop values are presented in

Figure 5.1. As expected increasing flow rate results in an increase in the pressure drop and decreasing the channel width at a fixed flow rate results in more pressure drop. Analytical and measured pressure drop results show a good match only for 300 and 900 micron channels, but larger deviations are seen for 500 and 600 micron ones.

73
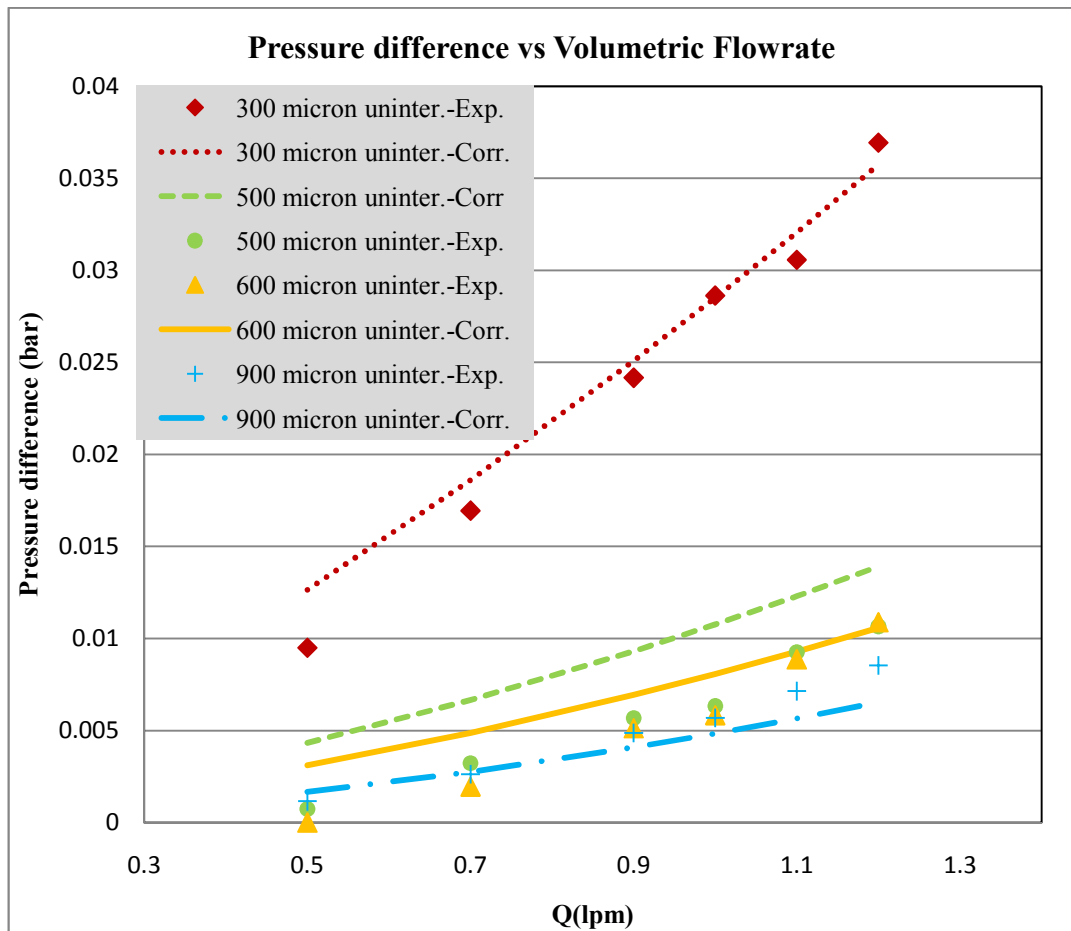
Figure 5.1: Variation of pressure drop with flow rate for uninterrupted channels

As mentioned by Bapat [59], there is not any analytical solution or experimental correlation for pressure drop along interrupted channels. However it is logical to compare the results with uninterrupted channels, as shown in Figure 5.2.
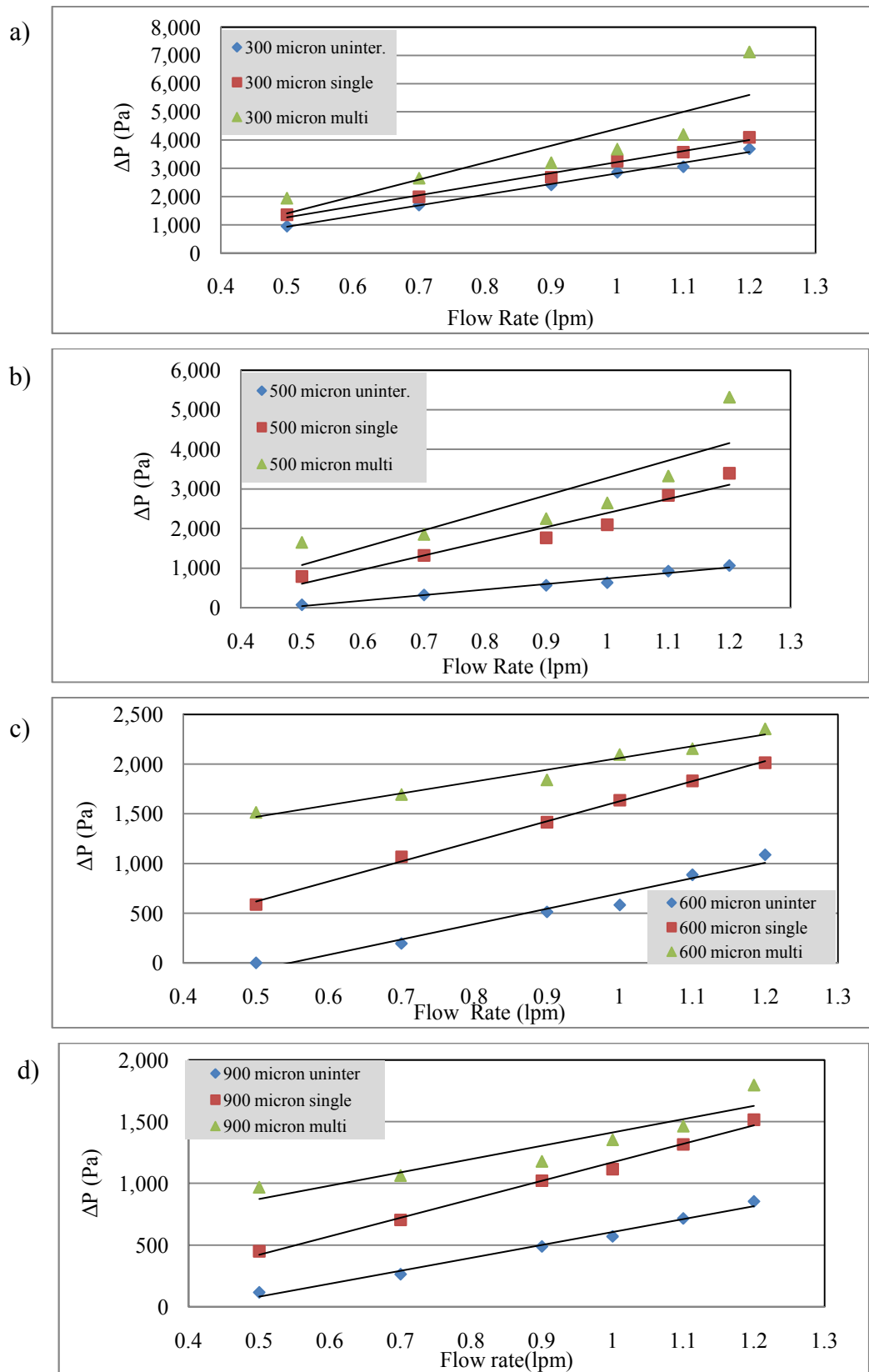
Figure 5.2: Pressure drop comparison for uninterrupted, single- and multi-interrupted channels (a) 300 micron, (b) 500 micron, (c) 600 micron and (d) 900 micron

5.3 Evaluation of Thermal Performance of Heat Sinks

During the tests, the power given to the system was adjusted so that the measured temperature difference between the inlet and the outlet of the microchannels result in a head load of 40 W. The heat loss to the surrounding was estimated using the temperature difference of bottom of the cap and the cold surface of the thermoelectric foil and checked with the difference of given power to the system and heat load of 40 W given to fluid. Heat transfer coefficients for all channels are found from Equation 40.

According to the current literature, it is possible to have higher thermal performance for carefully designed interrupted microchannels [19]. As presented in Figure 5.3, increasing trend in heat transfer coefficients and Nusselt numbers with increasing interruption grade is also observed in this study.
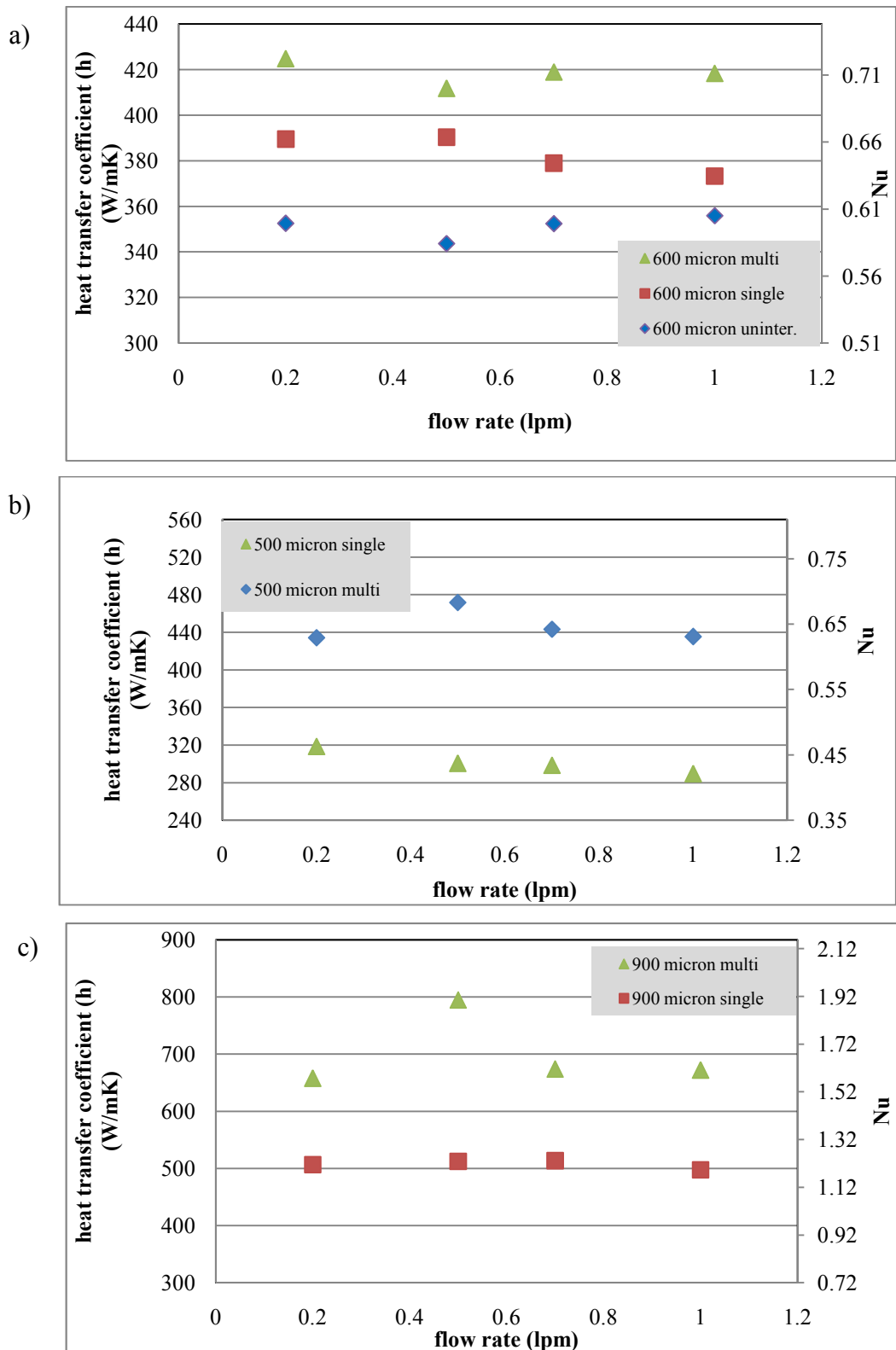
Figure 5.3: Heat transfer coefficients and Nusselt number for channels (a) 600 micron (b) 500 micron (c) 900 micron

Although in the literature it is said that interruption grade increases the thermal performance; the total fin area and the recirculation effects would degrade the thermal performance of the interrupted channels. For these reasons all channels tested in this study should be considered individually. Moreover; for a thermal designer, the main selection criterion is to have minimum reliable base temperature in order to run the electronic component for long periods; rather than having the maximum allowable heat transfer coefficients for the heat sink. Since liquid cooling technologies require secondary cooling cycles to cool down the cooling liquids; in order to minimize the volume occupied by secondary cycle; having minimum temperature difference between the inlet and the outlet of the heat sink is also a required design parameter. In addition to this parameter; availability of applying inlet cooling temperature as high as possible would also diminish the secondary cycle cooling capacity, thus its volume. These design parameters are summarized in Equation 41, by convective thermal resistance. The convective resistances of the 600 micron wide channels are given in the following figure
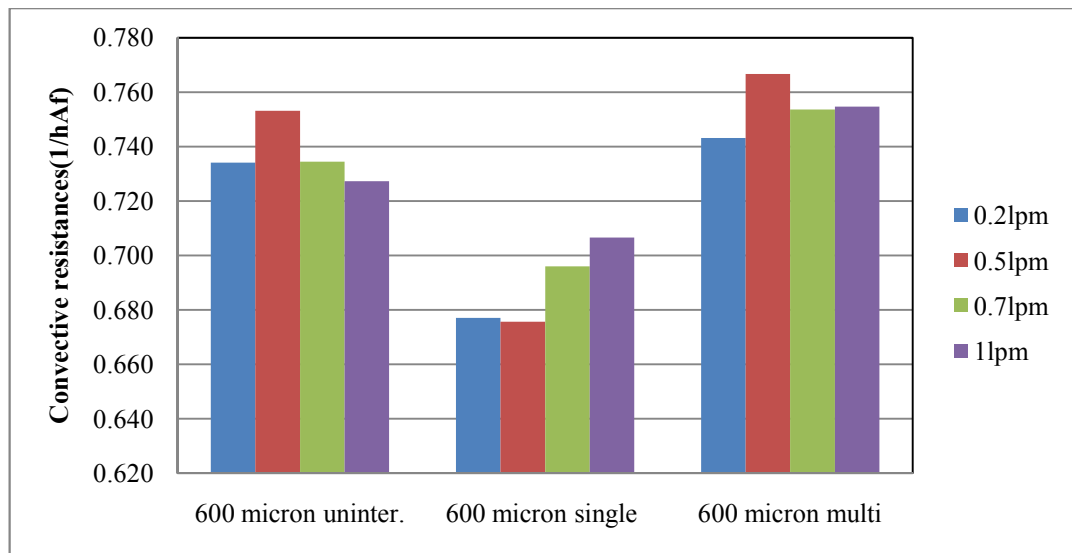
Figure 5.4: Convective resistance of uninterrupted, single-interrupted and multi-interrupted channels of 600 micron width

According to this figure, 600 micron wide single interrupted channel has the minimum convective resistance, even if; it does not have the maximum heat transfer coefficient as seen in Figure 5.3. The total fin area values have an effect in the sequence of convective resistance of the heat sinks. Unexpectedly, the minimum total fin area is obtained for the multi-interrupted channel as seen in Figure 5.5.
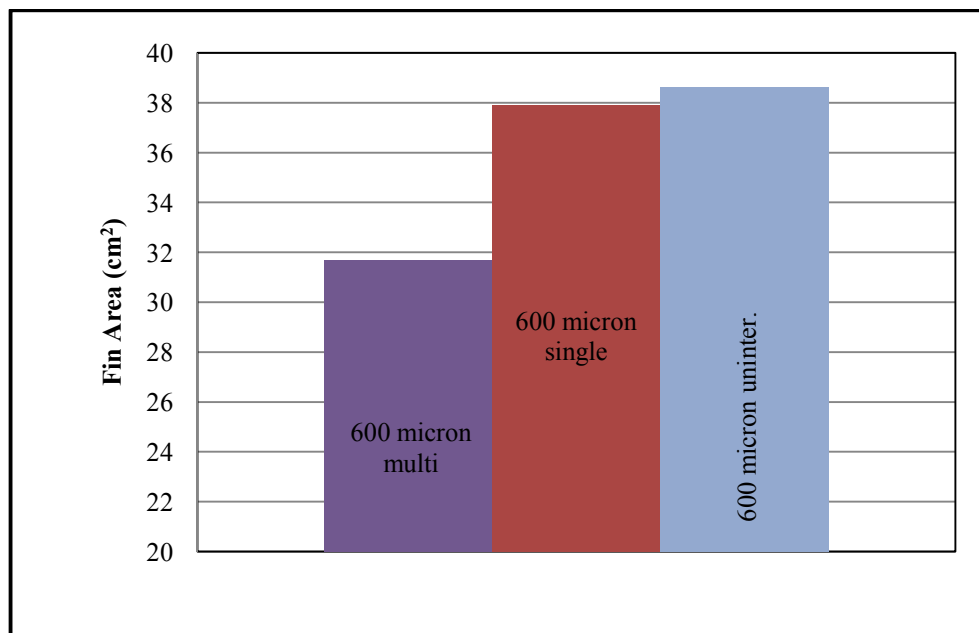
Figure 5.5: Fin areas of 600 micron wide microchannels

It is observed that increasing fin area decreased the product of heat transfer coefficient with temperature difference between the wall and the film as consistent with Equation 40. This trend is represented in the following figure
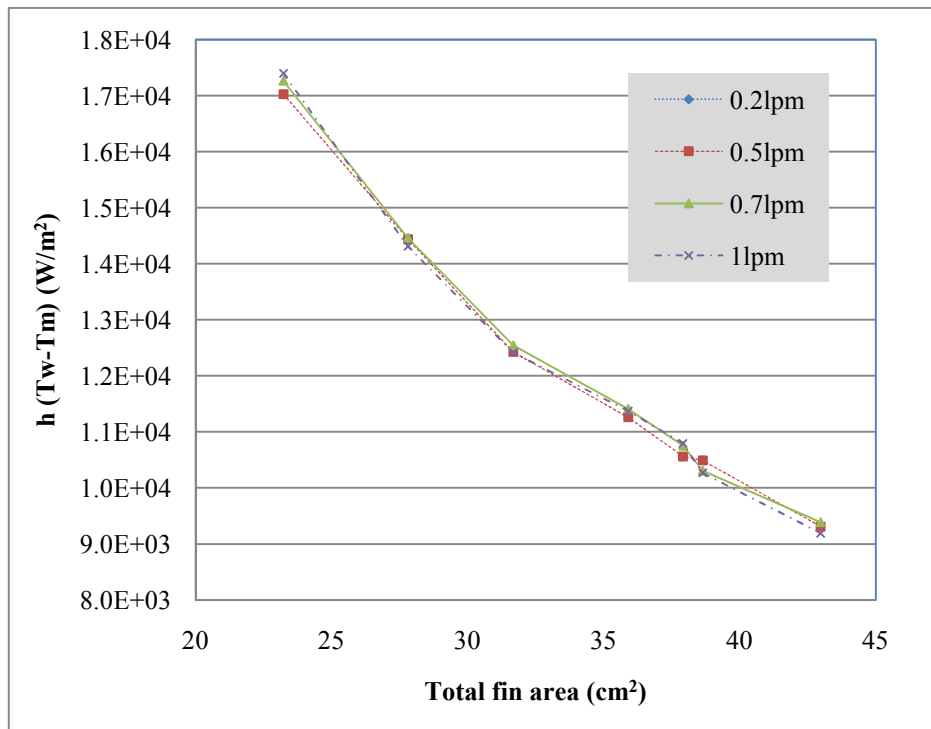
Figure 5.6: Heat transfer coefficients of channels with respect to fin areas

According to same equation it is expected to have a decreasing trend for temperature difference between the wall and the film as increasing fin area. However; increasing fin area resulted in wavy trend as seen in Figure 5.7.
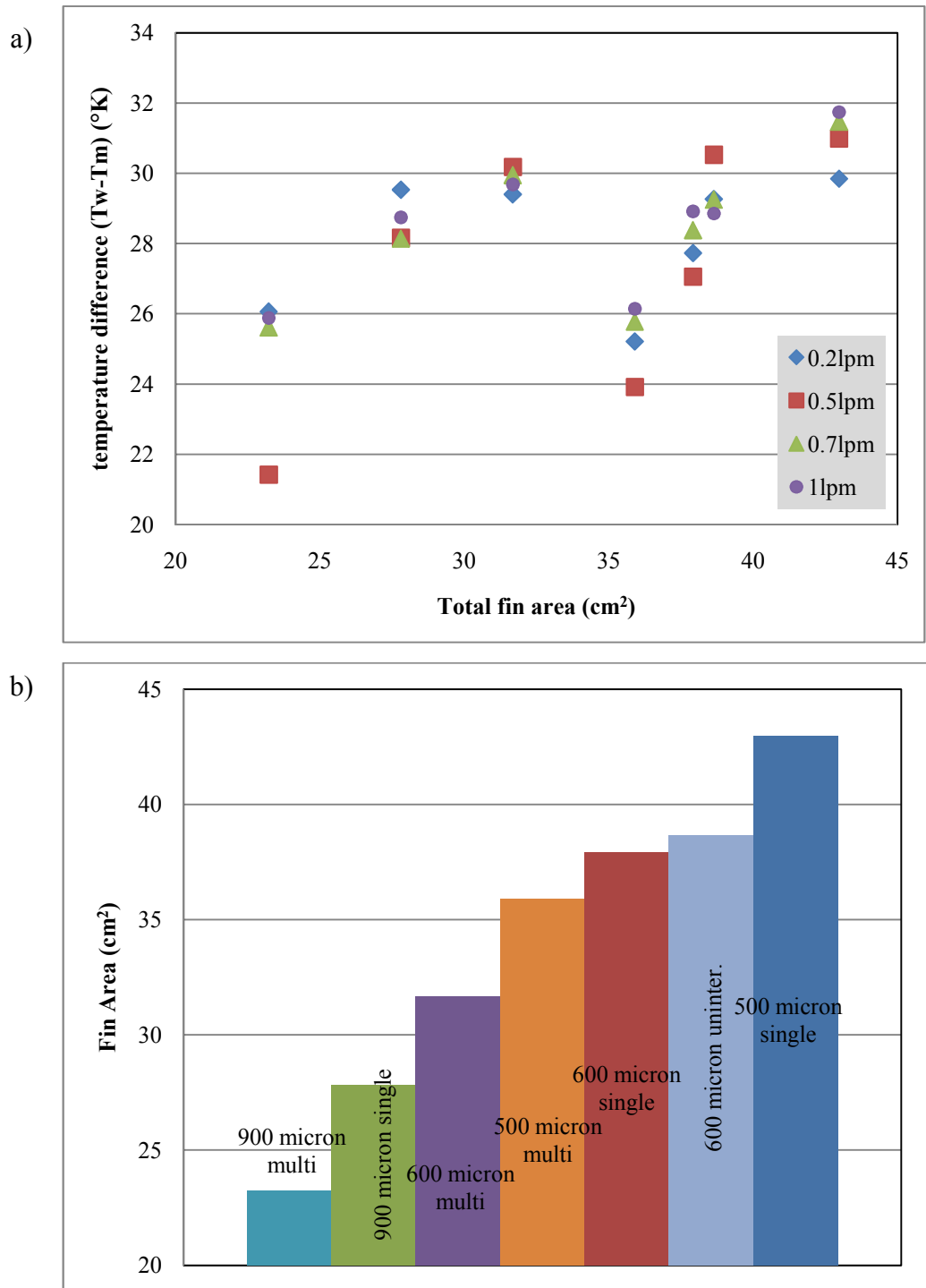
Figure 5.7: (a) Change of temperature difference between the wall and the film with fin areas of channels (b) channels with areas

This wavy trend in Figure 5.7 reveals that fin thermal performance is affected not only by the fin total area but also other dominant factors such as complex phenomena of enhanced mixing and channel width variation. Minimum thermal resistance is observed in multi-interrupted microchannel of 900 micron width. This result validates the suggestion of increasing channel hydraulic diameter and increasing interruption grade to avoid fully developed flow conditions and enhance thermal performance [19]. The entire results for convective resistance and channels are given at the following figure:
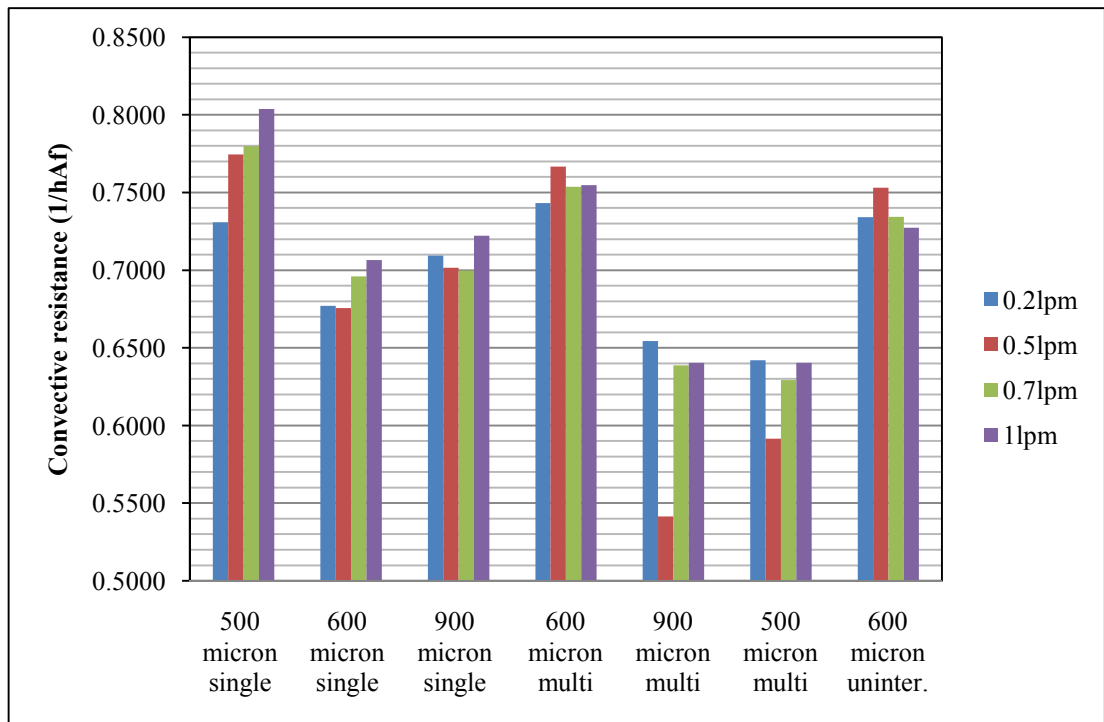
Figure 5.8: Convective resistances of channels

CHAPTER 6

CONCLUSION

6.1 Summary and Conclusion

During this thesis study 72 pressure and 28 thermal tests were conducted for 12 channels. Pressure drop increased for all channels with increasing flow rate and interruption grade. Owing to these reasons, the pressure drop across the 300 micron wide multi-interrupted channel at the maximum experimented flow rate was observed to be 3400 Pa higher than that observed for 300 micron wide uninterrupted channel.

The channels were produced under the limitations of the capabilities of OSTIM industrial zone. The minimum channel widths and maximum channel depth was limited by the EDM facilities. Secondary channels were produced under the limitation of possible minimum drill diameter. Under these restrictions, microchannel fin area could not be improved with interruptions. This situation caused evaluation of thermal resistance with respect to interruption grade impractical. However; under this limitation, improvement in Nusselt number was observed with increase in the interruption grade. In channels having a width of 600 microns, single interrupted serves a 13% increase in Nusselt number over an uninterrupted one and in the case of multi interrupted this improvement reaches 20%. For the same channel width, although the minimum area is calculated in multi interrupted channel, it has the highest heat transfer coefficient among the channels with this channel width.   In channels having a width of 900 microns, Nusselt number improvement of multi interrupted one over single interrupted was found as 55% and for channels having

width of 500 micron this value reached 56%. These improvements occurred under a negligible pressure drop, which would not require a pump replacement.

It was also observed that increasing the hydraulic diameter also increased the thermal performance. Even though the minimum fin area was calculated in the 900 micron multi interrupted channel, this fin served the best performance among all channels. Test results presented the expected trends with increasing the interruption grade and hydraulic diameter. Regrettably; having incomparable fin areas for different channel geometries made impossible to sequence and evaluate the convective resistances. In order to compare this parameter, fin areas had to be designed as equal.

Since there were limited number of heat simulators and thermoelectric foils, higher fluxes could not be investigated. However, higher heat loads should be applied in order to see the maximum available performance of channels under limited inlet temperature and limited base temperature situations.

6.2 Future Work

During the tests it has been observed that various improvements could be applied to the test system and the microchannel geometry. For the test system; the head load, flow rate, flow sensors, fluid type, the pump, and related power source could be improved and optimized. The simulated heat load could be increased to obtain high temperature differences between the inlet and the outlet of the fluid. High temperature difference facilitates a comparison of the microchannels' thermal performances. From a similar point of view, high pressure differences, achieved via high flow rates would make the comparison of the friction factors of heat sinks possible. Moreover; in order to see the extended trend for pressure drop with respect to Reynolds number higher flow rates should be applied. This development requires having a more powerful pump and a higher output power source. However; it should be noted that in the case of microchannel cooling, there will be a limit on the pump size, thus maximum allowable volumetric flow rate would also be limited. Testing

channels with commercial heat transfer liquids and nanofluids may help clarify the characteristics of the heat sinks. One other improvement could be on measurement tools, for example installing more sensitive pressure, volumetric flow rate and temperature sensors would yield more reliable and accurate results. Using a reservoir rather than an expansion tank would also lead to a controlled inlet temperature. Moreover, installing a temperature controller to the outlet of the heat exchanger would also satisfy this condition.

For the geometry of the heat sinks; interrupting channels with minimum possible drills would lead a logical consideration in thermal resistance. Different angles for the secondary channels rather than 90˚ could be applied to improve mixing of the fluid and the heat transfer performance. The arrow-shape secondary channels and diverging hydraulic diameters, through giving slopes to the base, may also improve the distribution of the heat load.

REFERENCES

1.   S.S. Anandan et al. Thermal Management of Electronics: A Review of Literature, Thermal Science: Vol. 12 (2008), No. 2, pp. 5-26

2.   W. A. Scott, Cooling of Electronic Equipment, John Wiley and Sons-Interscience, New York, USA, 1974

3.   C. Lasance, Technical Data column, ElectronicsCooling, January 1997.

4.   L.A. Florio, A. Harnoy, Combination Technique for Improving Natural Convection Cooling in Electronics, Int. Journal of Thermal Sciences, 46 (2007), 11,pp. 76-92

5.   Thermal and Mechanical Design Guide of Intel® Core™ i7-900 Desktop Processor Extreme Edition Series and Intel® Core™ i7-900 Desktop Processor Series and LGA1366 Socket

6.   S. M. Wait, S. Basak, S.V. Garimella, and A. Raman, Piezoelectric Fans Using Higher Flexural Modes for Electronics Cooling Applications, IEEE Transactions on components and packaging technologies, vol 30, No.1, March 2007

7.   D. Wolf, F. P. Incropera, R. Viskanta, Jet Impingement Boiling, Advances in Heat Transfer, 23(1993), pp.1-132

8.   H.C. Wang, A.V. Mamishev, Optimal Heat Transfer Performance of the Microfluidic Electrospray Cooling Devices, in 27th Annual IEEE Semiconductor Thermal Measurement and Management Symposium (SEMI-THERM 2011), 2011, pp. 35-42

9.   J. Toth, R. DeHoff, K. Grubb, Heat Pipes: The Silent Way to Manage Desktop Thermal Problems, presented at I-Therm 1998, Seattle

10.   H. Ryoson et al, Thermal Performance of Novel Thin Heat Pipe, IEEE, 987-1-4244-5343-6/10, 2010

11.   R. Palacios, J. Vazquez, M. A. Sanz-Bobi, Cooling Systems for Hermetic Devices Based on Thermoelectricity, 6th European Workshop on Thermoelectrics, Freiburg, Germany, Proceedings, 2001

12.   R.P. Feynman, "There's Plenty of Room at the Bottom", Miniaturization, H.D. Gilbert, ed., 282-296, Reinhold Publishing, New York, 1961.

13.   G. Moore, Cramming More Components Onto Integrated Circuits. *Electronics, 38,* 2., 1965

14.   D.B, Tuckerman, R.F.W. Pease, "High-Performance Heat Sinking for VLSI", IEEE Electron Device Letters, Vol. EDL-2, No.5, 1981

15.   H. Kristiansen, Thermal Managment in Electronics, Chalmers University ofTechnology,Göteborg,Sweden,2001,http://www.ppd.chalmers.se/edu/mpr235_thermgmnt.pdf

16.   M. Ohadi, and J. Qi, Thermal Management of Harsh Electronics, in 20th Annual IEEE Semiconductor Thermal Measurement and Management Symposium (SEMI-THERM 2004), 2004

17.   B. Xu, K.T. Ooi, N.T. Wong, W. K. Choi, Experimental Investigation of Flow Friction for Liquid Flow in Microchannels, Int. Comm. Heat and Mass Transfer, Vol.27, No.8, pp 1165- 1176, 2000

18.   P.Y. Wu and W.A. Little, Measurement of Friction Factor for the Flow of Gasses in Very Fine Channels Used for Micro Miniature Joule Thompson Refrigerators, Cyrogenics, vol. 23, pp. 273-277, 1983

19.   R.J. Phillips, Forced Convection, Liquid Cooled, Microchannel Heat Sinks, Msc Thesis, Mechanical Engineering Department, MIT, Massachusetts, 1987

20.   J. Pfahler, J. Harley, H. H. Bau and J. Zemel, Liquid Transport in Micron and Submicron Channels, J. Sensors and Actuators, A21-A23, pp.431-434 (1990). (Proceeding).

21.   J. Pfahler, J. Harley, H. H. Bau and J. Zemel, Micromechanical Sensors, Actuators, and Systems, ASME, DSC-Vol. 32, pp. 49-60 (1991) (Proceeding)

22.   X. F. Peng, G. P. Peterson and B. X. Wang. Frictional Flow Characteristics of Water Flowing through Microchannels, Exp. Heat Transfer, vol. 7, pp.249-264, 1994

23.   G. Hetstroni, A. Mosyak, E. Pogrebnyak, L. P. Yarin, Fluid Flow In Microchannels, Int. J. Heat and Mass Transfer, Vol.48, pp.1982-1998, 2005.

24.   M. E. Steinke and S. G. Kandlikar, Single Phase Liquid Friction Factors in Microchannels, International Journal of Thermal Sciences, vol. 45, pp.1073- 1083, 2006

25.   P. Y. Wu and W. A. Little. Measurement of the Heat Transfer Characteristics of Gas Flow in Fine Channel Heat Exchangers for Micro Miniature Refrigerators, Cryogenics, vol. 24, pp. 415–420, 1984.

26.   P.S. Lee, S. V. Garimella, D. Liu, Investigation of Heat Transfer in Rectangular Microchannels", Int. J. Heat and Mass Transfer, Vol.48, pp.1688-1704, 2005

27.   S. B. Choi, R. F. Barron, and R. O. Warrington. Fluid Flow and Heat Transfer in Microtubes, Micromech. Sensors, Actuators Syst., ASME DSC-Vol.32, pp. 123– 134, 1991.

28.   M.M. Rahman, F. Gui, Experimental measurements of fluid flow and heat transfer in microchannel cooling passages in a chip substrate, ASME EEP 4 (1993) 685– 692.

29.   D. Yu, R. Warrington, R. Barron, T. Ameel, An experimental and theoretical investigation of fluid flow and heat transfer in microtubes, in: Proceedings of ASME/JSME Thermal Eng. Joint Conference, 1995pp. 523-530.

30.   X. F. Peng, G. P. Peterson, B. X. Wang, Heat transfer characteristics of water flowing through microchannels, Exp. Heat Transfer 7 (1994) 265-283.

31.   T.S. Ravigururajan, M.K. Drost, Single-phase flow thermal performance characteristics of parallel microchannel heat exchanger, Enhanced Heat Transfer 6 (1999) 383-393.

32.   T. M. Adams, S. I. Abdel-Khalik, S.M. Jeter, Z.H. Qureshi, An experimental investigation of single-phase forced convection in microchannels, Int. J. Heat Mass Transfer 41(1998) 851-857.

33.   T. M. Harms, M. J. Kazmierczak, F. M. Gerner, Developing convective heat transfer in deep rectangular microchannels, Int. J. Heat Fluid Flow 20 (1999) 149- 157.

34.   W. Qu, I. Mudawar, Experimental and numerical study of pressure drop and heat transfer in a single-phase micro-channel heat sink, Int. J. Heat and Mass Transfer 45 (2002) 2549-2565.

35.   Y. J. Lee, P. Lee and S. Chou, "Experimental investigation of oblique finned microchannel heat sink", IEEE Electronic Device Letter EDL-2, 978-1-4244-5343-6/10, 2010

36.   J. Li and G. P. Peterson, "3-Dimensional numerical optimization of silicon-based high performance parallel microchannel heat sink with liquid flow", Int. J. Heat Mass Transfer 50 (15-16), pp. 2895-2904, 2007.

37.   A. Bejan and M. R. Errera, "Convective Trees of Fluid Channels for Volumetric Cooling", Int. J. Heat Mass Transfer 43, pp. 3105–3118, 2000.

38.   D. V. Pence, "Reduced Pumping Power and Wall Temperature in Microchannel Heat Sinks with Fractal-like Branching Channel Networks", Microscale Thermophys. Eng. 5, pp. 293–311, 2002.

39.   D. Heymann, et al., "Optimization of fractal-like branching microchannel heat sinks for single-phase flows", Int. J. Thermal Sciences (2010)

40.   Y. Chen and P. Cheng, "An experimental investigation on the thermal efficiency of fractal tree-like microchannel nets", Int. J. Heat Mass Transfer 32, pp. 931-938, 2005.

41.   J. H. Ryu, D. H. Choi, and S. J. Kim, , "Three-dimensional Numerical Optimization of a Manifold Microchannel Heat Sink", Int. J. Heat Mass Transfer 46, pp. 1553–1562, 2003.

42.   S. G. Kandlikar, and H. R. Upadhye, "Extending the Heat Flux Limit with Enhanced Microchannels in Direct Single Phase Cooling of Computer Chips", 21st IEEE SEMI-THERM Symposium, 2005.

43.   E. G. Colgan, B. Furman, M. Gaynes, W. S. Graham, N. C. LaBianca, J. H. Magerlein, R. J. Polastre, M. B. Rothwell, R. J. Bezama, R. Choudhary, K. C. Marston, H. Toy, J. Wakil, J. A. Zitz and R. R. Schmidt, "A Practical Implementation of Silicon Microchannel Coolers for High Power Chips", IEEE

Transactions on Components and Packaging Technologies 30 (2), pp. 218 – 225, 2007.

44. P.S. Lee, and S.V. Garimella , "Hot-Spot Thermal Management with Flow Modulation in Microchannel Heat Sink", Proceedings of 2005 ASME IMECE: International Mechanical Engineering Congress & Exposition, IMECE2005-79562, 2005

45. J.L. Xu, Y. H. Gan, D. C. Zhang, and X.H. Li, "Microscale Heat Transfer Enhacement Using Thermal Boundary Layer Redeveloping Concept", Int. J. Heat Mass Transfer 48, pp. 1662-1674, 2005

46. L., Gong et al. "Thermal Performance of Microchannels with Wavy Walls for Electronics Cooling", 12th IEEE ITHERM Symposium, 2010.

47. C.J. Ho, L.C. Wei, Z.W. Li, An experimental investigation of forced convective cooling performance of a microchannel heat sink with Al_2O_3/water nanofluid, Applied Thermal Engineering 30 (2010) 96–103

48. S.S. Bertsch, E. A. Groll, S. V. Garimella, Review and comparative analysis of studies on saturated flow boiling in small channels, Nanoscale and Microscale Thermophysical Engineering, 12:3, 187-227, 2008.

49. S.S. Mehendale, A. M. Jacobi, R. K. Shah, Fluid Flow and Heat Transfer at Micro- and Meso-scales with Application to Heat Exchanger Design", Applied Mechanics Reviews, Vol. 53, pp. 175-193, 2000

50. S. G. Kandlikar, W. J. Grande, "Evolution of Microchannel Flow Passages-Thermohydraulic Performance and Fabrication Technology", Heat Transfer Engineering, Vol.24, pp.3-17, 2003

51.   N. T. Obot, Toward a Better Understanding of Friction and Heat/Mass Transfer in Microchannels- A Literature Review", Microscale Thermophysical Engineering, Vol. 6, pp. 155-173, 2003

52.   Kandlikar S., Garimella S., Li D., Colin S., King M.R., Heat Transfer and Fluid Flow in Minichannels and Microchannels, Elsevier, 2006.

53.   S. Kakac, R. K. Shah and W. Aung, Handbook of Single-Phase Convective Heat Transfer, John Wiley and Sons Inc., New York, 1987

54.   R. K. Shah and A. L. London, Laminar Flow Convection in Ducts, Supplement to Advances in Heat Transfer, New York: Academic Press, 1978.

55.   J. O. C. Jones, An improvement in the calculation of turbulent friction in rectangular ducts, J Fluid. Eng., 98, 173-181, 1976.

56.   W. M. Kays and A. L. London, Compact Heat Exchangers, New York , NY: McGraw-Hill, 1984

57.   F.P. Incropera, D. P. DeWitt, Fundamentals of Heat and Mass Transfer, 5th edition, John Wiley & Sons, Indianapolis, 2002

58.   E. Alpsan, Experimental Investigation and Numerical Analysis of Microchannel Heat sinks for Phased Array Radar Cooling Applications, Msc Thesis, Mechanical Engineering Department, METU, Ankara, 2008

59.   A. V. Bapat, Experimental and Numerical Evaluation of Single Phase Adiabatic Flows in Plain and Enhanced Microchannels.

60.   A. M. Ateş, Experimental Comparison of Fluid and Thermal Characteristics of Microchannel and Metal Foam Heat Sinks, METU, Ankara, 2011

61.   D. B. Tuckerman and R. F. W. Pease, Ultrahigh Thermal Conductance Microstructures for Cooling Integrated Circuits, 32nd Electronics Components conference Proceedings, pp. 145-9.

62.   J. C. Lane and R. I. Loehrke, Leading Edge Seperation From a Blunt Plate at Low Reynolds Number, Journal of Fluids Engineering, Vol.102 pp.494-6

63.   N. Cur And E. M. Sparrow, Experiments on Heat Transfer and Pressure Drop for a Pair of Colinear, Interrupted Plates Aligned With the Flow, Internal Journal Of Heat and Mass Transfer. Vol.21, pp.1069-80

64.   C.O. Johnson and Loehrke R. I., An Experimental Investigation of Wake Edge Tones, AIAA Journal, Vol.22, pp.1249-53

65.   S., Garimella, "Microchannel Heat Exchangers Itherm Tutorial", 12th IEEE ITHERM Symposium, 2010.

66.   S.J. Kline, and F.A. McClintock, "Describing Uncertainies in Single-Sample Experiments", Mechanical Engineering, 75 (1), pp. 3-8, 1953

TECHNICAL DRAWINGS - TEST SPECIMENS
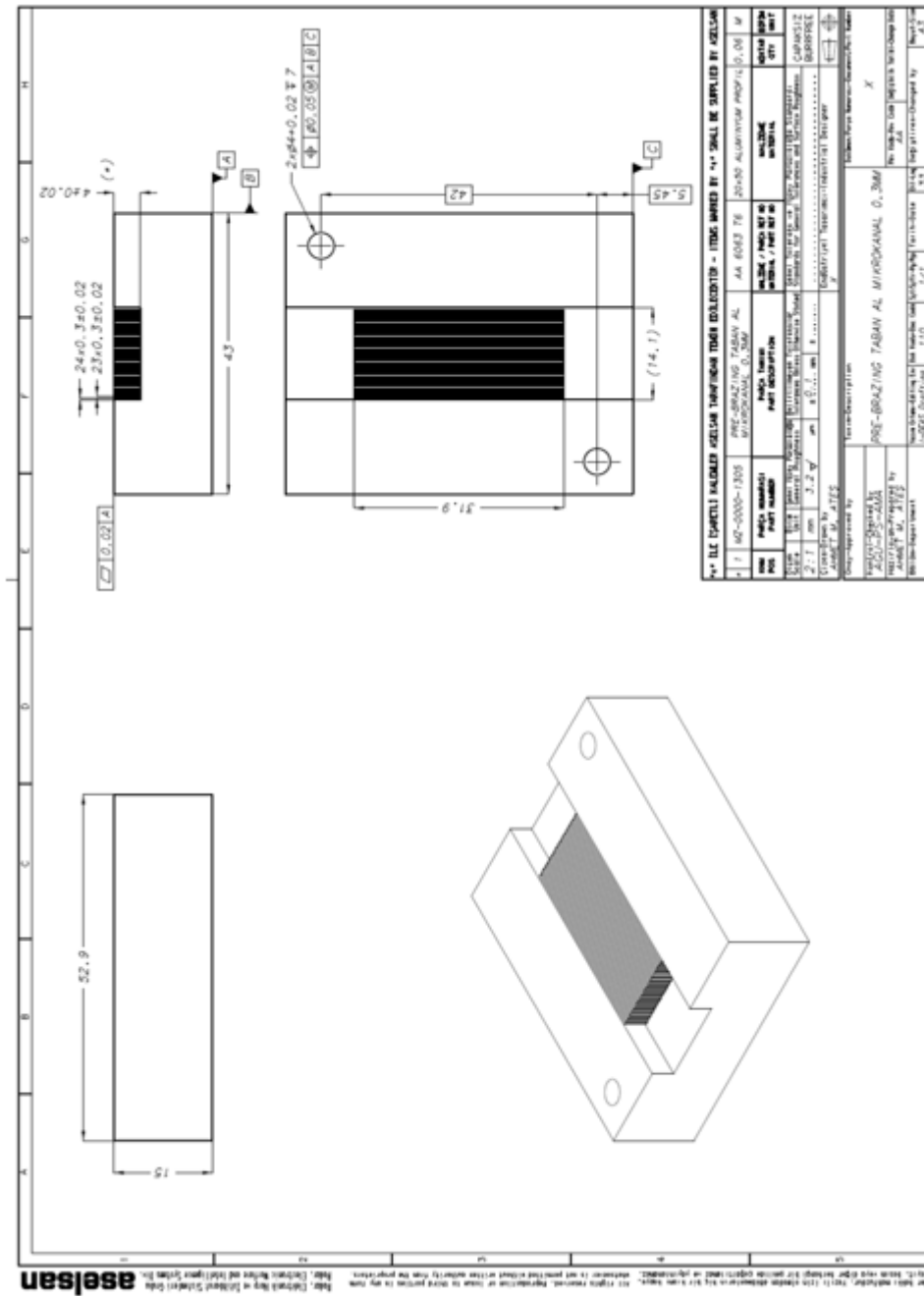
Figure A.1: Technical drawings of 300 micron wide uninterrupted channel

Figure A.2: Technical drawings of 300 micron wide single-interrupted channel

Figure A.3: Technical drawings of 300 micron wide multi interrupted channel
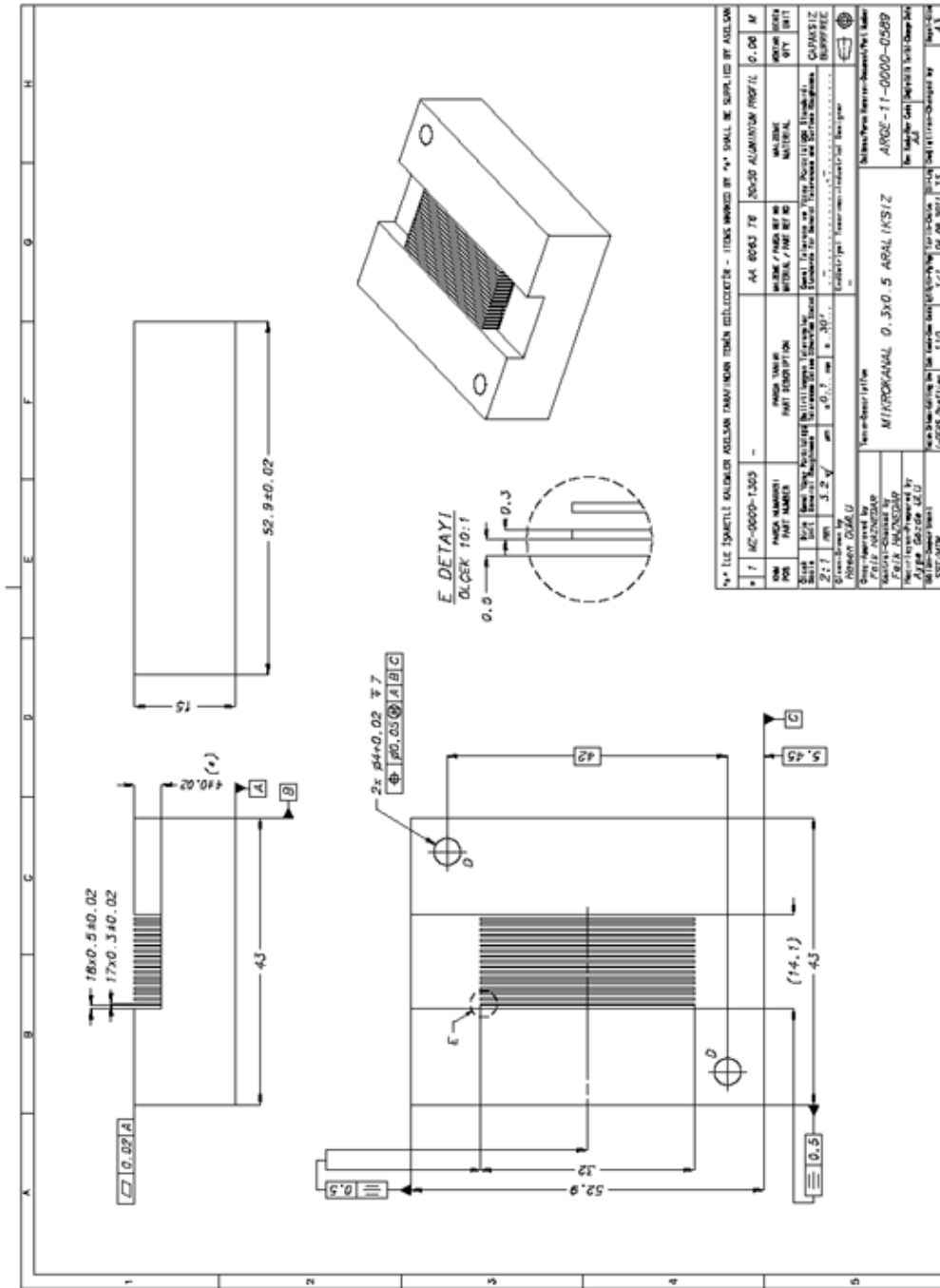
Figure A.4: Technical drawings of 500 micron wide uninterrupted channel
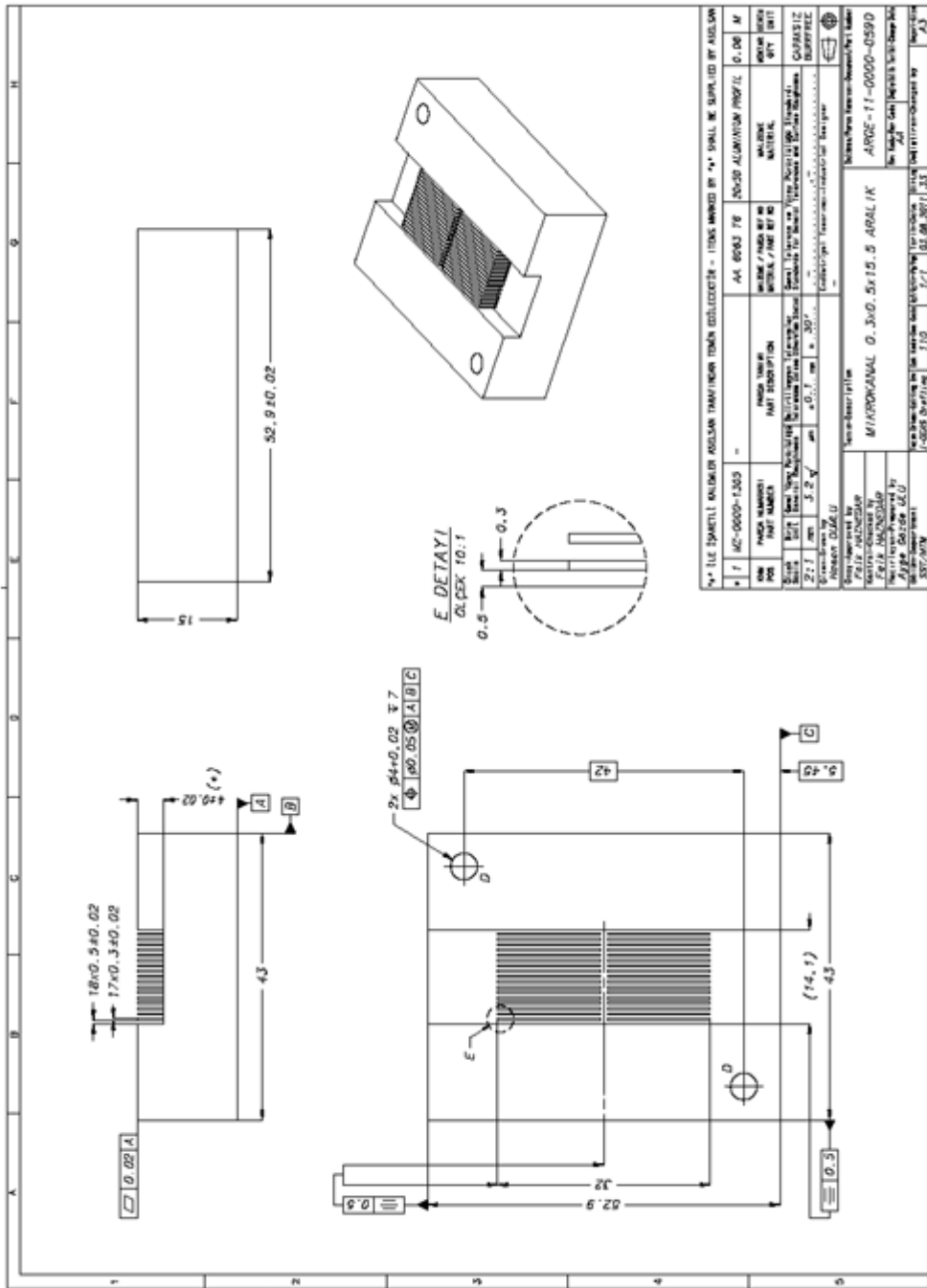
Figure A.5: Technical drawings of 500 micron wide singe interrupted channel
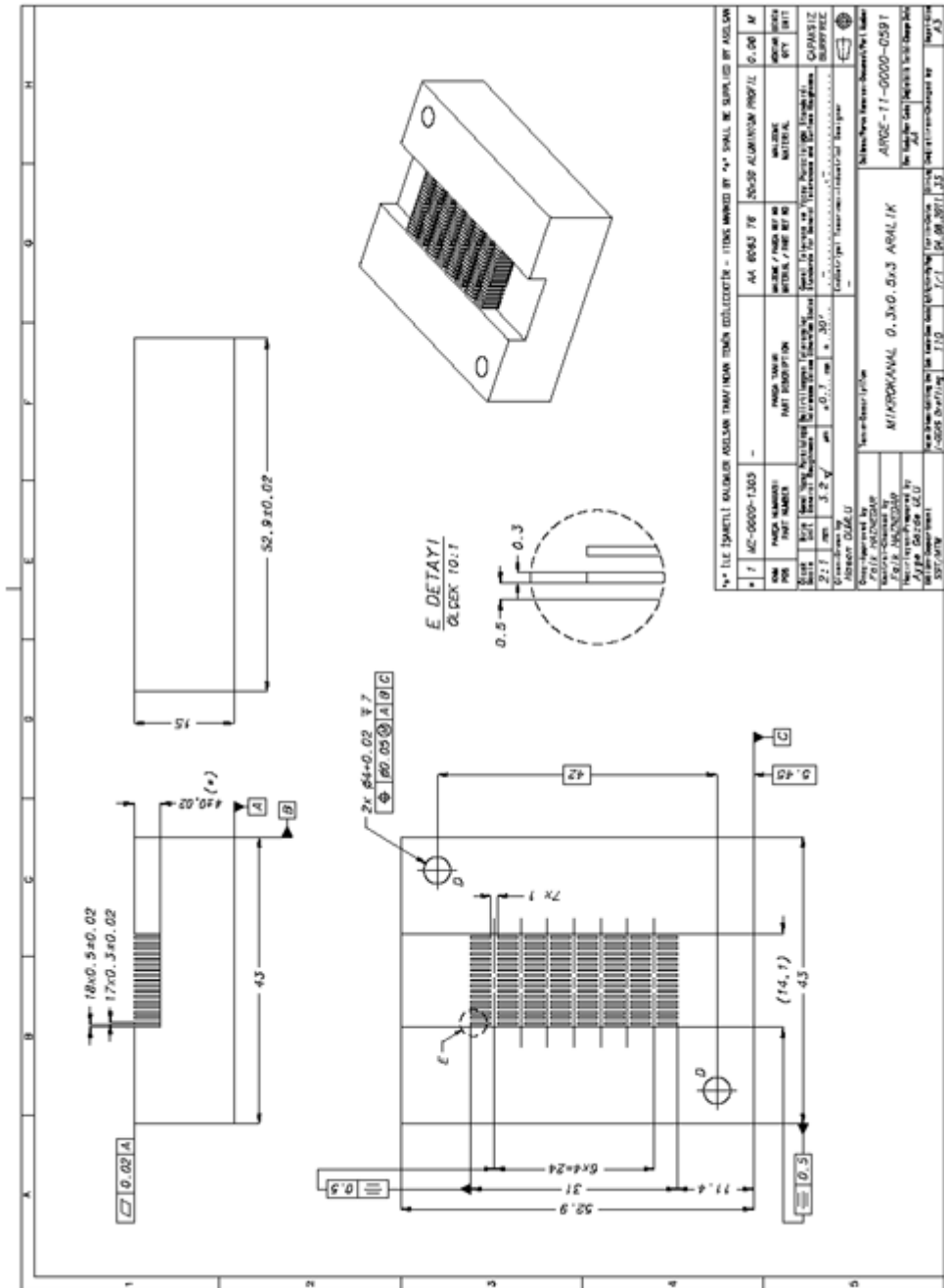
Figure A.6: Technical drawings of 500 micron wide multi interrupted channel

Figure A.7: Technical drawings of 600 micron wide uninterrupted channel

100
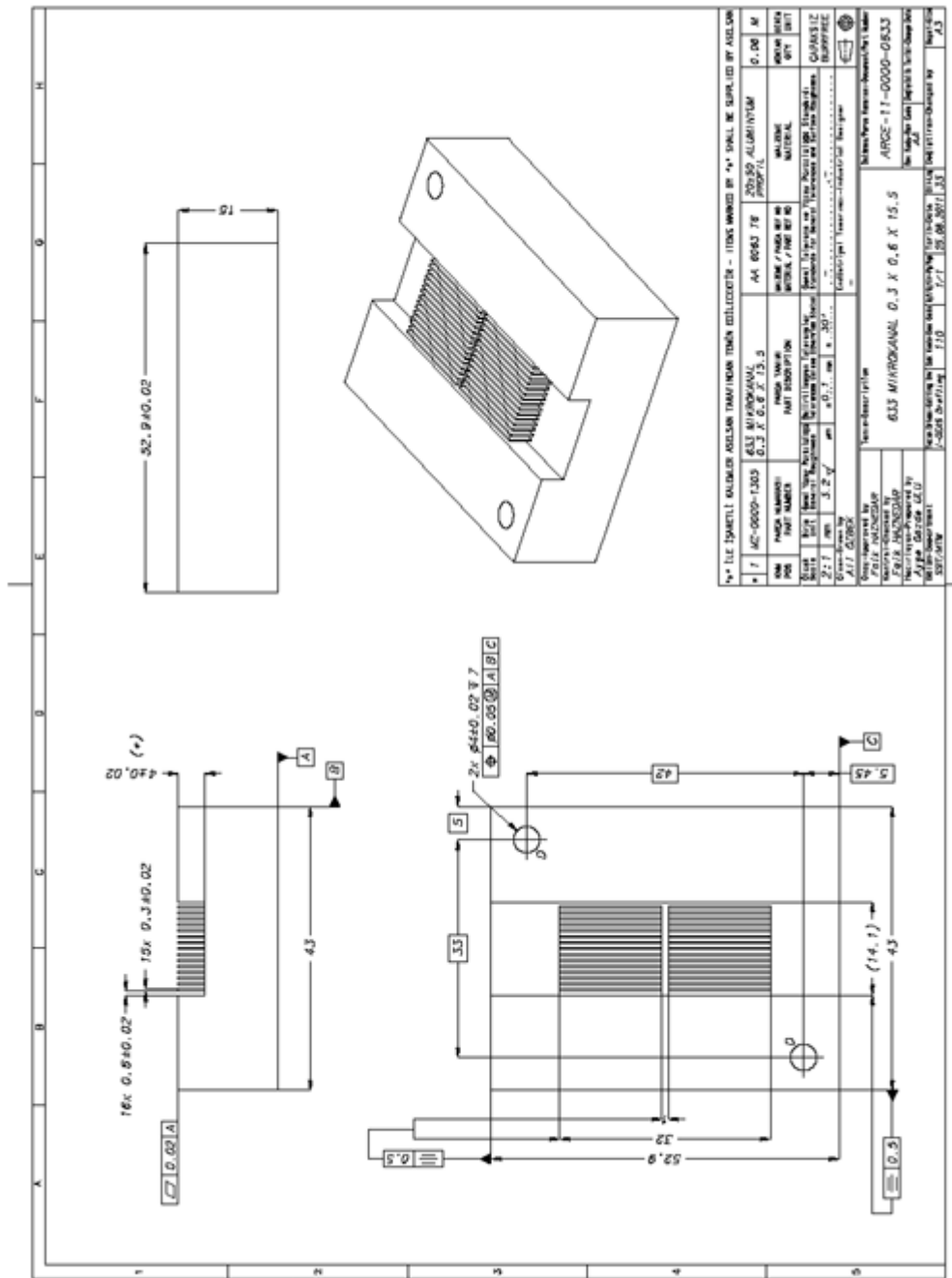
Figure A.8: Technical drawings of 600 micron wide singe interrupted channel

Figure A.9: Technical drawings of 600 micron wide multi interrupted channel

Figure A.10: Technical drawings of 900 micron wide uninterrupted channel
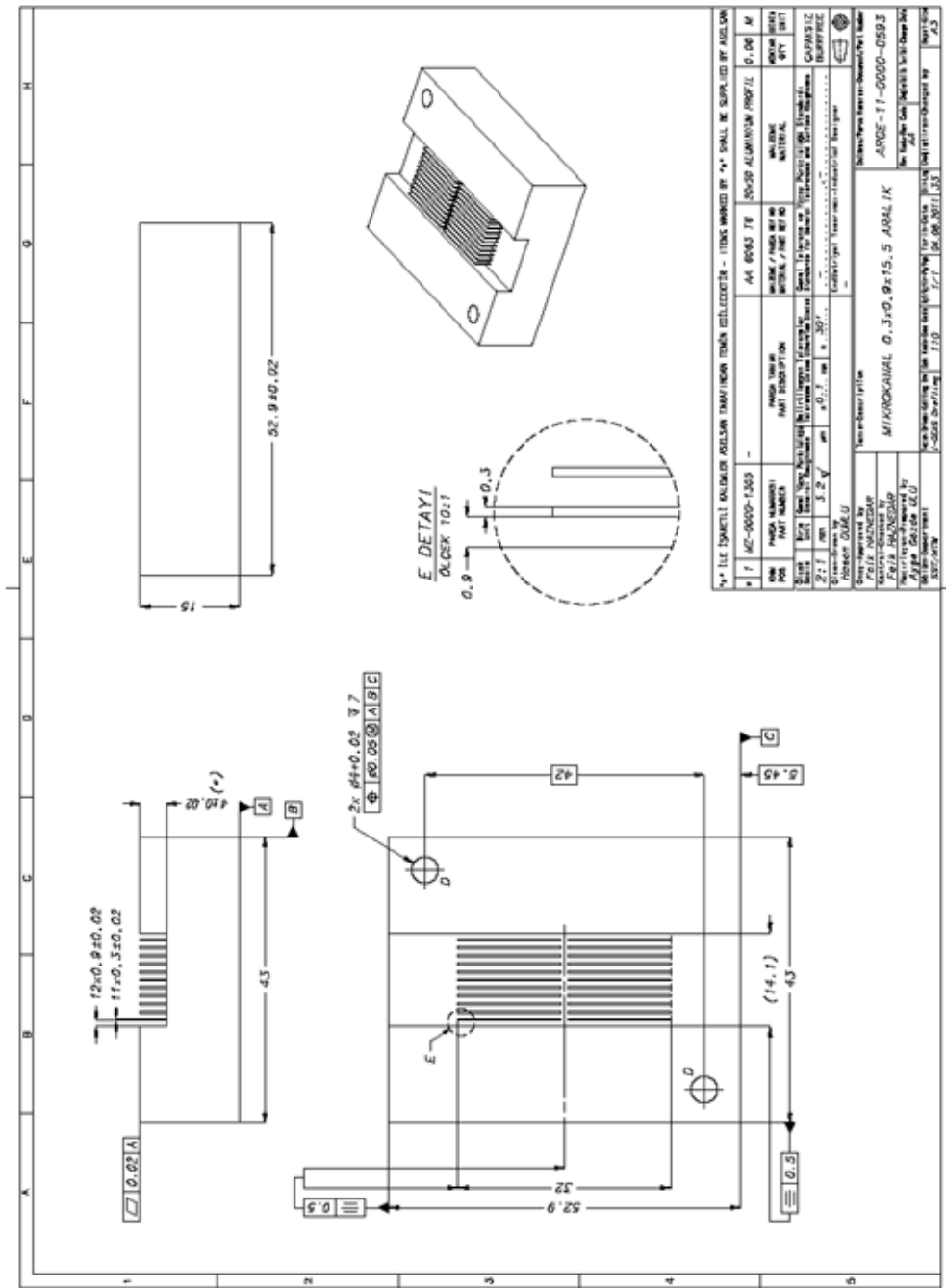
Figure A.11: Technical drawings of 900 micron wide singe interrupted channel

Figure A.12: Technical drawings of 900 micron wide multi interrupted channel

Figure A.13: Technical drawings of microchannel assembly

APPENDIX B

SAMPLE CALCULATIONS

A sample calculation for the microchannel heat sink of 500μm channel width, based on the relations presented in section 2.1, is given. Physical properties of water at 300K, on which the calculations are based, are given in Table B.1

Table B.1: Properties of water at 300 K

PROPERTY	SYMBOL	UNIT	WATER @ 300°K
Specific Heat	C_p	J/kg·K	4179
Dynamic Viscosity	μ	N·s/m^2	$8.55 \cdot 10^{-4}$
Thermal Conductivity	k	W/m·K	0.613
Prandtl Number	Pr	-	5.83
Density	ρ	kg/m^3	997

The set of sample calculations given below are for 500μm channel width. The aspect ratio and the hydraulic diameter for this channel is calculated as:

$$\alpha = \frac{a}{b} = \frac{0.5}{4} = 0.125$$

$$D_h = \frac{4A_{ch}}{P_w} = \frac{4 \times 0.5 \times 4}{2(4+0.5)} = 889\,\mu m$$

Volumetric flow rate: $Q = 1\text{lpm} = \dfrac{10^{-3}}{60}\,m^3/s = 1.667 \times 10^{-5}\,m^3/s$

For channel having cross sectional area of A_{ch} the flow velocity could be calculated as:

$$u_m = \frac{Q}{A_{ch}} = \frac{1.667 \times 10^{-5}\,m^3/s}{4mm \times 0.5mm \times 18} = 0.463\,m/s$$

Reynolds number for this flow rate:

$$Re = \frac{\rho \times u_m \times D_h}{\mu} = \frac{997 \times 0.463 \times 889 \times 10^{-6}}{8.55 \times 10^{-4}} = 479.9$$

Poiseuille number for this channel aspect ratio is found to be:

$$Po = f\,Re = 24(1 - 1.3553(0.125) + 1.9467(0.125)^2 - 1.7012(0.125)^3 + 0.9564(0.125)^4$$
$$- 0.2537(0.125)^5) = 20.59$$

From this equation the friction factor of the channel can be taken as:

$$f = \frac{Po}{Re} = \frac{20.59}{479.9} = 0.043$$

Entrance length of such a flow is defined to be:

$$L = 0.05 \times Re \times D_h = 0.05 \times 479.9 \times 889 \times 10^{-6} = 21.33\,\mu m$$

For channel having length of 31.9 mm, this entrance length means that the flow is not developed yet. For this flow Hagenberg factor is calculated as:

$$K(\infty) = 0.6796 + 1.2197(0.125) + 3.3089(0.125)^2 - 9.5921(0.125)^3 + 8.9089(0.125)^4$$
$$- 2.9959(0.125)^5 = 0.867$$

Pressure drop through the channel can be calculated as according to formula:

$$\Delta p = \frac{\rho u_m^2}{2}[(A_c / A_p)^2 (2K_{90}) + (K_c + K_e) + \frac{4f\, L_{ch}}{D_h} + K(\infty)]$$

$$\Delta p = \frac{997 \times (0.463 m/s)^2}{2}[(\frac{0.004 \times 0.0005 \times 18}{\pi \times (\frac{9.73}{2})^2})^2 (2 \times 1.1) + (0.8 + 0.98)$$
$$+ \frac{4 \times 0.043 \times 31.9 \times 10^{-3}}{889 \times 10^{-6}} + 0.867] = 750.7\, Pa$$

where 9.73 stands for the inner nominal diameter of the connectors, G1/8 thread.

The average heat transfer coefficient for frequently interrupted channel having 0.5mm channel width; 0.5x3 and is found from the following equations. The inside base temperature, T_b, is calculated from the Fourier law and the average of the base outside temperature, T_w.

$$T_b = T_w - \frac{t_b q^{''}}{k_{al}} = 60.98 - \frac{0.002 \times (40.83/(4.48 \times 10^{-4}))}{209} = 60.12$$

The heat transfer coefficient is calculated according to Equation 48 as below:

$$h = \frac{q}{A_f \times (T_b - T_m)} = \frac{40.83}{0.0035904 \times (60.12 - (34.27 + 33.68)/2)} = 434.99$$

Nusselt number for this flow is calculated as according to following equation:

$$Nu = \frac{hD_h}{k_f} = \frac{434.99 \times 889 \times 10^{-6}}{0.613} = 0.63$$

Convective and caloric thermal resistances are calculated as below:

$$R_{conv} = \frac{(\bar{T}_b - \bar{T}_f)}{q_{conv}} = \frac{60.12 - 33.97}{40.83} = 0.64$$

$$R_{cal} = \frac{(T_{fo} - T_{fi})}{q_{cal}} = \frac{1}{\rho \times Q \times c_p} = \frac{1}{\rho \times u_m \times n \times H \times w_c \times c_p} = \frac{34.27 - 33.68}{40.83} = 0.0144$$

EXPERIMENTAL RESULTS

Table C.1: Geometrical calculations

Fin type	600 micron uninter.	500 micron multi	900 micron multi	600 micron multi	900 micron single	600 micron single	500 micron single
Perimeter (mm)	64,40	6,60	6,60	6,60	31,60	31,60	31,60
Depth of a fin (mm)	4,00	4,00	4,00	4,00	4,00	4,00	4,00
Cross section area of a fin (mm^2)	9,57	0,90	0,90	0,90	4,65	4,65	4,65
Area of a fin (mm^2)	257,6	26,4	26,4	26,4	126,4	126,4	126,4
Number of fin in the channel (N)	15	136	88	120	22	30	34
Total fin area (mm^2)	3864	3590,4	2323,2	3168	2780,8	3792	4297,6
Un finned channel area (mm^2)	451,2	451,2	451,2	451,2	451,2	451,2	451,2
Total area (mm^2)	4315,2	4041,6	2774,4	3619,2	3232	4243,2	4748,8
Hydraulic diameter (mm)	1043	889	1469	1043	1469	1043	889

Table C.2: Nusselt number and heat transfer coefficient calculations at 0.2 lpm

Location of sensors		Types of channels						
		500 micron single	600 micron single	900 micron single	600 micron multi	900 micron multi	500 micron multi	600 micron uninter.
1	inlet of microchannel	30,4	30,5	32,5	32,1	31,9	30,7	31,4
2	outlet of microchannel	33,3	33,5	35,5	35,0	34,7	33,6	34,2
3	base of the channel 1	64,5	66,7	69,1	67,8	64,1	61,9	67,7
4	base of the channel 2	59,6	56,5	58,8	56,3	54,4	52,6	54,9
5	base of the channel 3	63,5	58,7	65,3	67,2	62,2	60,1	66,2
6	cold surface of heater	57,2	49,7	48,5	45,6	46,7	55,9	59,6
7	bottom surface of the cap	49,8	41,3	44,7	42,1	42,3	47,3	49,0
8	heater hot surface	115,1	98,9	106,7	95,8	89,7	89,6	95,4
Difference inlet-outlet		2.940	2,9	2,9	3,0	2,8	2,9	2,8
Rhs		2,07	1,67	1,78	1,61	1,45	1,50	1,61
q (W)		40,8	41,0	41,6	39,6	39,8	39,3	39,9
Pumping power	V	4,60	4,69	4,49	4,69	4,39	4,80	4,60
	I	0,04	0,04	0,04	0,04	0,04	0,05	0,05
	VI	0,18	0,19	0,18	0,19	0,18	0,22	0,21
Power given to heater	V	25,65	28,18	28,50	28,80	31,00	34,91	32,50
	I	2,05	1,77	1,82	1,85	1,65	1,47	1,50
	VI	52,48	49,88	51,98	53,22	51,06	51,35	48,62
Lost energy	k*A*Tdiff	3,48	3,95	1,79	1,65	2,10	4,05	4,95
Lost energy check	power given-taken	11,64	8,93	10,35	13,66	11,23	12,08	8,75
base average	average of 3, 4, 5	62,5	60,6	64,4	63,8	60,2	58,2	62,9
T_b		61,7	59,7	63,5	62,9	59,4	57,4	62,1
Fin total area (m^2)		0.004	0.004	0.003	0.003	0.002	0.004	0.004
T_b-T_m		29,8	27,7	29,5	29,4	26,1	25,2	29,3
h	$q/(A*(T_b-T_m))$	318,4	389,5	506,9	424,7	657,8	433,8	352,6
Nu	hD/k	0,462	0,663	1,215	0,723	1,576	0,629	0,600
R_{conv}	1/hA	0,73	0,68	0,71	0,74	0,65	0,64	0,73

Table C.3: Nusselt number and heat transfer coefficient calculations at 0.5 lpm

Location of sensors		Types of channels						
		600 micron single	900 micron single	600 micron multi	900 micron multi	500 micron multi	600 micron uninter.	500 micron single
1	inlet of microchannel	30,8	30,8	32,9	32,9	30,1	30,6	32,0
2	outlet of microchannel	31,9	32,0	34,0	34,1	31,2	31,7	33,1
3	base of the channel 1	65,0	66,1	67,3	69,2	55,8	59,8	68,9
4	base of the channel 2	60,0	54,9	57,0	56,1	48,1	50,5	56,1
5	base of the channel 3	64,6	57,0	63,1	68,2	54,8	57,6	66,8
6	cold surface of heater	62,4	50,5	45,9	45,9	36,5	52,2	66,8
7	bottom surface of the cap	51,0	40,9	42,6	42,4	34,5	44,4	52,4
8	heater hot surface	121,5	99,4	103,4	94,0	79,4	86,2	101,5
Difference inlet-outlet		1.152	1,2	1,2	1,2	1,1	1,1	1,2
Rhs		2.268	2,27	1,71	1,76	1,55	1,25	1,38
q (W)		40.010	40,0	40,0	40,1	39,4	39,6	40,4
Pumping power	V	10,30	10,30	10,20	10,80	10,00	10,10	10,70
	I	0,11	0,10	0,10	0,10	0,10	0,10	0,10
	VI	1,13	1,03	1,02	1,08	0,95	0,96	1,07
Power given to heater	V	26,30	28,60	28,20	30,10	28,50	34,51	34,40
	I	2,15	1,77	1,82	1,86	1,52	1,45	1,58
	VI	56,44	50,62	51,41	55,84	43,32	49,93	54,29
Lost energy	k*A*Tdiff	16,43	10,58	11,26	16,47	3,76	9,50	13,75
Lost energy check	power given-taken	16,43	10,58	11,26	16,47	3,76	9,50	13,75
base average	average of 3, 4, 5	63,2	59,3	62,5	64,5	52,9	55,9	63,9
T_b		62.326	62,3	58,5	61,6	63,7	52,1	55,1
Fin total area (m^2)		0.004	0.004	0.003	0.003	0.002	0.004	0.004
T_b-T_m		30.985	31,0	27,1	28,2	30,2	21,4	23,9
h	$q/(A*(T_b-T_m))$	300,5	390,3	512,6	411,7	794,9	470,8	343,6
Nu	hD/k	0,436	0,664	1,229	0,700	1,905	0,683	0,585
R_{conv}	1/hA	0,77	0,68	0,70	0,77	0,54	0,59	0,75

Table C.4: Nusselt number and heat transfer coefficient calculations at 0.7 lpm

		Types of channels						
Location of sensors		500 micron single	600 micron single	900 micron single	600 micron multi	900 micron multi	500 micron multi	600 micron uninter.
1	inlet of microchannel	31,2	32,7	33,0	33,7	32,8	33,4	31,9
2	outlet of microchannel	32,0	33,6	33,9	34,5	33,7	34,2	32,7
3	base of the channel 1	66,1	69,1	67,4	68,2	64,5	64,8	66,8
4	base of the channel 2	60,7	58,5	56,7	56,9	53,1	54,9	54,8
5	base of the channel 3	64,9	59,6	63,2	69,5	61,6	61,7	65,4
6	cold surface of heater	64,1	53,7	47,0	47,5	49,5	60,1	63,7
7	bottom surface of the cap	53,0	43,6	43,1	43,6	43,1	50,4	50,1
8	heater hot surface	121,8	98,0	105,3	95,8	88,2	99,5	99,4
Difference inlet-outlet		0.830	0,8	0,8	0,8	0,8	0,8	0,8
Rhs		2.246	2,25	1,60	1,80	1,56	1,38	1,61
q (W)		40.343	40,3	40,8	40,2	39,7	40,1	41,0
Pumping power	V	13,90	13,90	13,90	14,30	14,30	19,60	14,10
	I	0,15	0,16	0,16	0,16	0,16	0,25	0,16
	VI	2,09	2,15	2,22	2,29	2,29	4,98	2,18
Power given to heater	V	26,57	29,00	28,50	30,60	30,40	33,30	34,00
	I	2,16	1,82	1,83	1,88	1,86	1,67	1,56
	VI	57,28	52,90	52,21	57,65	56,39	55,61	53,14
Lost energy	k*A*Tdiff	16,94	30,98	12,00	17,92	16,29	14,64	13,32
Lost energy check	power given-taken	16,94	12,12	12,00	17,92	16,29	14,64	13,32
base average	average of 3, 4, 5	63,9	62,4	62,4	64,9	59,7	60,4	62,4
T_b		63.059	63,1	61,5	61,6	64,0	58,9	59,6
Fin total area (m^2)		0.004	0.004	0.003	0.003	0.002	0.004	0.004
T_b-T_m		31.463	31,5	28,4	28,1	29,9	25,6	25,8
h	$q/(A*(T_b-T_m))$	298,4	378,9	513,9	418,9	674,0	442,7	352,4
Nu	hD/k	0.433	0.645	1.232	0.713	1.615	0.642	0.600
R_{conv}	1/hA	0.780	0.696	0.700	0.754	0.639	0.629	0.734

Table C.5: Nusselt number and heat transfer coefficient calculations at 1 lpm

Location of sensors		Types of channels						
		500 micron single	600 micron single	900 micron single	600 micron multi	900 micron multi	500 micron multi	600 micron uninter.
1	inlet of microchannel	31,4	33,0	33,8	34,3	32,9	33,7	31,9
2	outlet of microchannel	32,0	33,6	34,3	34,8	33,5	34,3	32,4
3	base of the channel 1	66,4	70,0	68,7	68,5	64,6	65,4	66,0
4	base of the channel 2	61,0	59,1	58,0	57,1	53,3	55,5	54,5
5	base of the channel 3	65,4	60,3	64,2	69,7	62,0	62,1	65,0
6	cold surface of heater	66,4	56,2	48,7	47,5	51,3	62,0	63,0
7	bottom surface of the cap	53,9	44,7	44,0	43,8	43,8	51,4	49,6
8	heater hot surface	124,1	100,2	105,8	96,0	89,7	102,5	99,5
Difference inlet-outlet		0.569	0,6	0,6	0,6	0,6	0,6	0,6
Rhs		2.346	2,35	1,64	1,81	1,57	1,41	1,69
q (W)		39.492	39,5	40,9	39,8	39,3	40,4	40,8
Pumping power	V	19,40	19,20	19,30	19,80	19,00	19,60	19,10
	I	0,25	0,25	0,25	0,25	0,24	0,25	0,24
	VI	4,85	4,80	4,82	4,95	4,56	4,98	4,58
Power given to heater	V	27,00	29,60	28,90	30,60	34,00	33,70	34,00
	I	2,18	1,84	1,82	1,88	1,64	1,70	1,57
	VI	58,81	54,46	52,69	57,53	55,83	57,26	53,35
Lost energy	k*A*Tdiff	19,71	12,63	12,84	14,75	18,73	14,90	11,12
Lost energy check	power given-taken	19,31	13,54	12,89	18,20	15,41	16,43	13,67
base average	average of 3, 4, 5	64,3	63,1	63,6	65,1	60,0	61,0	61,8
T_b		63.458	63,5	62,3	62,8	64,2	59,1	60,1
Fin total area		0.004	0,0040	0,0040	0,0030	0.003	0.002	0.004
T_b-T_m		31.741	31,7	28,9	28,7	29,7	25,9	26,1
h	$q/(A*(T_b-T_m))$	289,5	373,2	497,9	418,3	672,1	435,0	355,9
Nu	hD/k	0,420	0,635	1,193	0,712	1,611	0,631	0,606
R_{conv}	1/hA	0,80	0,71	0,72	0,76	0,64	0,64	0,73

115